SOLUTE BIOCONCENTRATION MECHANISMS IN BIOLOGICAL MATERIAL

by

Rhys Colbran Trousdale

A dissertation submitted in partial fulfillment
of the requirements for the degree

of

Doctor of Philosophy

in

Chemistry

MONTANA STATE UNIVERSITY
Bozeman, Montana

May 2025

DEDICATION

This dissertation is dedicated to my amazing family and girlfriend for their love and support. Mom and Dad, thank you for your immense support and always pushing me to do my best in life and telling me how proud you have been, you're the reason I'm here doing what I love. Grandma and Papa and Granny and Gramps, I can't thank you enough for the love and support you have given me throughout my time in college, grad school and through life. Riley, thank you for being an ear to listen to and being my best friend through life. Niki, thank you for the love and always being there for me when things get tough.

ACKNOWLEDGEMENTS

First, I need to thank Dr. Rob Walker for being the best advisor one could ask for, the support, teaching and great scientific conversations were and always appreciated. I would also like to thank my committee members; Dr. Erik Grumstrup, Dr. Mary Cloninger, Dr. Brian Bothner, and Dr. Martin Mosquera, all of whom provided valued teaching, input and guidance throughout my time at MSU. I would also like to thank Dr. Doreen Brown for all of her help and support over the last five years.

An extended thank you to past and present Walker Research Group members, with a special thank you to Dr. Katelyn Duncan who mentored and instructed me, and taught me how to be a good scientist. Thank you to Tess Sobolewski for being a good friend and lab mate, and someone to always have a good conversation with. Past group members Josh, Tanner and Marshall for being good role models. The current WRG thank you for being a good community to do science with. Thank you to Will and Roark for the awesome adventures and great conversations.

I would like to thank EPSCoR for their funding of my studies. With a special thank you to those involved in EPSCoR who challenged me to think outside of my discipline. I would also like to thank SIGP Sloan Scholars for funding me personally. A special thank you goes to Barbara Komlos who got me into SIGP and wanted the best for the Sloan students at MSU. I would also like to thank Dr. Craig Ogilvie who took over Sloan and showed dedication and care for the graduate students of MSU. I would like to thank the whole SIGP Sloan scholar group for being an amazing group of people who gave me a community to join and express myself in.

I am, and always will be, forever grateful to my family and friends who supported me and fueled my drive to complete this Ph.D.

TABLE OF CONTENTS

TABLE OF CONTENTS CONTINUED

TABLE OF CONTENTS CONTINUED

LIST OF TABLES

Table Page

LIST OF TABLES CONTINUED

Table Page

LIST OF TABLES CONTINUED

Table Page

LIST OF FIGURES

Figure Page

LIST OF FIGURES CONTINUED

Figure Page

LIST OF FIGURES CONTINUED

Figure Page

LIST OF FIGURES CONTINUED

Figure Page

LIST OF FIGURES CONTINUED

Figure Page

LIST OF FIGURES CONTINUED

Figure Page

LIST OF FIGURES CONTINUED

Figure Page

ABSTRACT

Bioconcentration is a term used to quantify the concentration of a solute within an organism with respect to the source of exposure. Recently, bioconcentration has been a major field of study for analytical and environmental chemists since the rise of synthetic chemicals appearing within the environment. The work described here uses fluorescence spectroscopy, light scattering, and thermoanalytical techniques to describe the impact of bioconcentration mechanisms on the structure and function of biological material, including model biological membranes and transport proteins. The studies performed in this body of work investigate solute-membrane and solute-protein interactions by analyzing the behavior of both the solute, and the biological material of interest in order to uncover the wholistic effect of the solute on a biological system.

Each body of work either altered the solute studied for bioconcentration or the biological material itself, to get a deeper understanding of bioconcentration mechanisms. The first body of work describes a study looking into the partitioning behavior of the amino acid L-Phenylalanine into model biological membranes. Experiments showed that L-Phenylalanine integrates into the membrane and experiences a conformationally restricted environment. The second body of work inspects an environmental contaminant known as Perfluorooctanoic acid (PFOA), and the effects it has on lipid bilayer vesicles structure, as well as secondary solute partitioning behavior at concentrations close to the EPA regulatory limits. Experiments revealed that 100 nM PFOA increases membrane fluidity and increases secondary solute partitioning into the acyl chains of the lipid bilayer. The third body of work explores Perfluorooctanoic acid’s effects on the protein Human Hemoglobin, and discovered that PFOA induces a change in the fluorescence mechanism of the native Tryptophan residues, and binds at concentrations as low as 10 nM.

CHAPTER ONE

INTRODUCTION

Motivation

Bioconcentration and Bioaccumulation

Bioconcentration is a simple idea to describe: the tendency of solutes in aqueous solutions to concentrate within living systems. [1-3] Bioconcentration is generally construed as a harmful outcome of pollution or other contaminants adversely affecting an individual's health, but bioconcentration can also describe beneficial effects such as nutrient or pharmaceutical uptake. [4] Bioconcentration and bioaccumulation describe the absorption of a solute within an organism with respect to the source of exposure, and both are used as a descriptor for the potential toxicity of a solute. [2, 3, 5] However, the underlying mechanisms driving bioconcentration and bioaccumulation remain largely unexplored. Questions remain about not only where the solute will concentrate (lipid membranes, proteins, DNA), but also how these solutes affect the biological function of those structures into which they partition. Biological structures including lipid membranes and proteins are complex systems, with variable local solvation environments and a multitude of possibilities for chemical interactions. The research described in this dissertation uses complementary methods including optical spectroscopy, light scattering, and calorimetry to examine partitioning behavior of both environmentally and biologically relevant solutes with model lipid membranes and heme-proteins. The goal of this work is to develop a clear understanding of how the complexity found in biological systems controls solute partitioning. Our discoveries show that bioconcentration of biological solutes such as amino acids or synthetic solutes such as PFAS, are complex mechanisms which can significantly alter

the function of the target biological material. The impact of this work will show that bioconcentration mechanisms, while somewhat predictable, can be complicated and nuanced when interacting in a biological system.

Bioconcentration and bioaccumulation are both measures of a solute's uptake into organisms, with the difference being the source of exposure to the solute. [5] Bioconcentration is the most common measure of solute partitioning and analyzes solute absorption through respiratory and dermal surfaces. The bioconcentration factor (BCF) is calculated as the ratio of solute concentration in an organism (C_B) to solute concentration in the surrounding aqueous environment (C_W) (Equation 1). [5-7]

$$BCF = \frac{C_B}{C_W} \qquad \text{Eq. 1}$$

The bioaccumulation factor (BAF) takes into consideration how solute uptake can occur from other environmental sources, dietary uptake, inhalation, metabolic transformation, dilution of the solute from organism to organism, and excretion. BAFs are calculated as the ratio of the solute concentration within an organism relative to the sum of the concentration of the solute in the water, sediment (C_S), and food (C_F) (Equation 2).[7]

$$BAF = \frac{C_B}{C_W + C_S + C_F} \qquad \text{Eq. 2}$$

An important point to note is that both BCFs and BAFs are purely empirical, based solely on observation and measurement, and provide only a simple, single quantity to describe solute uptake. Although BCFs and BAFs are instructive, they fail to provide any direct chemical insight into the phenomena they describe.

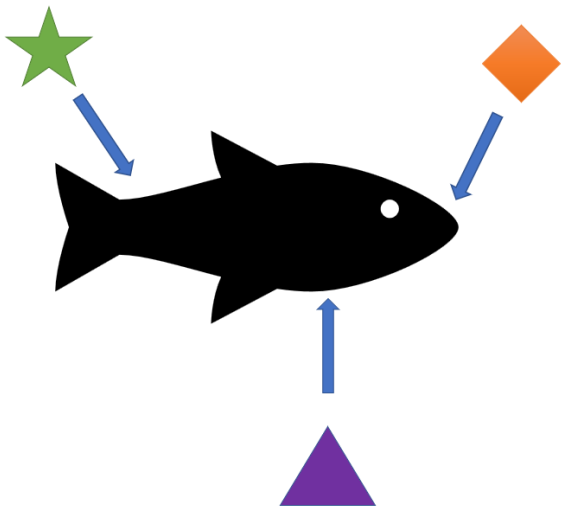

Figure 1.1: Schematic representation of bioconcentration of different solutes partitioning into an organism from the surrounding environment

BCFs and BAFs are often used to characterize a solute's persistence in the environment, although these numbers can be difficult to measure directly. A solute's partitioning coefficient, known as log P, is one empirical way to predict partitioning behavior of a solute, and this information is then used to determine the BCF. Log P is the log of the equilibrium partitioning of a solute between an organic phase (1-octanol) and an aqueous phase (water) (Equation 3). [1, 7, 8]

$$\log P = \log\left(\frac{[solute]_{octanol}}{[solute]_{water}}\right) \qquad \text{Eq. 3}$$

While log P can be a useful indicator of solute-membrane affinity, the scale is a simple solubility description and has shortcomings. One major fault of the log P measurement is that it fails to account for ionizability of the solute. log D, also known as the distribution coefficient, is another partitioning description intended to account for pH-dependent solubility of ionizable compounds. Like the log P scale, the log D scale considers the equilibrium distribution of solutes between 1-octanol and water, but accounts for both the ionized and nonionized population of the solute. [9]

$$\log D = \log\left(\frac{[solute]_{octanol}}{[solute]_{aq}^{ionized}+[solute]_{aq}^{nonionized}}\right) \quad \text{Eq. 4}$$

Another more advanced prediction technique is K_{mw} or is the phospholipid membrane-water partition coefficient, that replaces the 1-octanol used in log P and log D descriptors with a lipid membrane. This technique is an inherently more useful prediction tool as it directly measures concentrations of solutes between an aqueous environment and biologically-similar membranes to gauge solute tissue distribution and cell membrane penetration. [10, 11]

$$\log k_{mw} = \log\left(\frac{[solute]_{membrane}}{[solute]_{water}}\right) \quad \text{Eq. 5}$$

More recently, molecular modelling and computational chemistry approaches have been used to more accurately predict log P, log D, and log K_{mw} values. [12, 13] Computational methods can be more beneficial than experimental methods for predicting partitioning values since they allow more high-throughput screening of solutes, reducing the time required to predict solute lipophilicity. Multiple public log P calculators currently exist, and can be classified into four families, 1) atom-based methods, 2) fragment-based methods, 3) topology or graph-based methods and 4) structural property-based methods. [13] Atom-based methods sum the contribution from each individual atom of the molecule. While this approach has proven suitable for small molecules, it becomes increasingly inaccurate with more complex molecular structures, or when the electronic structure of the overall molecule effects the log P value. Some methods attempt to overcome these shortcomings by using additional corrections to account for neighboring atom interactions. [13]

Fragment-based methods are another additive approach that considers the summation of molecular fragments that contribute to a molecule's hydrophobic character. These calculations also consider interactions such as hydrogen bonding, proximity interactions, and hydrophobic-shielding effects. However, fragment-based methods require rigorous interpretation of solvation

interactions, and the computations tend to be expensive, making them less attractive for widespread screening. Topology or graph-based models use topological descriptors to generate models, typically using 2-D generated structures. Structure-property based methods are more robust, requiring 3-D structures to perform quantum-mechanical computations to develop a chemically specific perspective into the forces that control partitioning. These computational methods have made predicting solute lipophilicity much more accessible and for a larger range of molecules than the traditional experimental methods. Unfortunately, shortcomings of computational methods are still present insofar as predictions from these studies have not been experimentally validated. Furthermore, these computational methods are also expensive, and the they have not been employed to predict the effects that partitioned solutes have on subsequent biological structure and function. [13]

Another shortcoming of the log P, log D, and log K_{mw} techniques is their primary focus on membranes as the target for solutes since these descriptors are all a measure of a solute's general lipophilicity. However, membranes are not the only biological material that can bioaccumulate secondary solutes. DNA and proteins are also capable of attracting solutes in ways that build up secondary solute concentrations within organisms. [14, 15] Proteins such as Serum Albumins are widely recognized as candidates to accumulate hydrophobic solutes due to the large hydrophobic "pocket" within the protein that can act as an energetically favorable site for these molecules. [16, 17] However, with thousands of different proteins in organisms, identifying protein specific solute affinities as well as solute binding effects on protein structure and function is a daunting challenge.

Protein affinity experiments typically quantify solute binding using either an equilibrium association constant, or dissociation constant. Equilibrium dialysis measurements are the gold

standard for evaluating these descriptors. [18] In an equilibrium dialysis experiment, the solute or ligand is separated from the protein or macromolecule by a semi-permeable membrane where the solute can permeate through, but the protein remains on one side. Once the system reaches an equilibrium, or steady state, the amount of free solute should be equal on both sides of the dialysis membrane. The solute concentration on the protein side is the combination of bound and free solute, whereas the concentration on the other side is simply free solute. The concentration of bound solute can be found by taking the difference between the total solute concentrations present in both compartments. Careful consideration must be exercised when choosing a dialysis membrane, as thickness, membrane type, and membrane impurities can impact the values measured in an equilibrium dialysis experiment. [18] Equilibrium dialysis is the standard method for examining solute binding, however, like most affinity techniques, dialysis data lack the insight into how solute binding affects protein structure and function. Most systems that use equilibrium dialysis pair results with LC-MS measurements to determine ligand binding amount, but not many directly study the protein after reaching steady-state.

While these experiments provide insight into the toxicity limits and bioconcentration factors, they fail to capture the specific solute-lipid and solute-protein interactions responsible for solute accumulation mechanisms in biological systems. Work described in the following chapters tackles questions about solute affinity for membranes and proteins with the intent of developing quantitative and chemically specific descriptions of solute partitioning. Fluorescence spectroscopy in combination with thermoanalytical and dynamic light scattering methods were employed to address the following questions:

1. Do specific solutes partition into the biological material?
2. If so, where in the biological material do solutes accumulate?

3. What is the quantitative distribution of solutes within membranes and proteins?
4. Do partitioned solutes alter membrane/protein properties?

Each chapter in this body of work analyzed different classes of solutes, or different biological materials to develop a quantitative, mechanistic understanding of solute partitioning behavior. Specifically, this work focused on amino acids and PFAS interacting with model biological membranes, and PFAS binding to the protein human hemoglobin (Hb).

Membrane Complexity

Biological cellular membranes are a complex network of phospholipids, cholesterol, proteins, and carbohydrates following the fluid mosaic model or the raft hypothesis. [19, 20] Due to their heterogeneous structures and varied functions, biological membranes are often modeled using phospholipid bilayers as surrogates. [21, 22] The amphiphilic nature of the lipid is the source of the bilayer, the polar headgroups will orient themselves to the surrounding aqueous environment while the non-polar tails will orient towards the center of the membrane. These hydrophobic forces are the main source of bilayer formation, while van der Walls and electrostatic interactions stabilize the bilayer structure. [23] The phosphatidylcholine membranes used in this study create a heterogenous chemical environment across a membrane width of ~7nm. To fully understand solute partitioning behavior complex lipid bilayer environments, first the solute must be characterized in a variety of bulk solvents which model the local solvation environment that solute might experience in the membrane. Carbonate buffer was chosen to model the aqueous environment surrounding the membrane. Acetonitrile was used to model the polar aprotic head groups before membrane hydration takes place, and methanol was used to model the polar protic head groups after membrane hydration occurs. Cyclohexane was chosen to model the non-polar environment of the long carbon chain tails of the lipid.

An important point to remember is that the glycerol 3-carbon chain backbone is naturally polar aprotic and is a hydrogen bond acceptor but not a donor, until water can penetrate the membrane at the lipid bilayer gel to liquid-crystalline phase transition known as $T_{gel\text{-}lc}$. This phase transition occurs at a specific temperature for a given lipid, and can vary based on carbon chain length, or having other molecules within the bilayer such as cholesterol. From a physical perspective, $T_{gel\text{-}lc}$ is where the lipid bilayer goes from a more rigid and ordered structure in the gel state to a more loosely associated structure called the liquid crystalline state. [24] At this point, water can enter the membrane and hydrate the polar aprotic headgroups, making them have a polar protic local solvation environment. This liquid-crystalline state also opens new opportunities for solute interactions which might not occur in the gel state.

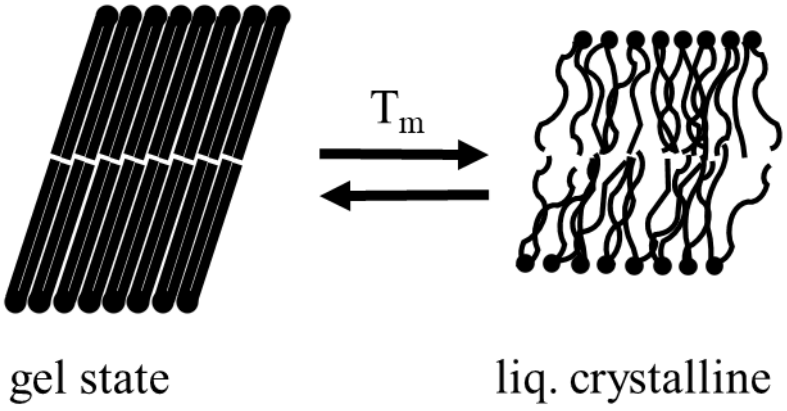

Figure 2.1. Schematic representation of a lipid bilayer going from the rigid, and more ordered gel state to the less ordered liquid-crystalline state caused from an increase in temperature.

Time-Resolved Fluorescence Emission

Time-resolved emission studies are based on the delayed detection of an emission photon following electronic excitation, where the excitation laser pulse is shorter than the fluorescence lifetime of the molecule of interest. Time-resolved emission can provide important insight into

the relaxation dynamics of a solute, including energy transfer between molecular states, molecular rotation, and fluorescence quenching dynamics.

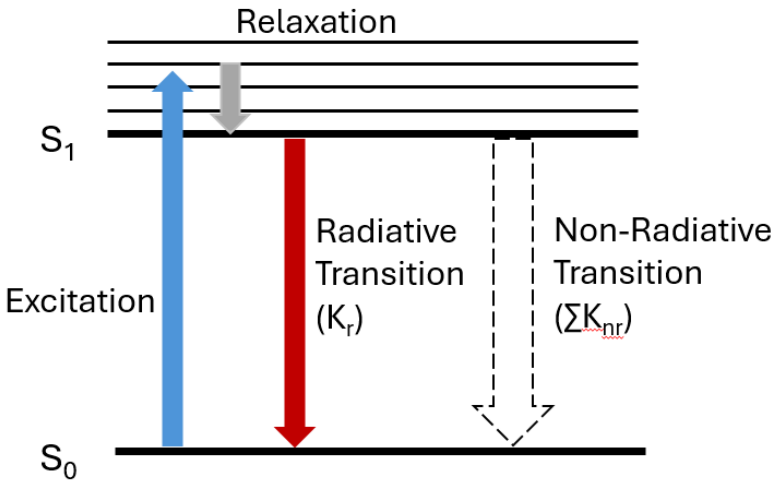

Figure 3.1: A simplified Jablonski diagram representing the excitation of a molecule to a higher electronic energy level, and the resulting possible relaxation mechanisms the molecule can have. A radiative transition will result in the release of a lower energy photon whereas a non-radiative pathway will result in no emission photon.

Fluorescence decay of an excited molecule can be described by first-order rate kinetics and depends on the radiative lifetime (τ_i) of the solute. The fluorescence lifetime of a molecule can be described by eq. 2, which considers the radiative (k_r) and non-radiative (k_{nr}) decay of the molecule. On a molecular level, τ describes the time required an excited state population to its 1/e value and contains information about a molecule's radiative and non-radiative lifetimes.

$$\tau = \frac{1}{k_r + \sum k_{nr}} \qquad \text{Eq. 6}$$

Tau (τ) can be experimentally determined by exciting the population of molecules and recording the fluorescence intensity decay. The intensity decay follows a single exponential model when the population of molecules exhibits a single lifetime and is described by Eq. 3.

$$I(t) = I_0 e^{-(\frac{\tau}{t})} \qquad \text{Eq. 7}$$

Where t is the time from excitation, I_0 is the initial intensity, and (τ) is the time it takes to decrease 1/e of its initial value. Fluorescence decay plots are typically plotted on a logarithmic scale. For the most part, fluorescence decays are fit with a single exponential decay model, however for more complex decays with two or more lifetimes, a more complicated fitting model, such as Eq. 8, is required to determine the lifetimes and corresponding amplitudes.

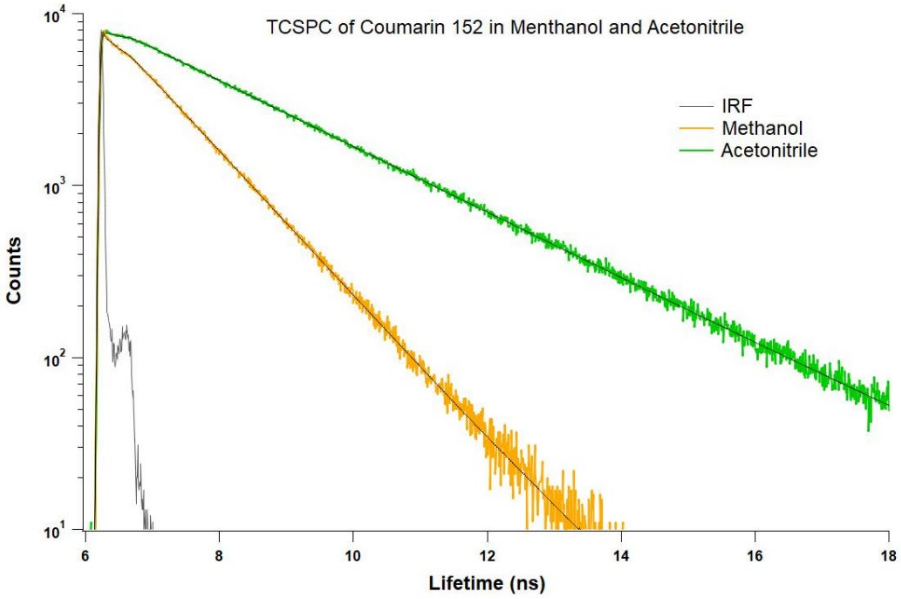

Figure 4.1: Example of time-resolved fluorescence of laser dye Coumarin 152 in methanol and acetonitrile. This figure shows how solvent can play a role in the time-resolved emission of a solute.

If only one single exponential decay for a molecule is measured, there is one radiative decay mechanism, whereas if a decay is characterized by two or more lifetimes, multiple independent decay mechanisms are occurring. The lifetime itself is also an indicator of the non-radiative decay, if a long lifetime (~2+ ns) exists for a solute, the non-radiative decay is very slow, but if the lifetime is short (~0.5 ns) the non-radiative decay becomes more important. Understanding these fluorescence decay characteristics is vital to determining the behavior of a solute in solution, especially when in complex systems like model biological membranes.

L-Phenylalanine (L-Phe) is one of three naturally fluorescent amino acids, the other two being L-Tryptophan (Trp) and L-Tyrosine (Tyr). Due to the low quantum yield of L-Phe in aqueous solutions at 0.023, it is the least studied of the fluorescent amino acids; with Trp and Tyr having quantum yields of 0.14 and 0.13 respectively. [25, 26] Fluorescent lifetimes of L-Phe are dependent on solvent interactions with the molecule. In solvents with higher polarity, such as water or methanol, the lifetime of L-Phe remains long (~6 ns), whereas in less polar solvents such as acetonitrile and cyclohexane, the lifetimes are reduced due to the polarity of the solvent at 3.3 ns and 1.1 ns respectively. Additionally, L-Phe can experience other lifetimes not represented by any bulk solvent, due to rotamer states of L-Phe which can occur when either at higher temperature (~60°C), when sterically trapped inside a peptide, or when physically trapped by a lipid bilayer and accessible to water molecules. Greater detail on this subject will be covered in Chapter 2.

Coumarin 152 (C152) is a common laser dye and the bulk solvent fluorescence behavior, as well as the behavior when in a solution with model biological membranes, has been studied extensively by the Walker Research Group. C152 has distinct behavior in the bulk solvents, making it a phenomenal solute to understand solute-membrane behavior. In an aqueous solution such as carbonate buffer, C152 has two distinct lifetimes, a short (0.5 ns) lifetime and a long (3.52 ns) lifetime. The short lifetime which comprises a majority of the fluorescence decay (~85%) is due to a twisted intramolecular charge transfer (TICT) state which occurs due to solvent interactions with C152. However, some of the population of C152 (~15%) does not undergo TICT, and this is reflected in the long lifetime due to a lower non-radiative decay. This short lifetime due to TICT reflected in the methanol lifetime which is measured as a single exponential decay and a lifetime on the order of 1 ns. In polar aprotic (Acetonitrile) and non-

polar solvents (non-polar), the TICT state cannot occur, and results in longer measured lifetimes of ~2.2 ns and 3.7 ns respectively. [27] Findings described in Chapter 3 of this dissertation rely on changes to the fluorescence of C152 within membranes with and without the presence of PFOA.

Unlike the previously described fluorescence mechanisms which were focused on a loose solute within a given solution, Chapter 4 discusses the fluorescence of Tryptophan residues within the protein structure of Human Hemoglobin (Hb). Hb is a heme-based oxygen transport protein consisting of a dimer of dimers, with each dimer containing one alpha and one beta subunit, and each subunit containing an iron-heme complex. Each alpha subunit contains one Trp residue and each beta subunit contains two Trp residues, resulting in six total Trp residues which can be utilized for fluorescence studies without the need for a fluorescent marker. Due to the complex nature of Hb, each Trp residue experiences a distinct conformation and fluorescence due to solvent accessibility and fluorescence quenching. Trp residues which are structurally close enough to the heme complex have fluorescence lifetimes which are defined by fluorescence quenching due to Forster Resonance Energy Transfer (FRET) with the heme group, which causes a fast non-radiative decay and therefore an ultrafast lifetime on the order of 0.05 ns. Additionally, fluorescence quenching can also occur from Trp residues to the peptide backbone resulting in vibrational relaxation, or other amino acid residues which are able to accept electronic energy such as Tyrosine, and is defined by a lifetime around 0.5 ns. Some Trp residues are solvent accessible and go through neither of these quenching pathways, resulting in a lifetime reminiscent of free Trp, with a lifetime on the order of 2 ns. [28-30] Overall, the natural fluorescence of Hb when using the native Trp residues becomes quite complicated, but the lifetimes due to quenching can be diagnostic of protein conformation and stability.

Perfluorooctanoic acid

Solute partitioning into biological membranes can also depend on other species in solution. Specifically, if a contaminant alters the cohesive properties of a biological membrane, secondary solute accumulation may be enhanced. Chapter 3 of this dissertation examines how one of the legacy 'forever chemicals', perfluorooctanoic acid (PFOA), affects secondary solute partitioning. PFOA, along with several other perfluoro alkyl substances (PFAS), has been among the most concerning environmental contaminants of the 21st century. PFOA has been linked to a multitude of health effects such as reduced vaccine response, high cholesterol, and a variety of cancers. Recently, the U. S. Environmental Protection Agency (EPA) mandated a maximum allowable drinking water concentration of 4 ppt for several PFAS species. PFOA itself has long been used as antifire foams, as well to waterproof products including cookware (Teflon), textiles, and food packaging material. While PFOA is no longer produced for commercial use, the molecule's chemical stability means it will remain an environmental and health hazard for decades. More discussion on the environmental and health impacts of PFOA will be discussed in Chapter 3.

A major concern for PFAS and PFOA is the fact that it can bioconcentrate in organisms. With a half-life in the human body on the order of 7 years, PFOA is expected to interact with biological material such as membranes and proteins by accumulating in hydrophobic environments. This behavior will lead to bioconcentration and may influence secondary solute accumulation. For example, if PFOA bioconcentrating alters the cell structure and causes structural defects, bioconcentration mechanisms of other environmentally relevant synthetic organic solutes such as herbicides, pesticides, or pharmaceuticals may be impacted. Chapter 3

considers how PFOA affects model membrane structures, as well as the impact PFOA has on the partitioning behavior of secondary solutes.

Experimental Methods

Sample preparation The lipid bilayer vesicles used in Chapters 2 and 3 were created from monomers of the lipid dipalmitoylphosphatidylcholine (DPPC) at concentrations of 1.5 mM for optical studies and 20 mM for calorimetry studies. Vesicle solutions used for optical studies were extruded and filtered using an Avanti Lipid Mini-Extruder (Alabaster, AL) to create large unilamellar vesicles (LUVs) having ~200 nm diameters. A defining feature of this lipid bilayer membrane, like most other lipids, is a transition temperature known as $T_{gel\text{-}LC}$ which occurs at 40.5°C. This transition describes bilayer melting when the bilayer goes from having a more rigid and structured gel phase with 'frozen' acyl chains to a less ordered and more fluid structure known as the liquid-crystalline phase. At temperatures slightly lower than $T_{gel\text{-}LC}$ the membrane experiences a pre-transition known as the ripple phase, where water can intercalate into the polar head group. Studies described in Chapters 2 and 3 were performed as a function of temperature to investigate solute interactions with lipid bilayers across $T_{gel\text{-}LC}$, as well as study the reversibility of observed partitioning mechanisms.

As mentioned previously, Human hemoglobin is a complex transport protein which functions as a dimer of dimers, the dimers consisting of one alpha subunit and one beta subunit. Each subunit has its own heme group, which is responsible for binding oxygen for transport throughout the body. Hemoglobin is an allosterically modulated protein, meaning that the solute binding at one site can cause conformational changes to the global structure of the protein. The study described in Chapter 4 uses lyophilized human hemoglobin that was rehydrated for

experiments. Before experiments were conducted, the solution containing Hb was spun in a microcentrifuge to reduce major aggregates of the protein that could be present. For native mass spectrometry experiments, this step was taken further, and the solution was spun in a microcentrifuge using 30 kDalton filters to remove additional fragments having sizes lower than the native quaternary structure.

Time-resolved emission studies on human hemoglobin were performed using the intrinsic fluorescence of the Tryptophan residues of the protein. Human hemoglobin has six Trp residues, two on each beta subunit and one on each alpha subunit. Due to the presence of a conjugated porphyrin (heme) within each subunit, time resolved fluorescence emission is dominated by an ultrafast (50 ps) fluorescence lifetime that reflects efficient fluorescence quenching of the Trp to the heme via Forster Resonance Energy Transfer. While this lifetime is outside the capabilities of our TCSPC to accurately measure, this ultrafast lifetime becomes a significant diagnostic of the protein structure.

Steady-State Fluorescence Spectroscopy.

The steady-state excitation and emission behavior of solutes in all bulk solvents were characterized using a Horiba Fluorolog-3 (Irving, CA). To understand each solutes interaction in each of the lipid local solvation environments, a wavelength that overlapped for each solvent was chosen for excitation and emission in a lipid vesicle solution to probe all possible solvation environments. Steady-state spectroscopy was also used to characterize human hemoglobin's natural fluorescence, targeting the Trp residues as the major contributor to the protein's fluorescence.

Time-Correlated Single-Photon Counting

The TCSPC assembly was built around a Ti:sapphire oscillator (Coherent Chameleon, 80 MHz, 85 fs pulse length, 680-1040 nm wavelength range, Santa Clara, CA) coupled with an APE autotracker harmonic generator (Berlin, Germany). The harmonic generator was used to frequently double (second harmonic generation) and triple (third harmonic generation) the fundamental wavelength. For second and third harmonic generation, a Conoptics Model 350-10 modulator, and a Conoptics 350-80 modulator (Danbury, CT), respectively, was used to reduce the repetition rate to 4 MHz. Picoquant Picoharp 300 and FluoTime 200 software were used for data collection. Samples were equilibrated at the reported temperature for 7 minutes using a Quantum Northwest TC125 control (Seattle, WA). A long pass filter was placed after the sample and before the detector to cut any fundamental excitation wavelength. The filter was sample specific and chosen to be an intermediate wavelength between excitation and emission wavelengths to reduce scattering from the sample and set-up. For experiments with vesicle-containing solutions, the excitation wavelength chosen was one that overlapped with all four bulk solvents in steady-state spectra.

All time-resolved emission data in vesicle containing solutions were fit independently and all determined lifetimes and amplitudes were obtained using fitting parameters adjusted to minimize residuals and optimize chi-square. A linear combination of lifetimes determined by fitting was used to determine the local solvation environment of the solute in vesicle containing solutions by comparing the lifetimes to bulk solvents. The fluorescence decay and amplitude expression are shown in Equation 8 where τ_i and A_i are the lifetime and amplitude if the i^{th} component, respectively.

$$I(t) = \int_0^t IRF\ (t') \sum_{i=1}^{n} A_i e^{-\frac{t-t'}{\tau_i}}\, dt' \qquad \text{(Eq. 8)}$$

Each decay trace was fit independently with no constraints for the lifetimes and amplitudes, with a typical chi-square between 0.9 – 1.1 when accounting for, at most, three lifetimes. Data presented herein represent an average of 3-5 independent, and equivalent experiments. Lifetime uncertainties are reported as +- 0.2 ns due to the TCSPC instrument response function (IRF); however, lifetimes reported here are an average of all 3-5 trials with a single standard deviation reported for the average of those trials. Uncertainty of amplitudes in time-resolved experiments is 0.4%. For temperature dependent and concentration dependent studies, this technique was done at each temperature or concentration independently, and only corresponding temperatures or concentrations were compared and averaged.

Differential Scanning Calorimetry (DSC)

A TA Instruments DSC2500 (New Castle, DE) was used for calorimetry experiments. Vesicle containing solutions were made at 20 mM concentrations for DSC experiments. To make the vesicles, the DPPC was dissolved in chloroform in a round bottom flask and the chloroform was subsequently evaporated via rotary evaporation at 50°C (10°C above the lipid gel-liquid crystalline transition) to form a thin film. The thin film was then rehydrated with either a pure buffer solution, or a solvent-buffer solution. Rehydrated vesicles were then sonicated at 50°C for 30 minutes to form vesicles. The resulting solution was not filtered to any specific size, and was left to sit in the fridge for a minimum of 10 minutes before calorimetry experiments were conducted. Hermetic Tzero pans and Tzero lids from DSC Consumables. Calorimetry experiments were performed by equilibrating the sample at 4°C and ramping the temperature at 1°C/min to 55°C. Temperature uncertainty from the DSC2500 is +-0.025°C. Data were analyzed using TA Instruments TRIOS software.

Dynamic Light Scattering (DLS).

DLS is a highly sensitive and non-invasive analytical method used to determine the size and size distribution of particles (typically sub-micron) in a solution. DLS works by using the light intensity autocorrelation function to determine the size of particles in suspension. An initial "snapshot" of the intensity of light coming through the sample us used as a reference before the experiment begins. Then, as time progresses, the light intensity changes as particles move around in solution due to Brownian motion. Faster changes to the light intensity mean the autocorrelation falls off sooner, and is representative of smaller particles. Slower changes to the light intensity result in a slower fall off of the autocorrelation and is representative of larger particles in solution. Solvent viscosity and refractive index can affect DLS results. For DLS experiments, a Malvern Panalytical (Malvern, UK) Zetasizer Pro was used. Sample preparation for DLS experiments followed the same lipid generation and filtration methods described in the Steady-state and TCSPC methods section. Each sample for DLS experiments was equilibrated at temperature for a minimum of 2 minutes, then subjected to 3 trials through the ZS Xplorer software provided by Malvern Panalytical. The software averages 3 trials to find an accurate size and size distribution of the vesicles within solutions. The polydispersity index (PDI) is a measure of the homogeneity of the solution, a PDI less than 0.2 means the size distribution of the particles is relatively homogenous, whereas a PDI of 0.7 and above represents a solution with a high variability in particles sizes. Reported DLS experiments were only taken for samples with PDI values below 0.35 to ensure dust or other contaminants were not affecting the results.

Thesis Outline

Research discussed in this work was all done to understand the bioconcentration mechanisms and consequences of biologically and environmentally relevant solutes with

biological material. The first part of this work (Chapter 2) focuses on the partitioning behavior of the amino acid L-Phenylalanine (L-Phe) with lipid bilayer vesicles, the effects on vesicle properties, and discoveries about L-Phe's fluorescent properties when in solution with vesicles. Chapter 3 consists of work done to understand how the forever chemical PFOA affects secondary solute bioconcentration mechanisms. This work uses a secondary solute Coumarin 152 (C152) to quantify partitioning and compares C152's behavior in vesicle containing solutions in studies. Chapter 4 studies PFOA binding and impact on Human Hemoglobin (Hb) at micro-molar and sub-micromolar concentrations using the fluorescence from Hb's native tryptophan residues as well as native mass spectrometry. Chapter 5 involves a study looking into phenylalanine-based dipeptide interactions with lipid vesicles, with the intention of increasing the complexity of the system of study to begin including peptide chains. Chapter 5 also presents experiments of lipid bilayer vesicle interactions with other PFAS molecules to see if trends are similar to PFOA. Chapters 2 and 3 are journal articles published in 2023 and 2024 respectively. Chapter 4 is a prepared manuscript which has been submitted to a journal for publication. Due to their publication in literature, information in the introduction, materials and methods sections of these chapters will, at times, be redundant.

Chapter 2. Quantitative Membrane Partitioning Studies of L-Phenylalanine

Motivated by previous work done in the Walker group looking into amino acid affinity for model biological membranes, this study was done in an effort to confirm the hypothesis that L-Phenylalanine integrates into the polar head group of the bilayer and disrupts cohesive lipid-lipid chain forces. Time-resolved emission studies comparing L-Phe in bulk solvents to L-Phe in vesicle solutions showed, initially, at 10°C, all of the L-Phe in a vesicle solution is within the surrounding buffer environment. However, as the temperature of the system gets closer to the

$T_{gel\text{-}LC}$, a second lifetime appears, which does not correspond to any bulk solvent lifetime. As the temperature passes $T_{gel\text{-}LC}$ and gets closer to 70°C, this 2nd lifetime comprises ~30% of the overall fluorescence from L-Phe. We interpret this 2nd lifetime as an optically trapped rotamer state of L-Phe, which has integrated with the bilayer before $T_{gel\text{-}LC}$, but only becomes optically visible when water is able to intercalate into the membrane during the membrane pre-transition. To confirm this, multiple lipids were examined for this behavior, all phosphocholine lipids with the same head group as DPPC, but with varying chain length which will change $T_{gel\text{-}LC}$. Results from these studies showed that the second lifetime of L-Phe becomes optically visible around the pre-transition in each different chain length membrane. This body of work confirms the hypothesis that L-Phe integrates into lipid bilayer membranes. All supplemental work can be found in appendix A and is indicated as such within the chapter. This work was published by the ACS journal *Journal of Physical Chemistry B* in 2023.

Chapter 3. Nanomolar PFOA Concentrations Affect Lipid Membrane Structure: Consequences for Bioconcentration Mechanisms

Motivated by recent EPA federal regulations declaring a maximum allowable drinking water concentration of 4 ppt for several PFAS species, this body of work delves into low concentration PFOA effects on the structure, function, and secondary solute accumulation of model biological membranes. This study was done in an effort to test the hypothesis that PFOA will bioconcentrate and effect the structure and function of lipid bilayer vesicles at concentrations close to the EPA regulatory limits. Results from Dynamic Light Scattering and Cryo- Electron Microscopy revealed significant changes to the structure of the vesicles when generated in the presence of just 100 nM PFOA. Notably, these studies revealed that the overall vesicle size is increased, and the lipid bilayer width is decreased with 100 nM PFOA present.

Alongside this, both Cryo-EM and DLS studies revealed the appearance of secondary structures, smaller than the average vesicle which were determined to be noisome-like structures. Cryo-EM also unveiled significant structural defects within the lipid bilayer structures including the appearance of multilamellar vesicles and more faceted bilayers. Time-resolved emission studies were used to determine if secondary solute partitioning is affected by the presence of PFOA with the vesicles. Using a laser dye, Coumarin 152, which has been well characterized in the Walker Research Group, we discovered that PFOA has a significant impact on the partitioning mechanism of the laser dye. In particular, we found that there was a ~30% increase in the non-polar lifetime contribution of the laser dye across temperature ranges, and a ~15% decrease in the contribution from the aqueous and polar lifetimes; leading us to the conclusion that PFOA is causing defects in the lipid bilayers which drives more C152 into the non-polar region of the membranes, increasing bioconcentration of the laser dye. All supplemental work can be found in appendix B and is indicated as such within the chapter. This work was published by the ACS journal *Environmental Science and Technology* in 2024.

Chapter 4. Perfluorooctanoic Acid Destabilizes Hemoglobin Structure at sub-Micromolar Concentrations

Bioconcentration targets are not only membranes but rather any biological material including proteins and DNA. This study was performed to broaden the understanding of bioconcentration mechanisms of PFOA specifically with Human Hemoglobin. Motivated by the previous body of work, this study looked at the impact PFOA has on protein structure when PFOA concentrations begin to increase as bioconcentration would, to confirm the hypothesis that PFOA will interact at with Hb at low concentrations, and due to the allosteric nature of the protein, cause conformational changes, which also result in functional changes to the protein.

Time-resolved emission experiments unveiled a change in the fluorescence quenching mechanism which occurs in heme-based proteins. When exciting the native tryptophan residues of the protein, Forster Resonance Energy Transfer (FRET) occurs from the excited Trp residue to the heme group, resulting in an ultrafast lifetime, deterministic of fluorescence quenching. However, as PFOA concentration increases into the 100 uM range, there begins to be a shift from the major quenching mechanism of FRET, to fluorescence quenching via the peptide backbone, suggesting that a structural change is causing heme loss, or significant structural changes to the protein. Native mass spectrometry was performed to examine changes in structure when PFOA is present, and results showed that PFOA binds to Hb at concentrations as low as 10 nM. NMS – Ion mobility experiments also revealed that at 20 uM PFOA, Hb experiences two distinct conformations, and we also witness loss of the alpha subunit from the overall protein structure, confirming the time-resolved emission studies. All supplemental work can be found in appendix C and is indicated as such within the chapter. This work is currently under review with the ACS journal *Journal of Physical Chemistry B.*

CHAPTER TWO

L-PHENYLALANINE PARTITIONING MECHANISMS IN MODEL BIOLOGICAL MEMBRANES

Contribution of Authors and Co-Authors

Author: Rhys C. Trousdale
Contributions: Reproduced and analyzed TCSPC and DLS data, generated figures, assisted in writing manuscript, and wrote SI.
Co-Author: Katelyn M. Duncan
Contributions: Collected and analyzed TCSPC and DSC data, generated figures, and wrote manuscript.
Co-Author: Christina Gonzolas
Contributions: Assisted with data accumulation.
Co-Author: William H. Steel
Contributions: Assisted with data accumulation, assisted with editing of manuscript.
Co-Author: Robert A. Walker
Contributions: Contributed important insight into performing experiments and interpreting results. Edited and assisted in preparation of manuscript.

Manuscript Information

Rhys C. Trousdale, Katelyn M. Duncan, Christina Gonzales, William H. Steel, and Robert A. Walker
Journal of Physical Chemistry B
State of Manuscript
_____ Prepared for submission to a peer-reviewed journal
_____ Officially submitted to a peer-reviewed journal
_____ Accepted by a peer-reviewed journal
__x__ Published in a peer-reviewed journal
Published by the Journal of Physical Chemistry B
In Volume 127, Issue 25, 5633-5644, 2023
https://doi.org/10.1021/acs.jpcb.2c08582

L-PHENYLALANINE PARTITIONING MECHANISMS IN MODEL BIOLOGICAL MEMBRANES

Katelyn M. Duncan[†,a], Rhys C. Trousdale[†,a], Cristina Gonzales[‖], William H. Steel[‡], and Robert A. Walker[†§]*

[†]Department of Chemistry and Biochemistry, Montana State University, Bozeman, Montana 59717, United States.

[‖]Department of Chemistry, Reed College, Portland, Oregon 97202, United States

[‡]Department of Chemistry, York College of Pennsylvania, York, Pennsylvania 17403, United States

[§]Montana Materials Science Program, Montana State University, Bozeman, Montana 59717, United States

[a]Both authors contributed equally to this work.

Abstract.

Time-resolved fluorescence spectroscopy in combination with differential scanning calorimetry (DSC) was used to study the chemical interactions that occur when L-Phenylalanine is introduced to solutions containing phosphatidylcholine vesicles. Studies reported in this work address open questions about L-Phe's affinity for lipid vesicle bilayers, the effects of L-Phe partitioning on bilayer properties, L-Phe's solvation within a lipid bilayer, and the amount of L-Phe within that local solvation environment. DSC data show that L-Phe reduces the amount of heat necessary to melt saturated phosphatidylcholine bilayers from their gel to liquid-crystalline state but does not change the transition temperature ($T_{gel\text{-}lc}$). Time-resolved emission shows only a single L-Phe lifetime at low temperatures corresponding to L-Phe remaining solvated in aqueous solution. At temperatures close to $T_{gel\text{-}lc}$, a second, shorter lifetime appears that is assigned to L-Phe already embedded within the membrane that becomes hydrated as water starts to permeate the lipid bilayer. This new lifetime is attributed to a conformationally restricted rotamer in the bilayer's polar headgroup region and accounts for up to 30% of the emission amplitude. Results reported for dipalmitoylphosphatidylcholine (DPPC, 16:0) lipid vesicles

prove to be general with similar effects observed for dimyristoylphosphatidylcholine (DMPC, 14:0) and distearoylphosphatidylcholine (DSPC, 18:0) vesicles. Taken together, these results create a complete and compelling picture of how L-Phe associates with model biological membranes. Furthermore, this approach to examining amino acid partitioning into membranes and the resulting solvation forces points to new strategies for studying the structure and chemistry of membrane soluble peptides and selected membrane proteins.

Introduction.

Small molecule accumulation in lipid membranes can have far reaching effects on membrane properties. Solutes such as chloroform, diethyl ether, and others have long been known to have anesthetic effects.[31, 32] Fat soluble vitamins such as vitamins A and E serve as antioxidants, protecting lipid membranes from reactive oxygen species.[33] Small molecule partitioning into lipid membranes can also result in cell death through deactivating transmembrane ion channels and subsequent accumulation of reactive oxide species.[34-36] Historically, a solute's tendency to partition is empirically predicted by the partitioning coefficient (logP) that calculates a solute's solubility preference for an organic (1-octanol) phase in comparison to an aqueous phase.[37] LogP has long historical relevance and is still being used today in agriculture and pharmaceuticals.[12, 38] While logP is a useful, zeroth-order predictor, it is still a solubility argument and therefore does not account for the chemical complexity found within biological membranes. Understanding specific chemical interactions that occur is important as actual partitioning behavior depends on much more than calculated and measured molecular properties used to develop quantitative structural activity relationships (QSARs) and linear solvation free energy relationships (LSERs).[39-42]

To identify and isolate solute-membrane interactions, biological membranes are often simplified and represented by pure lipid bilayer vesicles. Real biological membranes are decidedly complex in nature as they include proteins, carbohydrates, and cholesterol within the bilayer as depicted in the fluid mosaic model.[19, 43] In this context amino acids play an important role as changing individual residues on membrane peptides and proteins can change structure, orientation and stability.[44-46] Amino acids in membrane proteins have also been used as sensors of a membrane's physical state.[47, 48]

Specific to Phenylalanine (Phe or L-Phe), L-Phe aggregate interactions with membranes is responsible for the inherited disease, phenylketonuria (PKU). Model membranes were used to study how phenylalanine interacts with biological membranes.[49, 50] One study analyzed oleic acid vesicles and a fluorescent probe to analyze Phe's effects on vesicle properties and found Phe reduces vesicle rigidity and changes membrane hydration.[51] Another study analyzed L-Phe's effects on lipid monolayers and discovered L-Phe integrates into the film and affects surface tension, phase morphology and ordering of the lipid film.[52] While instructive, neither of these studies were able to quantify the amount of L-Phe that could be accommodated by a lipid membrane, nor *where* within the membrane L-Phe or its aggregates were accumulating.

A recent study by Perkins *et. al.* found that Phenylalanine (L-Phe, Phe) increases membrane permeability.[49] Using cryo-TEM, the authors proposed that Phe aggregated to form fibrils that reduced membrane rigidity making it more permeable. Motivated by this study, recent work in our lab studied the effects that the isomer L-Phe has on coumarin partitioning in lipid bilayer vesicles.[53] Results showed that L-Phe increased *relative* solute partitioning into the lipid bilayer's nonpolar region but blocked a large amount of solute from partitioning while the lipid was in the rigid and structured gel phase.[53]

The calculated logP value for L-Phe is -1.4 in the uncharged, neutral phase indicating a solubility preference for the aqueous environment rather than the organic phase.[37, 53, 54] However, at a biologically relevant pH (~7.4), L-Phe is zwitterionic, and although the net charge is zero, its logP value rises to 0.12 predicting that L-Phe is just as likely to partition into a polar organic phase as remain in an aqueous phase. Initial literature reports by Chakrabarti et al. predicted that only the uncharged neutral – not zwitterionic – form of L-Phe permeates into the membrane and comprises only a small fraction of the total amount of L-Phe in solution.[55, 56] However, more recent studies determined L-Phe in its zwitterionic form permeates deeper into the membrane allowing L-Phe monomers to be more dynamic as they interact with the lipid.[52] The zwitterionic L-Phe intercalates into the polar headgroup of the lipid, primarily through membrane deformities when the membrane is in its frozen gel phase.[52, 54-57] Computational studies show that L-Phe's aromatic ring increases the solute's tendency to enter into the lipid bilayer displacing the water that is in the polar headgroup creating a polar aprotic environment.[54] L-Phe then arranges itself with its aromatic ring aligning normal to the nonpolar acyl chains.[58-61]

L-Phe is one of three aromatic amino acids that are naturally fluorescent and contribute to protein fluorescence. L-Phe is the least fluorescent of the three of aromatic amino acids with a quantum yield of 0.023 in an aqueous solution. For comparison, the quantum yields for Tyrosine (Tyr) and Tryptophan (Trp) are 0.14 and 0.13, respectively.[26, 62-64] Interestingly, L-Phe does not directly contribute to a protein's fluorescence emission as it efficiently transfers its energy to Tyr then to Trp. Because of this lack of direct contribution to protein fluorescence and low quantum yields, the excited state photochemistry of L-Phe has not been studied as thoroughly as for Tyr and Trp.[62, 65-69] The emission behavior of L-Phe has been studied with differing functional groups in effort to understand how each addition affects its photophysical properties.[70, 71]

Phenylalanine's behavior in a short peptide was characterized when phenylalanine and serine were analyzed as monomers in the gas phase and then again in its excited state as the two monomers dimerized and relaxed to form a short chain dipeptide.[67]

In most of the studies described above, L-Phe and other amino acids have been analyzed indirectly either by using a fluorescent probe or through computational studies intended to predict L-Phe partitioning into membranes.[72] These surrogate studies were simpler to carry out relative to direct measurements due to L-Phe's intrinsically low fluorescence yields. Findings reported below measure L-Phe's partitioning behavior *directly* using time-resolved fluorescence spectroscopy in four different lipid bilayer systems. Using time-resolved and steady-state fluorescence spectroscopy, this work examines the chemical interactions that occur when L-Phe is introduced to a model biological membrane. Specifically, these studies identify *where* within the membrane does L-Phe integrate; *how much* L-Phe partitions within the heterogeneous membrane environment; and the effects L-Phe has on the lipid bilayer properties.

Experimental Methods.

Materials

L-Phenylalanine (L-Phe) was purchased from Alfa Aesar and used as received. Organic solvents used were purchased from Sigma-Aldrich and used as received. Millipore water (18.2 MΩ) was used to make the vesicle solutions. The vesicle solutions consisted of an aqueous solution containing 0.84 g of sodium bicarbonate (Sigma Aldrich, 99.99%) with the pH adjusted to 7.0 ± 0.1 at 20˚C using concentrated HCl. Allowing for the Na^+ and HCO_3^- concentrations at pH 7, vesicle solution ionic strength 47.5 mM. 1,2-dilauroyl-*sn*-glycero-3-phosphocholine (12:0 DLPC), 1,2-dimyristoyl-*sn*-glycero-3-phosphocholine (14:0 DMPC), 1,2-Dipalmitoyl-*sn*-glycero-3-phsophocholine (16:0 DPPC), and 1,2-distearoyl-*sn*-glycero-3-phosphocholine (18:0

DSPC) were purchased from Avanti Polar Lipids (Alabaster, AL) and used as received. Vesicle solutions were prepared with 1.5 mM lipid content for fluorescence experiments and 20 mM lipid content for DSC measurements. Structures of all molecules can be found in Appendix A (Figure A-2.1).

Lipid Bilayer Vesicle Preparation

Lipid bilayer vesicles were prepared by dissolving the lipid in chloroform and subsequently drying the solution via rotary evaporation. The resulting thin lipid film was then rehydrated using a 10 mM L-Phe in the pH 7 carbonate solution to form a solution with multilamellae lipid bilayers. While the carbonate concentration of this solution is not sufficiently high to be considered a buffer, we noted that adding the L-Phe to the solution changed the overall solution pH by less than 0.02.

Our choice of 10 mM L-Phe for these experiments was the result of two conflicting considerations. The low quantum yield of L-Phe encouraged experiments to be performed at higher concentrations for better S/N. However, we also wished to work with low L-Phe concentrations to minimize the possibility of aggregation effects. To ensure that the 10 mM results were the result of L-Phe monomers either in bulk aqueous solution or partitioned into the bilayer, we performed a series of fluorescence emission measurements using 2.5 mM L-Phe. These results are shown in Appendix A (Figures A-2.2 and A-2.3 and Table A-2.1). Close agreement in the data from these two systems implies that L-Phe aggregation is not an important consideration at 10 mM.

Solutions were sonicated for 30 minutes at temperatures 10 °C higher than each lipid's respective gel-liquid crystalline transition temperature ($T_{gel\text{-}lc}$). The solution then extruded through a PTFE syringe filter (450 nm) to remove giant unilamellar vesicles. Solutions were

again heated to 10 °C higher than $T_{gel\text{-}lc}$ and extruded through an Avanti Mini Extruder 11 times with a membrane pore size of 200 nm. Vesicles sizes were determined via Dynamic Light Scattering analyses (Figures A-2.4 and A-2.5, and Table A-2.2), showing that the Pure DPPC and DPPC with L-Phe had diameters of 132 and 166 nm respectively.

Differential Scanning Calorimetry (DSC)

Differential scanning calorimetry (DSC) measurements were performed using a TA instruments Discovery DSC 2500. The vesicles for DSC experiments were not filtered to any specific vesicle size. For experiments, Tzero pans and Tzero hermetic lids (TA instruments) were used. To prepare the sample 2 ± 0.1 mg of a vesicle solution was added to the pans and the samples were sealed. Care was taken to ensure that the entire solution was deposited *in* the pan and no stray drops touched the pan. Except for experiments with DLPC, temperature scans began at 15 °C below the $T_{gel\text{-}lc}$ and heated 1°C/min to 15 °C above the $T_{gel\text{-}lc}$ to capture the full gel-liquid crystalline transition temperature ($T_{gel\text{-}lc}$). (DSC experiments with DLPC began at temperatures near -5˚C, only 3˚ below DLPC's $T_{gel\text{-}LC}$ of -2˚C.)

Time-Correlated Single-Photon Counting (TCSPC)

Fluorescence experiments were measured following L-Phenylalanine excitation by a Ti:sapphaire oscillator (Coherent Chameleon, 80 MHz, 85 fs pulse duration, 680-1040 nm wavelength range) coupled with an APE autotracker harmonic generator used to frequency triple the fundamental wavelength. A Conoptics model 350-80 modulator was used to reduce the repetition rate to 4 MHz. Picoquant PicoHarp 300 and FluoTime 200 software were used for data collection. Samples were equilibrated at the reported temperatures for 5 minutes using a Quantum Northwest TC125 control (Seattle, WA). A long pass filter (90% transmission >280 nm) was placed after the sample to reduce scattering from the vesicles. Photon emission was

collected at 290 nm, a wavelength that overlapped all emission spectra in bulk solvents. Excitation wavelength chosen was 260 nm for all solutes, a wavelength that overlapped in each of the bulk solvents.

Time-resolved emission data from vesicle-containing solutions were fit with a linear combination of independent lifetimes and amplitudes using fitting parameters that are adjusted to minimize residuals and optimize χ^2. The resulting fluorescent lifetimes were then compared to the lifetimes of the solute in different solvents chosen to mimic local solvation environments within the lipid bilayer. The fluorescence decay and amplitude expression are shown in Eq. 2.1, where A_i and τ_i are the amplitude and the lifetime of the i^{th} component, respectively.

$$I(t) = \int_0^t IRF\,(t') \sum_{i=1}^{n} A_i e^{-\frac{t-t'}{\tau_i}}\, dt' \qquad (2.1)$$

Each trace was fit independently, without any constraints, for the lifetimes and amplitudes. The typical χ^2 were from 0.9-1.1 when accounting for at most three lifetimes. Typically, uncertainties in lifetimes and amplitudes were 0.2 ns and 0.04, respectively. There is an inherent uncertainty in the lifetimes reported of ± 0.3 ns due to the detection limit of the instrument; however, the data and error bars presented in this work represent results from at least 3 independently prepared, equivalent trials averaged together with a single population standard deviation of those trials. The average lifetime and amplitudes and their respective standard deviations are reported for each specific temperature and only compared to their respective temperature.

Results.

Analyzing L-Phe's effect on DPPC lipid vesicles with DSC

To understand how, or even if, L-Phe interacts with DPPC bilayers, differential scanning calorimetry (DSC) was employed to understand the effect L-Phe has on bilayer properties. Two separate lipid vesicles solutions at a 20 mM concentration were hydrated with a carbonate-containing aqueous solution with and without L-Phe. Previous work has shown that small solutes associating with lipid bilayers can disrupt monomer-monomer interactions leading to a decrease in the bilayer gel to the liquid-crystalline phase transition temperature ($T_{gel\text{-}lc}$). [73, 74] Alternatively, some studies have reported that strong solute-headgroup association can dehydrate the membrane's outer layer, enhancing monomer-monomer interactions and *increasing* $T_{gel\text{-}lc}$.[75, 76]

The DSC traces of DPPC lipid vesicles with and without L-Phe show that the $T_{gel\text{-}lc}$ remained unchanged from the addition of the amino acid to the vesicle system (Figure 2.1). However, the addition of L-Phe to the lipid bilayer vesicle resulted in a decrease in the heat flow required to drive the gel phase into the liquid-crystalline phase transition with a slight, asymmetric widening of the peak base to lower temperatures.

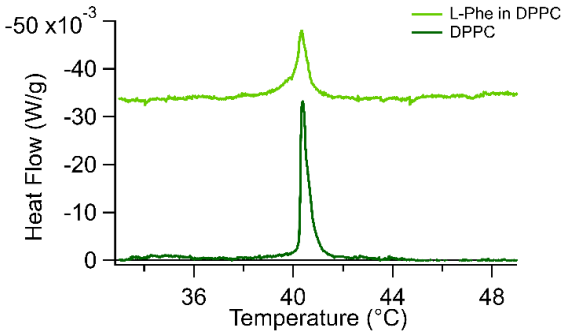

Figure 2.1. DSC spectra of pure DPPC vesicle solutions and DPPC vesicle solutions containing 10 mM L-Phe. The two endotherms are offset for the ease of viewing.

From this result, we infer that any L-Phe that does partition into the bilayer has minimal effect on the cohesive chain-chain interactions, although any impact is assumed to be weakly disruptive given the subtle low-temperature tailing in the DSC trace. Such a result could arise if L-Phe in the bilayer disrupted local acyl chain interactions without disrupting the overall long-range order characteristic of DPPC bilayers in their gel state. This suppression of heat flow is monotonic with L-Phe concentration. We performed equivalent experiments with solutions containing less L-Phe (1, 6, and 8 mM) and noted that while the endotherm grew in magnitude, even at 1 mM, the maximum heat flow was still 25% smaller than the pure DPPC endotherm. These data are shown in Appendix A (Figure A-6.1.)

DLS measurements of DPPC vesicles in aqueous solution both with and without L-Phe support this interpretation. Adding L-Phe to DPPC-containing solutions leads to a ~25% increase in the vesicle diameter and significantly broadens the distribution, again implying some disruption in the lipid bilayer, but not enough to changes the fundamental thermodynamics of the gel-liquid crystalline transition. (DLS results for DPPC vesicles in aqueous solution and solutions containing 5 and 10 mM L-Phe are shown in Appendix A, (Figures A-5.1 and Table A-2.1).

TCSPC of L-Phe in model bulk solvents.

To evaluate the partitioning mechanisms of L-Phe, we first analyzed L-Phe's fluorescence behavior in bulk solvents chosen to model the possible local solvation environments of a lipid bilayer vesicle: acetonitrile for a polar aprotic environment, methanol for a polar, protic environment, and cyclohexane to model the hydrophobic region created by the hydrocarbon tails. This approach has been used previously to identify changes in solvation opportunities within the membrane interior as the membrane melts.[53, 77-79] One important consideration is that the region created by the lipid glycero-backbones is polar and intrinsically aprotic. Only when water begins

hydrating this region is there any opportunity for hydrogen bond formation. Water is expected to percolate into the membrane as the membrane adopts its 'ripple phase' or, equivalently, in the vicinity of its gel-liquid crystalline pre-transition.[80] DPPC's ripple phase occurs at 35 °C.[81, 82] The lipid bilayer vesicles used in this study are prepared in a 10 mM a pH 7 aqueous solution. Consequently, similarities in L-Phe emission lifetimes in the aqueous solution and in solutions containing DPPC vesicles are attributed to L-Phe solutes that do not associate with the bilayer. L-Phe lifetimes in DPPC lipid vesicle solutions are determined independently from the daa without consideration of what was measured in the different bulk solvents (including bulk solution). After L-Phe's lifetimes were determined in DPPC vesicle solutions, results were compared to L-Phe behavior in the bulk solvents to assign L-Phe's local solvation environment within the lipid bilayer vesicle. The fluorescence properties of L-Phe in each of the bulk solvents are reported in Table 2.1.

The first observation from Table 2.1 is the quantum yield of L-Phe is extremely poor in aqueous solvents. The aqueous phase quantum yield of L-Phe is 0.023, much lower than Tyr and Trp where quantum yields are 0.14 and 0.13, respectively.[26, 62-64] The second observation is the quantum yield of L-Phe changes depending on the solvation environment with the largest quantum yield of 0.033 measured in a polar protic solvent, methanol. L-Phe's quantum yield decreases 5-fold to 0.006 in a polar aprotic environment (acetonitrile). A description of how the values reported for each quantum yield in Table 1 were calculated can be found in the Supporting Information. The quantum yield (ϕ_f) and radiative rate (k_f) of L-Phe in aqueous solution and methanol were calculated as a function of temperature with the full list found in the Supporting Information (Table A-2.3) with only those values calculated at 20 °C reported in Table 2.1. The calculated quantum yields of L-Phe in aqueous solution as a function of temperature closely

match those reported in literature.[83] The quantum yield and radiative rate of L-Phe in acetonitrile was only calculated at 20 °C due to poor solubility and low absorbance and emission intensities.

Table 2.1. Fluorescence properties of L-Phe in each of the bulk solvents at 20 °C. The steady-state spectra for L-Phe in each of the bulk solvents can be found in the Appendix (Figure A-2.9).

solvent	λ_{ex} (nm)	λ_{em} (nm)	τ_f (ns)	φ_f	k_f (10^6 s^{-1})
Aqueous	264	287	6.42	0.023[a]	3.52
Methanol	265	290	6.74	0.033	4.89
Acetonitrile	262	299	3.22	0.006	1.72
Cyclohexane	262	301	1.01 (0.85), 4.51 (0.15)		

[a] Quantum yield were calculated in this study but consistent with literature.[83]

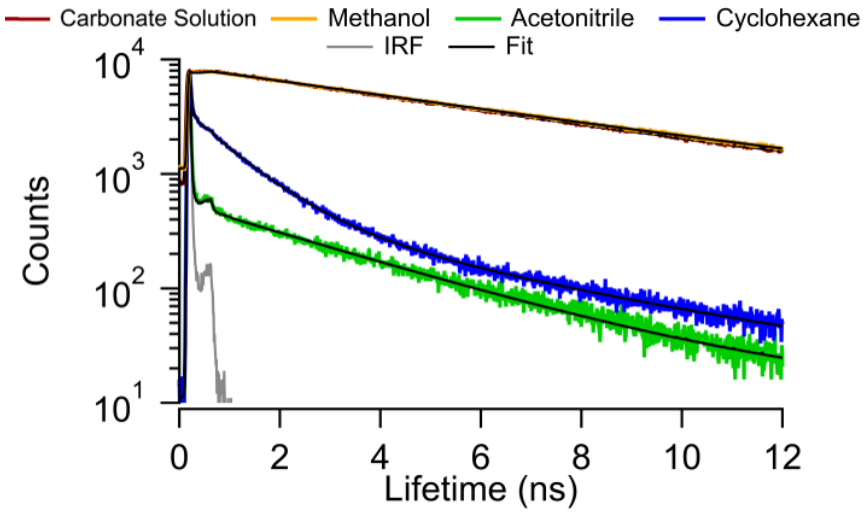

Figure 2.2. TCSPC spectra of L-Phe in each of the bulk solvents taken at 20 °C. Results from fitting these emission traces to Equation 1 are reported in Table 2.1. The gray trace is instrument response function (IRF).

The time-resolved fluorescence behaviors of L-Phe in all bulk solvents are shown in Figure 2.2 with the corresponding fluorescence lifetimes reported in Table 1. L-Phe fluorescence emission in cyclohexane was best fit to two fluorescence decays with the 1.01 ns lifetime as the

marker for a nonpolar environment due to the higher amplitude (0.85). The time-resolved fluorescence behaviors of L-Phe in bulk aqueous solution and bulk methanol were measured, separately, as a function of temperature and results are reported Appendix A (Tables A-2.3 and Figure A-2.8). The resulting L-Phe lifetimes in carbonate buffer matched those found in literature except for the appearance of a second lifetime at 60 and 70 °C not previously reported.[83] The significance of this second lifetime will be discussed below.

TCSPC in DPPC vesicle solutions

The time-resolved fluorescence behavior of L-Phe in aqueous solution containing DPPC lipid vesicles was characterized as a function of temperature through the $T_{gel\text{-}lc}$ of DPPC (41 °C) up to 70 °C. Time-resolved emission spectra were also acquired as the solution cooled to test for reversibility. The fluorescence decay data are shown in Figure 2.3 with the corresponding calculated lifetimes and amplitudes reported in Table 2.2. For each temperature, the lifetimes were calculated with the minimum number of lifetimes required for a χ^2 between 0.9 – 1.1. The resulting lifetimes for each temperature were compared to lifetimes found in bulk solvents to correlate local solvation environments experienced by L-Phe within the DPPC lipid bilayer. Each amplitude was radiative rate corrected using the fluorescence quantum yield of L-Phe in aqueous solution and methanol at each corresponding temperature. The explanation for why methanol was chosen to radiative rate correct the amplitude of the second fluorescence lifetime can be found in the Appendix A.

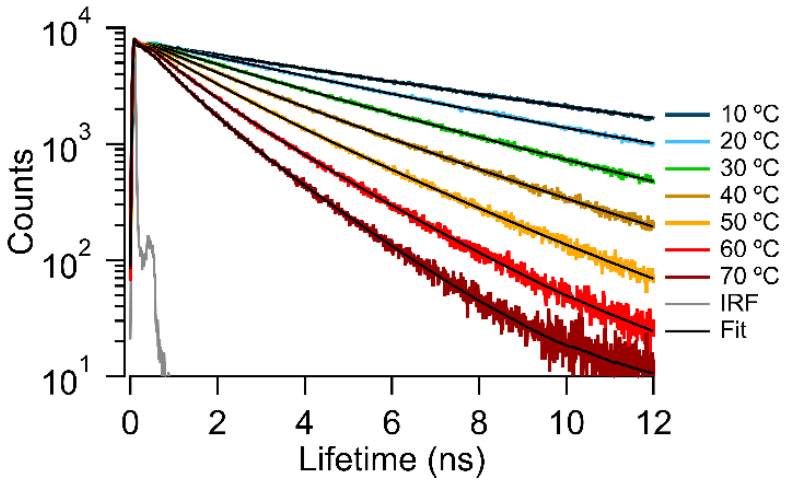

Figure 2.3. TCSPC spectra of L-Phe in DPPC vesicles as a function of temperature. Results from fitting these emission traces to Equation 1 are reported in Table 2.1.

Fitting the fluorescence decay traces in Figure 2.3 at both 10 and 20 °C requires only single lifetime (6.6 ns at 10˚C and 4.9 ns at 20˚C). While slightly lower than L-Phe's emission lifetime in the bulk aqueous solution, we assign this emission to L-Phe that remains in the water and not strongly associated with the DPPC vesicles. Once the temperature was raised to 30 °C, however, the decay trace required two lifetimes with the first lifetime corresponding to L-Phe in bulk solution and accounting for 85% of the overall fluorescence decay, and a second lifetime (1.8 ns, 15%) that does not match any result found in bulk solvents but *does* correspond to L-Phe in a polypeptide that is assigned to a different L-Phe rotamer state.[84] This temperature is approximately where the ripple phase (35 °C) occurs for DPPC lipid bilayers. As temperature increases the 2nd lifetime decreases (to 0.7 ns) and the amplitude increases 30%. These results are quantitatively reversible

Given this lifetime's clear correlation with L-Phe in vesicle containing solutions, we assign this lifetime to a new radiative decay pathway for L-Phe associated with the lipid bilayer. While the origin of this new pathway is not immediately apparent, we propose that it results from

L-Phe in the bilayer where rotational isomerization is restricted resulting in a shorter fluorescence lifetime (K_{rot}) that only becomes optically visible when water begins to penetrate into the lipid bilayer. The basis for this assignment is presented in discussion section below. These data summarized in Figure 2.4 where changes in the lifetimes and amplitudes are shown as a function of temperature. (The fitting parameters used to generate Figure 2.4 are reported in Table A-2.4 in Appendix A.) Also shown in Figure 2.4 is the dashed line corresponding to L-Phe's lifetime in bulk carbonate buffer and two vertical dashed lines that denote DPPC's $T_{gel\text{-}lc}$. Note that the x-axis reporting temperature starts at 10 °C, rises to 70 °C at the axis midpoint and returns to 10 °C. The symmetry shown by all traces about the 70 °C high temperature mark demonstrates reversibility of the observed effects.

Generalizing the effects of L-Phe
on vesicle bilayer properties

Given that the 2nd shorter lifetime was attributed to L-Phe associated with the DPPC bilayer that becomes hydrated as the system approaches $T_{gel\text{-}lc}$, additional experiments were carried out to test whether or not this phenomenon was general. These subsequent studies used three other lipid bilayer systems: DSPC (18:0, $T_{gel\text{-}lc}$ = 53.5 °C), DMPC (14:0, $T_{gel\text{-}lc}$ = 22.5 °C), and DLPC (12:0, $T_{gel\text{-}lc}$ = -1.2 °C). All three lipids are phosphatidylcholine (PC) lipids and contain the same headgroup with the only difference being in the length of the saturated acyl chains and corresponding phase transition temperatures.

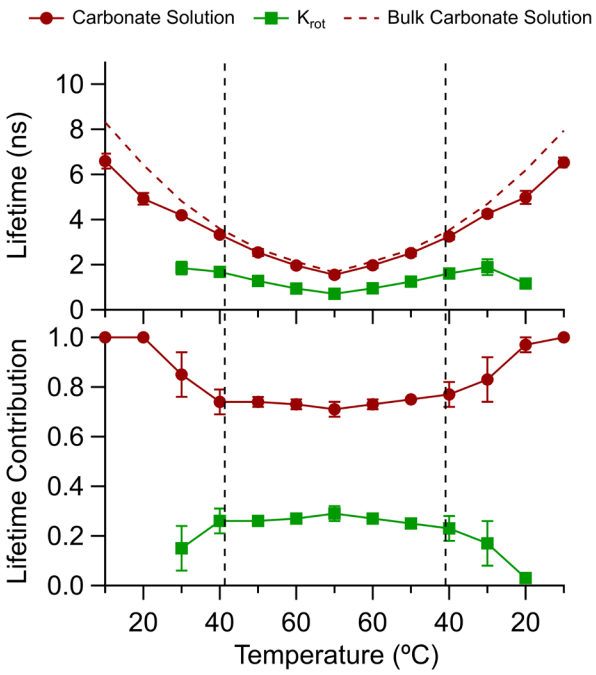

Figure 2.4. Fluorescence lifetimes (top) and respective radiative rate corrected lifetime contribution (bottom) of L-Phe in DPPC lipid vesicles. The major lifetime is assigned to L-Phe in carbonate buffer (τ_1, burgundy circles), and a restriction of L-Phe rotamer in the DPPC polar headgroup region (τ_2, green squares). The dashed lines indicate the $T_{gel\text{-}lc}$ of the DPPC lipid bilayer at ~41.5 °C. Each point is an average of 3 independent trials and the respective error bars are one standard deviation based on the results of those 3 trials. In some instances, the uncertainty is smaller than the marker used to represent that data point.

The effect L-Phe has on the $T_{gel\text{-}lc}$ was analyzed using DSC with lipid vesicles rehydrated in aqueous solutions (20 mM lipid) as well as with 10 mM L-Phe/vesicle aqueous solutions. Figure 2.5 shows the DSC traces of DSPC, DMPC, and DLPC in aqueous solution both with and without L-Phe. The same behavior observed in DPPC lipid vesicles is consistent with DSPC and DMPC. Namely, there was no change in the $T_{gel\text{-}lc}$ but there was a decrease in peak intensity. For DSPC and DMPC vesicles, the same peak broadening as in DPPC vesicles was observed. (L-Phe did not affect DLPC's $T_{gel\text{-}lc}$ (at -2˚C) nor did the amplitude of the endotherm change, in stark

contrast to DMPC, DPPC and DSPC. DSC data for DLPC with and without L-Phe is shown in Appendix A-2.10)

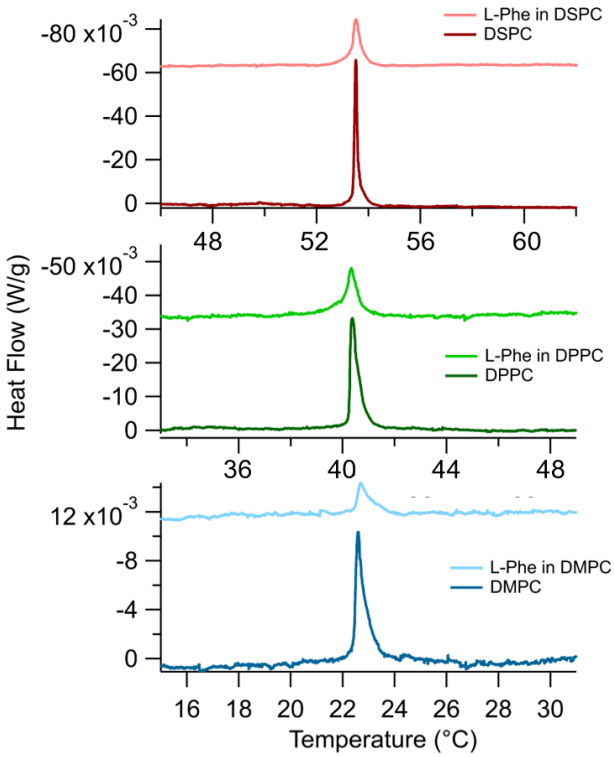

Figure 2.5. DSC spectra of DSPC (top, red), DMPC (middle, blue), and DPPC (previously shown, bottom, green) vesicle containing solutions rehydrated with carbonate solution and 10 mM L-Phe in carbonate solution. All transitions are endothermic and offset for the ease of viewing.

In a manner similar to studies performed with L-Phe in DPPC vesicle solutions, time-resolved fluorescence behaviors of L-Phe in DSPC, DMPC, and DLPC vesicle solutions were measured as a function of temperature (Figure 2.6). The temperature regions sampled were adjusted for each lipid vesicle system to capture any behavioral changes with respect to each bilayer's $T_{gel\text{-}lc}$. The data shown in Figure 6 were analyzed in the same way as the L-Phe/DPPC system. (Quantitative fitting parameters are reported in Appendix A, Table A-2.5.)

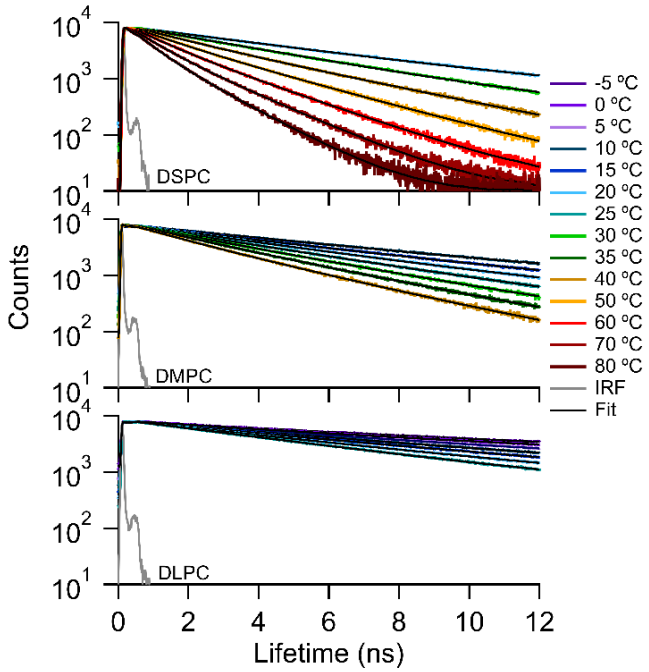

Figure 2.6. TCSPC spectra of L-Phe in DSPC (top), DMPC (middle), and DLPC (bottom) lipid vesicles as a function of temperature. Results from fitting these emission traces to Equation 1 are reported in Table 3.2.

L-Phe fluorescence emission in all lipid vesicle solutions is described by a single lifetime at low temperatures. For L-Phe in DSPC and DMPC, the appearance of a second lifetime occurs in the vicinity of the respective transition temperatures and, like DPPC, the second lifetime does not match behavior observed in bulk solvents. In DLPC, L-Phe fluorescence is characterized by a single lifetime corresponding to L-Phe fluorescence in bulk solution at all temperatures. From these data, we conclude that L-Phe does not partition into DLPC vesicles. The second general observation is that L-Phe in DSPC and DMPC vesicles behaves similarly to L-Phe in DPPC vesicles. A more detailed assessment is provided below. (Fitting parameters that resulted from analyzing these traces are reported in Appendix A, Table A-2.7.)

Starting with DSPC (18:0, $T_{gel\text{-}lc}$ = 53.5 °C), time-resolved emission was measured every 10 °C between 20 °C to 80 °C. Results in Figure 7 show a major lifetime that corresponds to L-Phe in a bulk solution. For the DSPC vesicle system, the appearance of a second lifetime does not appear until 40 °C, slightly below the ripple phase of pure DSPC lipid vesicles (~45 °C).[82] The reversibility of L-Phe in DSPC displays the same behavior as seen in DPPC vesicle solutions.

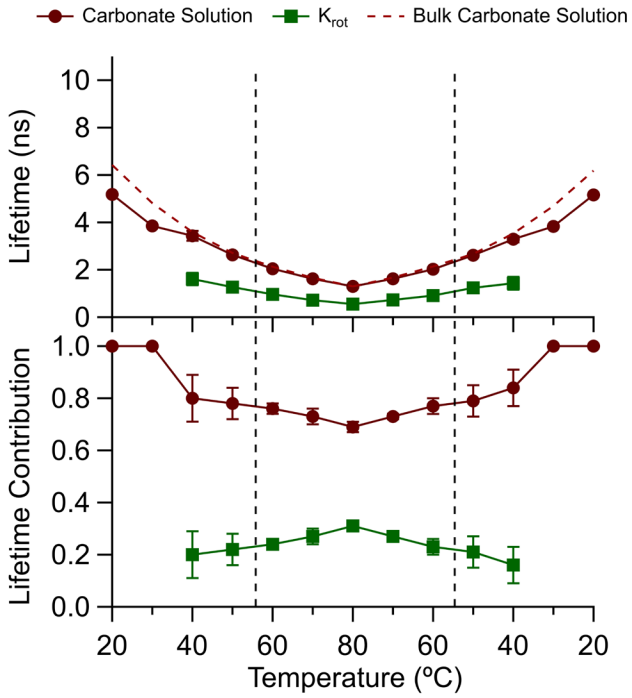

Figure 2.7. Fluorescence lifetimes (top) and respective radiative rate corrected lifetime contribution (bottom) of L-Phe in a DSPC lipid vesicle solution. The major lifetime is assigned to a L-Phe in carbonate buffer (τ_1, maroon circles), and a second lifetime assigned to L-Phe in the membrane appears at 40˚C (τ_2, dark green squares). The dashed lines indicate the $T_{gel\text{-}lc}$ of the DSPC lipid bilayer at ~53.5 °C. Each point is an average of 3 independent trials and the respective error bars are one standard deviation based on the results of those 3 trials. In some instances, the uncertainty is smaller than the marker used to represent that data point.

Results are not quite so definitive for L-Phe in DMPC vesicle containing solutions. Results in Table 2.3 are shown in Figure 2.8 and depict the same long lifetime corresponding to

L-Phe in in bulk solution. However, the appearance of the second lifetime does not occur until 25 °C or at approximately the same temperature as the DMPC $T_{gel\text{-}lc}$ (22.5°C). This is behavior differs from observations made in DPPC and DSPC lipid vesicle solutions where the second lifetime appeared ~10-12 °C before the $T_{gel\text{-}lc}$.

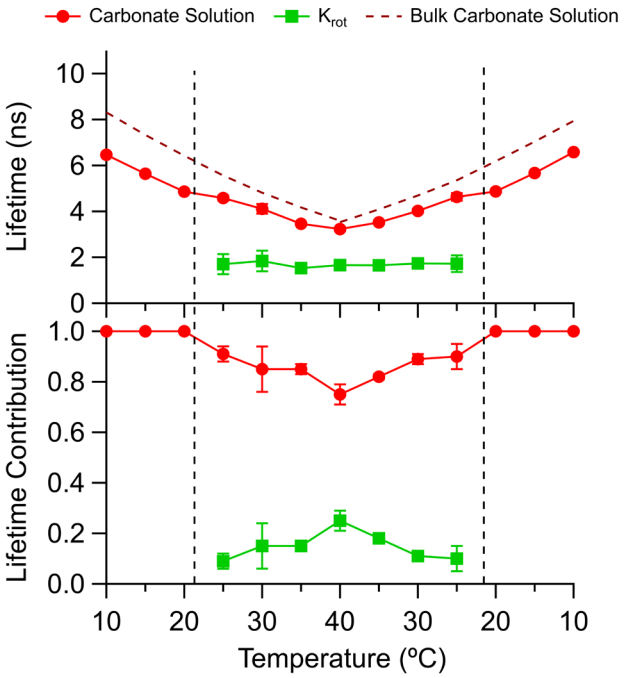

Figure 2.8. Fluorescence lifetimes (top) and respective radiative rate corrected lifetime contribution (bottom) of L-Phe in a DMPC lipid vesicle solution. The major lifetime is assigned to a L-Phe in carbonate solution (τ_1, red circles), and a second lifetime assigned to L-Phe in the membrane appears at 25 °C (τ_2, light green squares). The dashed lines indicate the $T_{gel\text{-}lc}$ of the DMPC lipid bilayer at 22.5 °C. Each point is an average of 3 independent trials and the respective error bars are one standard deviation based on the results of those 3 trials. In some instances, the uncertainty is smaller than the marker used to represent that data point.

Lastly, DLPC with a pair of C_{12} acyl chains and a $T_{gel\text{-}lc}$ = -1.2 °C shows L-Phe emission with only a single lifetime that is assigned to L-Phe in solution. From these findings, we conclude that L-Phe does not associate in any measurable way with DLPC lipid bilayers. The reasons for this pattern of L-Phe association with lipid bilayers – noticeably with DSPC and DPPC, modestly with DMPC, and not at all with DLPC – are discussed below.

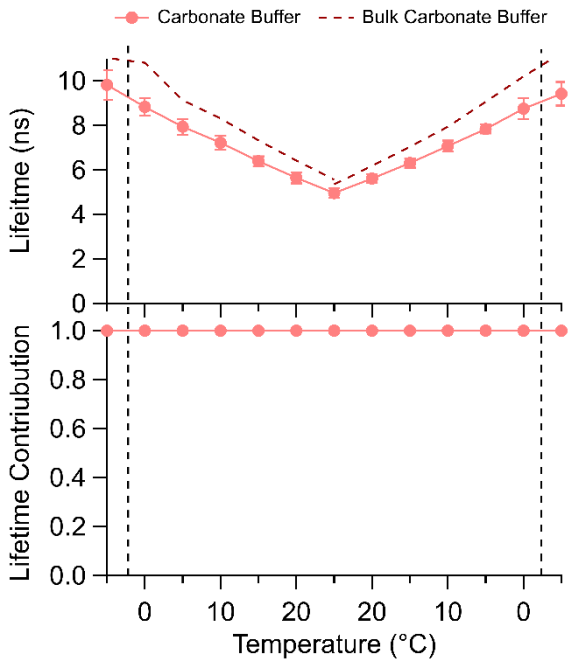

Figure 2.9. Fluorescence lifetimes (top) and respective radiative rate corrected lifetime contribution (bottom) of L-Phe in a DLPC lipid vesicle solution. The single lifetime is assigned to a L-Phe in carbonate buffer (τ_1, pink circles). The dashed lines indicate the $T_{gel\text{-}lc}$ of the DLPC lipid bilayer at -1.2 °C. Each point is an average of 3 independent trials and the respective error bars are one standard deviation based on the results of those 3 trials. In some instances, the uncertainty is smaller than the marker used to represent that data point.

Discussion:

The partitioning behavior of L-Phe in model biological membranes was characterized using time-resolved fluorescence spectroscopy in combination with differential scanning calorimetry. From results reported above, three discoveries stand out and require discussion:

- DSC data show that L-Phe does not alter bilayer $T_{gel\text{-}lc}$ but does decrease the energy required to melt the bilayer from its gel-phase to its liquid-crystalline phase. This finding applies to DSPC, DPPC and DMPC but *not* to DLPC.

- In the vicinity of $T_{gel\text{-}lc}$, L-Phe time-resolved emission in vesicle solutions begins showing a second, faster emission lifetime (< 2 ns) in addition to the persistent longer lifetime assigned

to L-Phe in bulk solution. The shorter L-Phe lifetime is readily apparent in DSPC, DPPC, and DMPC vesicle solutions but *not* in DLPC vesicle solutions. A short lifetime for L-Phe matching those observed in the vesicle solutions *does* appear in bulk solution at temperatures above 60 °C and this correlation forms the basis of our assignment of this lifetime to a rotamer of L-Phe.

- The 2nd, shorter lifetime in vesicle solutions can comprise up to 30% of the amplitude in the emission decay traces. In DSPC and DPPC vesicle solutions, this shorter lifetime decreases from ~1.8 ns at temperatures just below the $T_{gel\text{-}lc}$ to < 1 ns at 70 °C. Whereas in DMPC vesicles, the lifetime stays almost constant at ~1.6 ns. Furthermore, in DSPC, DPPC and DMPC vesicle solutions the amplitude of the short lifetime contribution rises with temperature.

The discussion below considers each issue individually.

<u>The L-Phe that integrates into the bilayer does not change $T_{gel\text{-}LC}$</u>

The DSC traces in Figures 2.1 and 2.5 display the $T_{gel\text{-}lc}$ phase transition behavior for each lipid system studied with and without L-Phe in solution. Two observations stand out. First, L-Phe does not affect the transition temperature for any of the lipid bilayers. The peak in the different endotherms remain at 53.5 °C, 40.4 °C, and 22.5 °C for DSPC, DPPC, and DMPC, respectively, regardless of whether or not L-Phe is present. (The transition temperature for DLPC (-1.2˚C) also remains unchanged as shown in Figure A-2.10.) Given that bilayer melting is controlled by van der Waals forces between acyl chains and Coulomb forces between the charged choline headgroups,[73,85] the DSC findings imply that some amount of L-Phe partitions into the gel state bilayer. MacCallum, *et al.* calculated that Phe in the carbonyl and acyl chain

region of the bilayer was ~10-12 kJ/mole more stable than in bulk aqueous solution, although these simulations were carried out using a model DOPC bilayer in its fluid, liquid crystalline state.[72] What is clear is that L-Phe accumulation into the bilayer does not disrupt the fundamental interactions responsible for the transition.

The second observation is that L-Phe *does* change quantitative details related to $T_{gel\text{-}lc}$. For DSPC, DPPC and DMPC, the presence of L-Phe significantly reduces the amount of heat needed to drive the gel-liquid crystalline transition to completion. For vesicle solutions in the absence of L-Phe, the heat required to drive the gel-liquid crystalline transition diminishes with shorter chain length: +60 mW/g for DSPC, +30 mW/g for DPPC and +10 mW/g for DMPC. When L-Phe is added to the solutions, these values drop to 20 mW/g, 14 mW/g, and 3 mW/g for DSPC, DMPC and DLPC respectively. (DLPC shows no change in its $T_{gel\text{-}LC}$ nor in the magnitude of the endotherm and is not considered in this discussion.). This 2-3-fold reduction in the heat required to melt the bilayer in the presence of L-Phe supports the hypothesis that L-Phe partitions into the gel-phase bilayers and disrupts *some* of the chain-chain interactions but this disruption is not extensive enough to completely fluidize the bilayer. In effect, we believe that incorporating L-Phe into the bilayer introduces defects into the long-range order within the frozen chains reducing cooperativity within the bilayer.[86] We note also that the L-Phe's effect on the DSC data scales with L-Phe concentration. As noted at the start of the Results section, we did perform equivalent experiments using solutions of DPPC containing 1, 6, and 8 mM L-Phe, and as L-Phe concentration diminished, the endotherm approached (but never converged) to the endotherm for DPPC vesicles in the absences of L-Phe. These data are shown in Appendix A, Figure A-2.6.

Assigning the 2nd lifetime

To demonstrate the universal behavior of L-Phe in the lipid bilayer vesicle systems, Figure 2.10 shows all fluorescence lifetimes of L-Phe in DSPC, DPPC, DMPC, DLPC, and bulk carbonate solution across the entire temperature range sampled. Also included on Figure 2.10 are L-Phe lifetimes in bulk carbonate solution including the second, shorter lifetime that appears only at elevated temperatures (labeled as CS τ_2).

In each vesicle-containing solution, the dominant contribution to the emission decay trace matches L-Phe emission in bulk carbonate solution. This agreement enables us to assign the major lifetime of L-Phe in vesicle-containing solutions to solutes that do not associate with lipid vesicles. In the DSPC, DPPC and DMPC vesicle solutions, the second, shorter lifetime appears at temperatures close to each lipid's respective $T_{gel\text{-}lc}$. As noted in the Results section, the time resolved emission of L-Phe in bulk carbonate solution also has a short lifetime that appears at temperatures ≥ 60 °C. This shorter lifetime does not coincide with emission behavior in any bulk organic solvent, although it does match closely the 1.7 ns lifetime assigned to L-Phe in the EGFRtm peptide as reported by Duneau, *et al.*[84]

Multiple studies have either inferred or predicted that the hydrophobic part of L-Phe should insert into the lipid bilayer membrane through membrane surface defects.[54-57, 59, 60] In its gel phase, the lipid bilayer is rigid and will limit the intramolecular conformational freedom of embedded L-Phe. The benzyl-group of L-Phe is believed to extend into the nonpolar tails and L-Phe's zwitterionic carboxylic acid and amino groups are directed towards the lipid's glycero-backbone and headgroup.[54, 60] Olsztynska *et. al.* reported the appearance of a second, shorter L-Phe emission lifetime (2.6 ns) and proposed that this behavior resulted either from protonation of the carboxylic acid or the formation of aggregates that enabled a faster radiative decay pathway.[87] Supporting this finding are reports of excimer excitation of 100 mM L-Phe in

aqueous solution, as evidenced by an emission peak at 320 nm that disappears with decreasing concentration.[83]

Findings presented in this work do not support the proposal that the short lifetime reflects L-Phe aggregation. First, in all three lipid systems where L-Phe shows membrane affinity, the short lifetime amplitude *increases* with increasing temperature. If the short emission lifetime observed in these systems were due to noncovalently bound aggregates, we would expect aggregation to play *less* of a role at higher temperatures, not more. Second, emission spectra of L-Phe in carbonate solution (Appendix A Figure A-2.9) show no evidence of excimer formation at the concentrations used in these experiments. Third, a 4-fold concentration decrease of L-Phe (2.5 mM) in DPPC vesicles showed no change in partitioning behavior from that of 10 mM L-Phe in DPPC lipid vesicles (Appendix A Figures A-2.2 and A-2.3 and Table A-2.1). The possibility that aggregation and excimer formation controls L-Phe photophysical behavior at high concentrations as reported by Leroy and Laustrait cannot be discounted,[25] but these effects are unlikely to be present at the 10 mM L-Phe concentrations employed in this work.

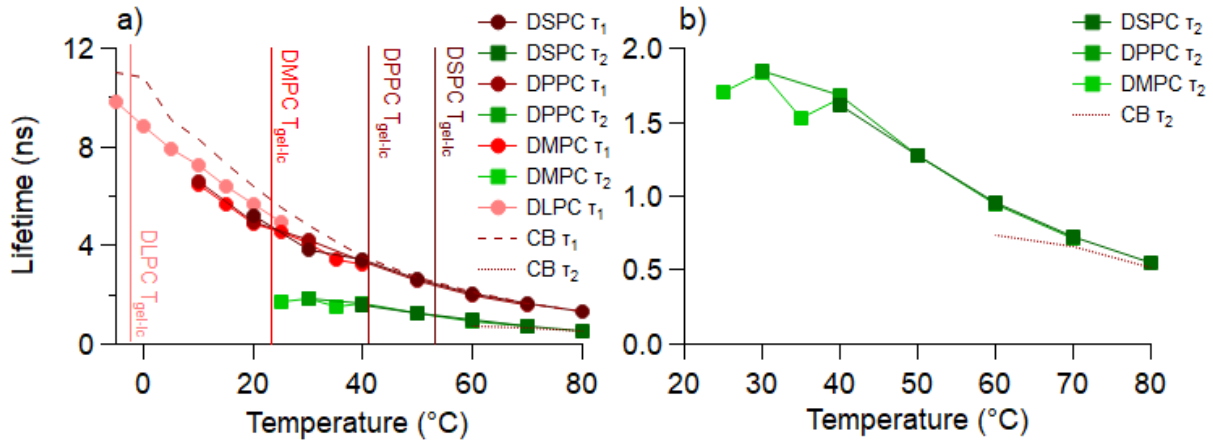

Figure 2.10. Fluorescence lifetimes of L-Phe in bulk carbonate solution, DSPC, DPPC, DMPC, and DLPC lipid vesicles. Left panel (a) overlays all major lifetimes assigned to a L-Phe in carbonate solution (τ_1: DSPC, maroon circles; DPPC, burgundy circles; DMPC, red circles, and

DLPC, pink circles), and a second lifetime assigned to L-Phe in the membrane appears (τ_2: DSPC, dark green squares; DPPC, green squares; and DMPC, light green squares). Dashed traces indicate L-Phe in bulk carbonate solution (CS) with long dashes indicating first fluorescent lifetime and short dashes indicating second fluorescence lifetime. Solid vertical lines indicate each lipid's $T_{gel\text{-}lc}$ and which are color coded using same scheme as color assignments for lifetime attributed to carbonate solution and labeled as such within figure. Right panel (b) is expanded view of 2nd lifetime alone attributed to restriction of L-Phe rotamer (K_{rot}) in the polar headgroup region of L-Phe in DMPC, DPPC, and DSPC, and bulk carbonate solution (CS). Each point is an average of 3 independent trials of each respective system.

An alternative hypothesis explaining the short L-Phe lifetime was proposed by Duneau, *et al.*, and attributed emission from L-Phe in two different peptides to L-Phe rotamer states at room temperature.[84] In the 29-mer peptide ErbB-2*tm, the single L-Phe residue shows three different emission lifetimes, two of which are sub-ns and a longer, 2.2 ns lifetime. The longer lifetime was assigned to different rotamer states that interconvert on timescales slower than the measured emission lifetimes. L-Phe emission from a second peptide, EGFRtm, is characterized by a single, 1.70 ns lifetime that matches the lifetime observed for L-Phe in the lipid vesicle solutions. The authors proposed that the single lifetime either reflects different rotamers that interconvert rapidly on the timescale of the experiment or L-Phe in a single rotamer state, before concluding that the first explanation, that of rapidly interconverting rotamers, is more consistent with their findings. Similarly, Rzeska *et. al.* analyzed analogues of L-Phe and determined that all possible rotamer conformations result in a similar fluorescence lifetime and are indistinguishable from one another.[70, 71]

In contrast to Duneau, *et. al*, we believe that the short lifetime emission we observe at higher temperatures is due to a single rotamer state. Cavanaugh *et. al.* studied the temperature variations of NMR chemical shifts and coupling of L-Phe rotational isomerization.[88] The authors reported that temperature played a large role in intramolecular and intermolecular parameters of

L-Phe, and the importance of these parameters changed depending on the local environment. This NMR study had two conclusions: either the rotamer energies are temperature dependent and gain stability as temperature increases, or the results require a deviation from the original proposed rotamer structures to understand experimental data.[88] Our findings support the conclusion that a distinctive rotamer structure is stabilized at higher temperatures long enough for a radiative decay pathway to contribute to the overall fluorescence behavior. This stabilization effect of high temperatures is evident in the appearance of a second fluorescence lifetime in bulk carbonate solution starting at 60 °C.

We propose that L-Phe in the bilayer experiences a conformationally restricted environment that forces L-Phe to adopt conformations that decay nonradiatively (as is the case in polar, aprotic environments). As the membrane begins to become more fluid, L-Phe can adopt a rotamer state that *does* decay radiatively. We expect that this emissive state is stabilized by water as water will begin to percolate into the lipid bilayer's polar glycero-backbone region as the system temperature approaches $T_{gel\text{-}lc}$.[89, 90] We believe the second lifetime found in bulk carbonate buffer at 60 °C arises from this same rotamer conformation that is only accessible in bulk solution at higher temperatures, consistent with the first hypothesis proposed by Cavanaugh.[88]

To assess what role the water plays in assisting rotamer formation, the fluorescence lifetimes of L-Phe in a deuterated water (D_2O) carbonate solution were measured as a function of temperature (Appendix A Table A-2.6.) L-Phe in D_2O carbonate solution displays an increase in fluorescence lifetimes (τ_f at 10 °C = 10.81 ns) at low temperatures in comparison to H_2O carbonate solution (τ_f at 10 °C = 8.00 ns). Similarly, the appearance of a second lifetime (0.88 ns, 11%) at 60 °C also occurs in D_2O carbonate solution. However, the amplitude of the second,

short lifetime is significantly different as temperature increases from 60 – 80 °C. Namely, the second lifetime displays a sharp increase in amplitude of up to 57% (80 °C) in D_2O carbonate solution in comparison to 20% (80 °C) in H_2O carbonate solution. In D_2O, the hydrogen-bonding capabilities are stronger than in H_2O. This finding supports our premise that the new emissive rotamer state observed in bilayers close to $T_{gel\text{-}LC}$ and in carbonate solution at elevated temperatures is stabilized by hydrogen bonding and stronger hydrogen bonding (by D_2O) stabilizes this new rotamer even further.

Local solvation environment dependence of
the 2nd lifetime of L-Phe in lipid vesicles

The results described above show a strong dependence of L-Phe behavior on bilayer phase with the appearance of the second lifetime. For the DSPC and DPPC lipid vesicles, the appearance of the second lifetime occurs ~10°C before the transition temperature of the lipid bilayer. Uniquely, the second lifetime of L-Phe in DMPC lipid vesicles does not appear until $T > T_{gel\text{-}lc}$. No second lifetime is apparent In DLPC vesicles solutions across the entire temperature range. We propose this second lifetime, assigned to a confined L-Phe rotamer, becomes 'optically visible' only when water is present.

L-Phe in the polar headgroup of the lipid bilayer in its gel phase is subject to a polar, aprotic solvation environment. Our studies of L-Phe in bulk acetonitrile show that in such an environment, fluorescence is weak with the quantum yield of less than 0.01. (In acetonitrile, L-Phe's quantum yield is 0.006 (Table 2.1.).) However, as temperature increases and water percolates into the polar headgroup, hydrogen bonding opportunities become available, and

L-Phe can sample a polar, protic solvation environment where its quantum yield is > 5-fold larger (0.033 in methanol) than in polar aprotic environments.

Consequently, we believe that L-Phe in the tightly packed, anhydrous, gel-phase bilayer interior is optically invisible. Bilayer hydration near the gel-liquid crystalline transition temperature allows L-Phe to become optically active and contribute to the overall fluorescence decay. This result explains why the second lifetime appears at different temperatures for each of the different lipid vesicle systems and in the vicinity of the $T_{gel\text{-}lc}$. For DSPC and DPPC, the second lifetime appears ~10°C before the $T_{gel\text{-}lc}$ and for DMPC, the lifetime appears shortly after the $T_{gel\text{-}lc}$.

Before the lipids fully transition from the gel-phase into the liquid-crystalline phase, they pass through a pre-transition (also known as the ripple phase) where water begins to percolate into the lipid bilayer vesicle.[80, 82] The ripple phase occurs at 16.5 °C, 35 °C, and 46.7 °C for DMPC, DPPC, and DSPC, respectively.[81, 82] Shinoda *et. al.* studied transition temperatures with MD simulations and found the insertion of ethanol into the bilayer creates defects where water can hydrate into the bilayer before the ripple phase and this effect is more pronounced for larger lipids.[91] Therefore, we propose that the L-Phe in the membrane creates a pathway for water to enter the bilayer at or near the ripple phase transition. The onset of the ripple phase and additional membrane hydration is then responsible for the appearance of the second lifetime of L-Phe in DSPC and DPPC vesicles.

As water begins to percolate into the membrane, the bilayer expands by ~25% for DPPC vesicles[92] and transitions into the liquid-crystalline phase of the bilayer where the local solvation environment is polar protic, and solutes have the conformational freedom, the hydrogen bonding and sufficient thermal energy to adopt the new rotamer conformation having the shorter emission

lifetime. As seen in Figures 2.4, 2.7, and 2.8, the concentration of L-Phe in the bilayer increases in concentrations up to 30% at high temperatures.

The increase in concentration of the rotamer state implies one of two things: (1) more L-Phe is entering the bilayer as the bilayer expands and experiences this rotamer state. Or (2), as the bilayer expands and water increases concentration within the bilayer, more of the L-Phe that is already in the bilayer becomes optically visible. Scenario (2) seems more likely as the free L-Phe in bulk solvent would not experience a conformational restriction as the vesicles increase and should be free to adopt a new, thermally accessible rotamer conformation. Instead, the more likely explanation is that L-Phe already in the bilayer becomes optically active (or visible) as the lipid bilayer becomes hydrated.

There is still a remaining question of the second lifetime *after* the $T_{gel\text{-}lc}$ of DMPC lipid vesicles and the absence of a second lifetime in DLPC lipid vesicles. Literature has reported a large temperature dependence of the fluorescence lifetimes of L-Phe in an aqueous solvent.[83] The large temperature dependence is attributed to a switch in the non-radiative decay pathways as a function of temperature. Leroy *et. al.* noted that at temperatures above 0˚C, the main non-radiative decay pathway of L-Phe in aqueous solvents is internal conversion.[83] However, at low temperatures (< 0 °C), the main non-radiative decay pathway begins changing from internal conversion to intersystem crossing.[83] If this switch from internal conversion to intersystem crossing begins to happen at higher temperatures (0-20 °C), then we would not expect to observe a second lifetime in DLPC vesicles and, perhaps, observe a second lifetime in DMPC vesicle solutions above $T_{gel\text{-}lc}$.

Conclusion:

Studies reported in this work used time-resolved fluorescence spectroscopy in combination with differential scanning calorimetry to understand the partitioning behavior of L-Phe into model biological membranes. Results show that most L-Phe remains in the carbonate solution, but the L-Phe that *does* partition into the bilayer does not significantly impact the $T_{gel\text{-}lc}$. Evidence of a conformational rotamer fluorescence lifetime of 1.8 ns is seen in DSPC, DPPC, and DMPC lipid vesicles close to their $T_{gel\text{-}LC}$ phase transition temperature. We propose that this rotamer lifetime only becomes optically visible when water penetrates into the bilayer and the local solvation environment switches from a polar aprotic to a polar protic environment, increasing the quantum yield by an estimated factor of ~5 based on data from L-Phe in methanol and acetonitrile. The L-Phe rotamer lifetime increases slightly in amplitude, eventually comprising up to 30% of the time resolved emission at elevated temperatures. This behavior is predicted to come from L-Phe already in the bilayer that becomes more optically visible as the bilayer expands and increasing amounts of water make the bilayer headgroup region more protic. We hope work reported here sparks further studies into the specifics of the rotamer conformation and related photophysical behaviors of L-Phe, a naturally fluorescent amino acid whose optical properties have been largely overlooked compared to the attention received by other fluorescent amino acids, tyrosine and tryptophan. We also expect that findings reported here will aid in quantifying the behavior of other aromatic amino acids and small peptide chains in lipid vesicle bilayers.

CHAPTER THREE

NANOMOLAR PFOA CONCENTRATIONS AFFECT LIPID MEMBRANE STRUCTURE: CONSEQUENCES FOR BIOCONCENTRATION MECHANISMS

Contributions of Authors and Co-Authors

Manuscript in Chapter 3

Author: Rhys C. Trousdale

Contributions: Co-author with equal contribution to Tess Sobolewski. Collected and analyzed experimental TCSPC data, analyzed Cryo-EM data, and assisted in writing and editing manuscript

Author: Tess N. Sobolewski

Contributions: Co-author with equal contribution. Collected and analyzed experimental DSC and DLS data, assisted in writing and editing manuscript

Author: Colin L. Gauvin

Contributions: Collected experimental Cryo-EM data and data analysis

Author: C. Martin Lawrence

Contributions: Assisted in Cryo-EM data analysis

Author: Robert A. Walker

Contributions: Assisted with data analysis, writing, and editing of manuscript

Manuscript Information

Rhys C. Trousdale, Tess N. Sobolewski, Colin L. Gauvin, C. Martin Lawrence, and Robert A. Walker
Environmental Science & Technology
State of Manuscript
_____ Prepared for submission to a peer-reviewed journal
_____ Officially submitted to a peer-reviewed journal
_____ Accepted by a peer-reviewed journal
__x__ Published in a peer-reviewed journal
Published by Environmental Science & Technology
In Volume 59, Issue 1, 709-718, 2024
https://doi.org/10.1021/acs.est.4c03652

NANOMOLAR PFOA CONCENTRATIONS AFFECT LIPID MEMBRANE STRUCTURE: CONSEQUENCES FOR BIOCONCENTRATION MECHANISMS

Tess N. Sobolewski[a,‡], *Rhys C. Trousdale*[a, ‡], *Colin L. Gauvin*[a], *C. Martin Lawrence*[a], *and Robert A. Walker*[a,b,*]

[a]Department of Chemistry and Biochemistry
Montana State University
Bozeman, MT 59717

[b]Montana Materials Science Program
[‡]Both students contributed equally to this work
[*]corresponding author

Abstract

Independent methods show that sub-microMolar concentrations of perfluorooctanoic acid (PFOA), a member of the PFAS family of 'forever chemicals', change the properties of DPPC vesicle bilayers. Specifically, calorimetry measurements show that PFOA at concentrations as low as 0.1 nM lowers DPPC's gel-liquid crystalline transition enthalpy by several J/g without changing the transition temperature ($T_{gel\text{-}LC}$), and dynamic light scattering (DLS) data illustrate that PFOA markedly broadens the size distribution of DPPC vesicles. Furthermore, DLS results from PFOA-containing, DPPC vesicle solutions also contain smaller objects having diameters of 30-50 nm. Close inspection of cryo-EM images reveals that DPPC vesicles formed in the presence of PFOA are multi-lamellar and the smaller objects have a clear bilayer structure making them resemble niosomes. A consequence of these PFOA-induced changes to DPPC bilayer structure is that the bilayers themselves are more susceptible to

secondary solute accumulation. Time resolved emission measurements of Coumarin 152 (C152) report that C152 is 3-fold more likely to partition into the bilayer's acyl chain, hydrophobic interior when PFOA is present, and fluorescence lifetimes from C152 partitioned into the polar region of the lipid bilayer show evidence of PFOA-induced membrane hydration below $T_{gel\text{-}LC}$.

Introduction

Per- and polyfluorinated alkyl substances, or PFAS, are a class of molecules that threatens community and ecosystem health. PFAS are often called 'forever chemicals' because of their environmental persistence, and PFAS have been linked to reduced vaccine response, high cholesterol, compromised immune system function, and certain types of cancer.[93-97] Despite the hazards they pose, PFAS have only recently been federally regulated as environmental contaminants under the U. S. Clean Water Act, although previously at the state level, more than 20 jurisdictions had imposed maximum allowable PFAS limits in drinking water. These local regulatory limits ranged from 5 ppt (CA) to over 650 ppt (NV).[94, 98] New federal limits released in 2024 by the U. S. Environmental Protection Agency (EPA) mandate a maximum allowable drinking water concentration of 4 ppt for several PFAS species.[94, 98-100] Such low concentrations can be challenging to quantify reliably, and the effects of these low concentrations on biological materials are not well characterized. Findings presented below show how one of the most common PFAS species – perfluorooctanoic acid (PFOA) – affects model lipid membrane properties at concentrations approaching regulatory limits. Additional experiments illustrate how sub-micromolar PFOA concentrations render model membranes more susceptible to bioconcentration of secondary solutes, with implications for how pollutant bioconcentration factors change in the presence of PFAS contaminants.

PFOA is a legacy member of the PFAS family, having long been used as an aqueous film foaming fire (AFFF) suppression agent as well a means of waterproofing products including cookware, textiles, and food packaging material.[94] While no longer produced for commercial use, PFOA is expected to remain an environmental and human health hazard for decades.[101, 102] PFOA is a per-fluorinated, linear, eight carbon carboxylic acid. Considerable uncertainty surrounds PFOA's membrane affinity. Publicly available data compiled by ADC/Labs and made available from the Royal Society of Chemistry ChemSpider site[103] report that PFOA in its protonated form has a predicted logP value on the order of 7.7, and a predicted logD value of 1.8 at a biologically relevant pH (7.4), when it is deprotonated.[104] (The logD scale considers solution phase pH as a part of the partitioning scale.) We note that reports predicting octanol partitioning behavior (log P) should be viewed with caution. Many algorithms do not differentiate behavior between PFOA's neutral and deprotonated forms. Nevertheless, both the logP and logD scales predict that PFOA should be lipophilic regardless of charged state, although one expects PFOA's neutral protonated form should show much stronger affinity than the deprotonated PFOA anion.[105] Despite early controversy concerning an anomalously large apparent pK_a (of 3.8),[106-108] calculations and experiments now agree that PFOA's pK_a is in the vicinity of -0.1 - +0.7[109-113] although this value is expected to rise if monomers aggregate.[114-116] A consequence of this behavior is that PFOA should be exclusively in its anionic form under physiological conditions.

To our knowledge, PFOA's membrane partitioning coefficient, K_{mem-w} has not yet been directly measured, although the logP scale has been reported as an adequate surrogate for K_{mem} for solutes having log P values ≤ 5.[7] Several studies using independent methods have examined deprotonated PFOA's membrane affinity for synthetic lipid bilayers, and results all show deprotonated PFOA to be lipophilic. Ebert, *et al.* used dialysis measurements to quantify PFAS

partitioning behavior into POPC liposomes and noted that experimental results generally agreed well with predicted log $K_{mem/w}$. Specific to PFOA, the authors reported experimental and predicted partition values of 3.52 ± 0.08 and 3.93, respectively.[117] PFOA affinity for lipid bilayers has also been noted by Droge who measured PFOA sorption to supported lipid bilayers using liquid chromatography.[118] Fluorescence anisotropy and calorimetry measurements have noted that deprotonated PFOA partitioning into phosphatidylcholine bilayers is independent of lipid chain length.[119, 120]

With its elevated partitioning tendencies, even at a biological pH, PFOA is a strong candidate to bioconcentrate in lipid membranes, although PFOA's effects on membrane properties remain largely uncharacterized. By analogy, alkyl surfactants have long been used to solubilize lipid membranes, and surfactants have also been shown to induce structural transitions in membranes and micelles.[121] Mechanisms describing surfactant-lipid bilayer interactions begin by assuming that the surfactant partitions into the bilayer up to a membrane solubility limit. Surfactant accumulation leads to bilayer expansion, shape changes, and an increase in membrane permeability.[121-123] Typically, these effects become pronounced for surfactant concentrations ≥ 0.5 mM.[122, 124] Even in studies focused on low surfactant:lipid ratios, surfactant concentrations are rarely less than 100 μM. For PFOA and other PFAS species, these concentrations are close to five orders of magnitude higher than the sub-nM PFOA regulatory limits. (For reference, a the 4 ppt regulatory limit for PFOA corresponds to an aqueous concentration of ~10 pM.)

PFAS are distributed widely throughout the environment given their high solubility in ground and surface water[125,126,127] as well as their ability to be transported through air.[128, 129 130] This pervasive presence, coupled with PFAS tendency to bioconcentrate in wildlife has been well documented.[131] Long chain PFAS (C ≥ 6) accumulation has been measured in species including

striped dolphins,[132] carp,[133, 134] and other members in aquatic food webs.[107, 135-139] Individual PFAS concentrations (including PFOA) vary widely ranging from ≤10 ppt (by mass) to ≥ 7 ppm, with higher concentrations found in organs known to be susceptible to bioaccumulation.[140] While numbers vary from study to study, a growing body of literature cites PFAS bioconcentration factors in excess of 100 and as high as 23,000.[101, 141-144]

From a human health perspective, PFAS exposure has been correlated with liver disease,[145] reduced birth weights,[146] compromised immune response,[147] impaired platelet aggregation,[148] and a host of other conditions. Given PFOA's ability to bioconcentrate, lipid membranes become effective storage media, even when ambient environmental PFOA concentrations are low. [149] The effects of PFOA on membrane properties, however, remain largely unexplored especially at low PFOA concentrations. Recently reported surface pressure measurements and Brewster Angle Microscopy experiments demonstrated that PFOA and related PFAS fluidize lipid monolayers formed from both synthetic and bacterial lipid mixtures.[150] These studies, however, considered PFAS concentrations on the order of 10-100 μM, considerably higher than concentrations relevant to current regulatory limits.

Studies described in this work are motivated by the hypothesis that PFOA concentrations approaching regulatory limits will affect lipid membrane structure and function. While such an assumption is implicit in many of the reports cited above, never before have the effects of such low PFAS concentrations on biological macrostructures been evaluated quantitatively. Data presented below show that sub-μM PFOA concentrations lower DPPC bilayer transition enthalpies and preferentially promote secondary solute accumulation in the bilayer's hydrophobic interior. Furthermore, these low PFOA concentrations interfere with lipid vesicle formation and promote

niosome creation at surfactant:lipid ratios that are orders of magnitude smaller than previously reported. This concerted investigation into PFOA affinity for lipid membranes and the resulting consequences demonstrate sub-μM PFOA concentrations change lipid bilayer properties, and these changes disrupt chain-chain interactions within the membrane making the lipid bilayer intrinsically less cohesive. As scientists and public health officials continue to focus on the physiological effects of PFOA and other PFAS on human and ecosystem health, findings reported in this work will provide the insight necessary to anticipate how PFOA and other members of the PFAS family affect membrane stability and bioconcentration in the low PFAS concentration limit.

Experimental materials and methods

Materials.

Perfluorooctanoic acid (95% purity) was purchased from Sigma Aldrich (St. Louis, MO) and used as received. For carbonate buffer solutions, sodium bicarbonate was purchased from Sigma-Aldrich (St. Louis, MO), dissolved in Millipore water, and set to a pH of 7.2 using 1 M NaOH. PFOA was dissolved in either 10- or 50-mM carbonate buffer (pH 8) to make PFOA solutions. Solutions having low PFOA concentrations were prepared by serial dilutions from 0.1 mM stock solutions. To aid in converting between concentrations expressed in Molar units and in parts per billion and parts per trillion (ppb and ppt, by mass), Table 3.1 presents conversions relevant for the concentrations used in these studies.

Table 3.1. PFOA concentrations in units of molarity and ppb/ppt (by mass)

PFOA Concentration	
nM	ppb/ppt
1000	400 ppb
100	40 ppb
10	4 ppb
1	400 ppt
0.1	40 ppt[a]
0.01	4 ppt[b]

[a]The following states had previously set jurisdictional regulatory limits ≤40 ppt PFOA in drinking water: California, Michigan, New York, New Hampshire, New Jersey, Massachusetts, Vermont, Minnesota

[b]EPA PFOA regulatory limit for drinking water.

1,2-Dipalmitoyl-*sn*-glycero-3-phosphocholine (DPPC, powder, >99%) was purchased from Avanti Polar Lipids (Birmingham, Alabama). All chemicals were used without further purification. Millipore water (resistivity of 18.2 MΩ·cm) was used for all aqueous sample preparations. Coumarin 152 (C152) was purchased from Exciton (Edmonton, Canada) and used as received. The bulk buffered C152 solution had a concentration of 6 μM.

Processing

Vesicle Preparation: Lipid vesicles were prepared by dissolving 16:0 PC (DPPC) 1,2-dipalmitoyl-sn-glycero-3-phosphocholine in chloroform. Chloroform was then evaporated off using a rotary evaporator at 45°C. A thin film results and was then rehydrated using 10mM carbonate buffer (pH = 7.2) for a pure DPPC vesicle solution. The solution was sonicated for 30 minutes at 45°C.

The solution temperature was held constant as the solution was filtered ten times through an Avanti Mini Extruder from Avanti Polar Lipids with a membrane pore size of 200 nm. For most studies (DLS, Cryo-EM and TCSPC) DPPC vesicles were generated from solutions having 1.5 mM DPPC concentration; for calorimetry studies the lipid concentration was increased to 20 mM to ensure high S/N.

Methods.

Differential Scanning Calorimetry

DSC measurements were performed using a TA Instruments Discovery Q2000 DSC (Hüllhorst, Germany) that can measure transition temperatures with +/- 0.1 °C accuracy. Vesicle solutions were made of 20mM DPPC vesicles rehydrated with 10 mM carbonate buffer (pH 7.2). For DPPC vesicle solutions with PFOA, the 20mM DPPC samples were rehydrated with PFOA solutions prepared in 50mM carbonate buffer (pH 7.2). Tzero pans and hermetic lids were purchased from DSC Consumables Inc. (Austin, MN) and were used to hold the sample as it was heated from 10 °C at a ramp rate of 1 °C/min to 55 °C to quantify the gel to liquid-crystalline transition temperature. Samples for DSC experiments were not extruded unlike the DLS and TSCPC experiments that were filtered to create a more uniform distribution of vesicle sizes (< 200 nm). DSC data are reported as the averages of five runs completed on separate days.

Dynamic Light Scattering

DLS measurements measuring DPPC vesicle size distributions were performed using a Malvern Zetasizer Pro Red from Malvern Instruments Ltd. (Worcestershire, England) which utilizes a non-invasive back scattering method at a measurement angle of 173° to measure particle sizes ranging from 0.3 nm to 10 µm. Samples are loaded into disposable polystyrene cuvettes (Malvern Instruments Ltd.) and were run in triplicate after calibrating at the desired temperature

for 60 seconds. The average of each run is reported. Samples were analyzed using L-curve analysis with automatic attenuation. DLS experiments used 633 nm light for all scattering instruments.

Cryo-Electron Microscopy

Samples were plunge frozen on Quantifoil 200 mesh R2/1 Cu grids using a Vitrobot Mark IV plunge freezer set at 4° C and 95% humidity with cellulose blotting paper on both sides. Sample sizes were 4 μL, blot times were 4 seconds at blot force 5. Frozen grids were then imaged on a Talos Arctica transmission electron microscope operating at 200 kV. Images were recorded with a Gatan K3 camera using SerialEM at magnification of 44,700x and defocus value of -3.0 μm. Exposure times were 5 sec at approximately 15 electrons per pixel per second. Magnified pixel size was 1.104 e-/Å^2 and total dose was 45 e-/Å^2.

Time-Correlated Single Photon Counting

TCSPC is used to determine a solute's excited state lifetimes in the sample. The TCSPC assembly used in these experiments has been described previously.[151-153] Briefly, the assembly consists of a Ti:sapphire oscillator (Coherent Chameleon, 80 MHz, 85 fs pulse length) with a fundamental output range of 690-1040 nm. Doubling and tripling harmonic assemblies enable output ranges of 345-520 nm and 230-346 nm respectively. A modulator (Conoptics Model 350-10) is used to reduce the repetition rate of the laser to 4 MHz before entering the sample chamber. Samples are excited using vertically polarized light, and fluorescence emission is collected at the magic angle (57°). To reduce background scattering from the sample, a long pass filter is used between the sample and the monochromator. Picoquant PicoHarp 300 and FluoTime 200 packages

are used for data acquisition and analysis. The time-resolved emission data are fit to a linear combination of lifetime decays alongside the relative amplitudes. By correlating solute lifetimes measured in vesicle containing solutions with solute lifetimes in different bulk solvents, we can approximate a solute's local solvation environment and quantify where within a lipid bilayer the solutes have accumulated. TCSPC has been used in our group previously to quantify how solute partitioning depends on temperature and, more importantly, determine *where* in a membrane the solutes accumulate.[79, 154-156]

For Coumarin 152 fluorescence lifetimes measurements, the samples were excited at 400 nm and emission was collected at 500 nm. A 455 nm long pass filter was used before the PMT to limit noise from scattering. Temperature dependent studies were performed using a Quantum Northwest TC125 temperature control sample chamber. Samples were held at temperature for 7 minutes before performing each scan to allow for equilibration.

Results.

Differential Scanning Calorimetry.

Surfactants have long been used to solubilize lipid membranes and isolate membrane proteins.[157, 158] Membrane solubilization requires that the lipid bilayer become saturated by the surfactant before the membrane/surfactant system begins to form micelles having mixed composition. Typically, this transformation occurs when surfactant:lipid molar ratios approach unity.[159-161] At lower surfactant concentrations (surfactant:lipid ratios ≤ 0.1), surfactants will partition into the membrane and increase membrane permeability. All these phenomena reduce lipid-lipid interactions resulting in a more fluid bilayer structure.[124, 162] Figure 3.1 shows DSC results from DPPC vesicle solutions having different PFOA concentrations. In the absence of PFOA, the DSC trace is characterized by a sharp endothermic feature at 40.5˚C corresponding to

the DPPC bilayer's gel to liquid crystalline transition. As PFOA is added to solution, the transition temperature does not change, but the amount of heat required for this melting transition diminishes.

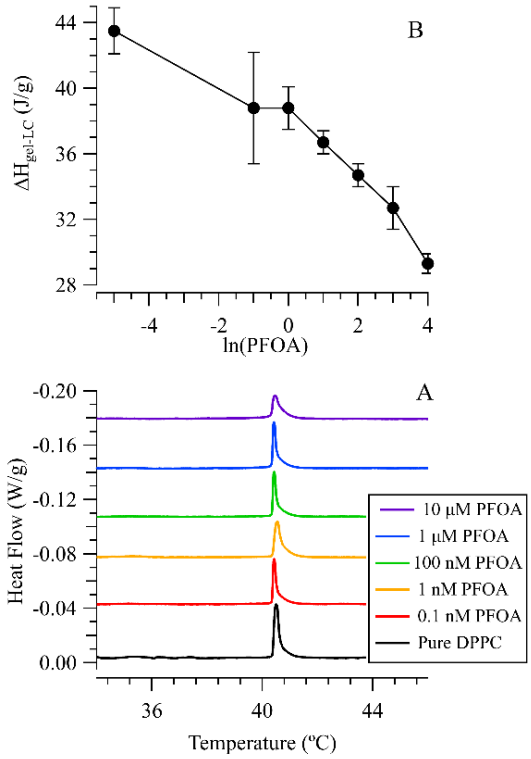

Figure 3.1. (A) Differential scanning calorimetry isotherms of pure DPPC and DPPC with increasing [PFOA] ranging from 0.1 nM to 10 μM. Isotherms have been offset vertically for clarity. (B) Average enthalpies of the gel-liquid crystalline transition as a function of [PFOA]. The inset shows an expanded view of ΔH for [PFOA] ≤ 100 nM. At a concentration of 10 μM, the peak shows noticeable broadening. Note that the calculated enthalpy for pure DPPC vesicles is assigned an arbitrarily low PFOA concentration of 10^{-5} nM to place it on scale.

Integrating the peak area results in a calculated gel-liquid crystalline transition enthalpy, ΔH_{gel-LC}. (Figure 3.2b) The 44 ± 1 J/g transition enthalpy measured for pure DPPC vesicles is consistent with values reported in the literature.[163-165] As expected, higher PFOA concentrations (≥ 1 μm) lower the transition enthalpy. (Figure 3.2 and Table 3.2) Surprisingly, nM and even sub-nM PFOA concentrations also lower DPPC bilayer transition enthalpies. Neither the

transition temperature nor the width of the endotherm changes significantly for PFOA concentrations ≤ 1 μM. The diminished enthalpy coupled with a sharp and invariant $T_{gel\text{-}LC}$ implies that PFOA penetrates the bilayer and reduces the extent but not the nature of lipid-lipid interactions.

Table 3.2. Average enthalpies of DPPC in the PFOA containing solutions. $T_{gel\text{-}LC}$ = 40.4-40.5 ˚C for all PFOA concentrations. ΔT (FWHM) = 0.2˚C. $\Delta H_{gel\text{-}LC}$ values are the averages of ≥ 9 measurements and uncertainties are reported to one standard deviation.

[PFOA] nM	$\Delta H_{gel\text{-}LC}$ (J/g)
0	44 ± 1
0.1	39 ± 3
1	39 ± 1
10	37 ± 1
100	35 ± 1
1000	33 ± 1
10000	29 ± 1

We note that the constant lipid gel-liquid-crystalline transition temperature coupled with decreasing transition enthalpy is relatively common in solutions containing low concentrations (≤ 1μM) of simple surfactants such as SDS or octanoic acid. [166] (See Reference 71 and Appendix B.) Lung surfactant proteins have been known to modestly increase DPPC's $T_{gel\text{-}LC}$ by up to 2˚C, an effect assigned to enhanced interactions between the negatively charged DPPC phosphate and positively charged residues within the proteins.[167] In contrast, Maiti *et al.* studied the effects of cationic gemini lipids on DPPC bilayer stability and discovered that these surfactants *lowered* $T_{gel\text{-}LC}$ implying that these linked, charged, lipids (present at a 5-10 mole% concentration) *disrupted* DPPC monomer-monomer interactions destabilizing bilayer structure.[168] Even PFOA has been reported to lower DPPC's $T_{gel\text{-}LC}$ by 1˚C but not until PFOA concentrations reaches ~200 μM.[120] From these and other reports, we conclude that while the low PFOA concentrations

are sufficient to lessen the heat required to melt the lipid bilayer, the intermolecular forces between DPPC monomers remain unchanged within detection limits.

Dynamic Light Scattering.

As described in the Methods section, DPPC vesicle solutions were prepared by extrusion above $T_{gel\text{-}LC}$. DLS measurements from samples created in the absence of PFOA show a narrow distribution of vesicles with a diameter centered at 115 nm and a 6 nm FWHM. (Figure 3.2) Creating DPPC vesicles in solutions containing PFOA changes the distribution in several ways. First, while the distribution center does not change systematically with PFOA concentration, the distribution does become much broader. (Table 3.3) Second, addition of PFOA creates to a second population of smaller bodies in solution having diameters between 35 and 40 nm. (Figure 3.2, Table 3.3)

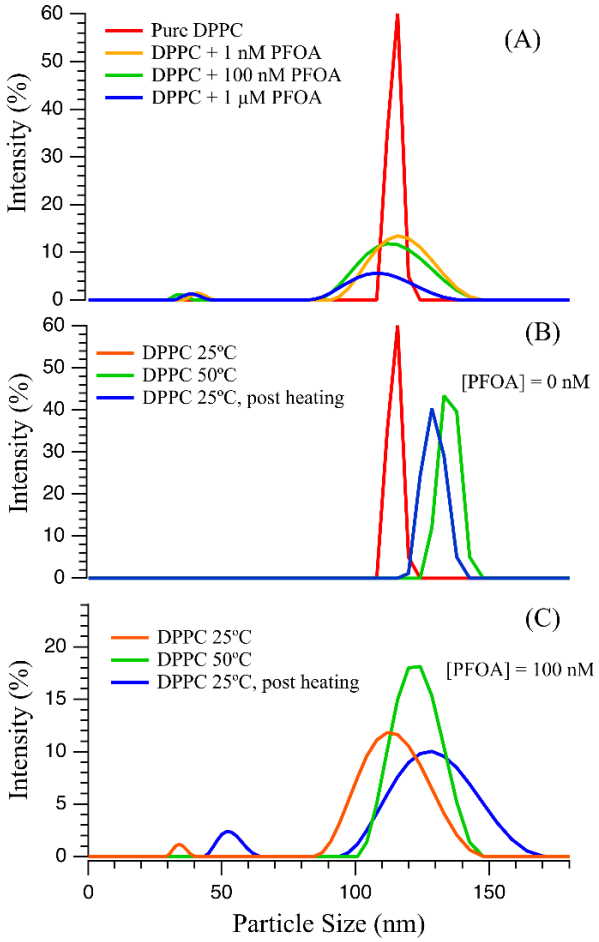

Figure 3.2. (top) Dynamic light scattering from DPPC vesicle solutions containing 0 nM, 1 nM, 100 nM, and 1 μM PFOA. (middle) DPPC vesicle size as a function of temperature in the absence of PFOA. (bottom) DPPC/PFOA solutions at 25˚C, heated to 50˚C, and then returned to 25˚C.

Heating the pure DPPC vesicle solutions above $T_{gel\text{-}LC}$ increases vesicle size by ~15%. The process is not reversible as cooling the sample results in a broader distribution having a larger average diameter than the original sample. (Figure 3.3b, Table 3.3). This result is consistent with literature reports and has been attributed to thermally induced deformation of the bilayer and a changing bilayer compression modulus.[169] Interestingly, heating the DPPC vesicle/PFOA solutions shows the same increase in vesicle size, but the smaller 35 nm objects disappear from the DLS traces, only to reappear when the solution is returned to temperatures below $T_{gel\text{-}LC}$.

Table 3.3. DPPC vesicle diameters (d) from the top panel of Figure 3.2 and size distributions (Δ) at room temperature. Uncertainties in diameter (d) are ±4 nm and in FWHM (Δ) are ±8 nm except for the pure DPPC vesicle solutions where uncertainties in d_2 and Δ_2 are ±2 and ±4 nm, respectively. Uncertainties reflect one standard deviation calculated from 9 measurements.

[PFOA] (nM)	d_1 (nm)	Δ_1 (nm)	d_2 (nm)	Δ_2 (nm)
0	—	—	115	6
1.0	40	7	116	28
100	35	5	112	32
1000	38	8	108	31

We note that the smaller objects are >10-fold larger than traditional micelle structures. For reference, sodium dodecyl sulfate and sodium octanoate solutions above their CMCs form micelles having diameters of 2.7 nm and 2.1 nm, respectively. Furthermore, the CMC for these surfactants (8.3mM for SDS and 347 mM for sodium octanoate) are much higher than the PFOA concentrations used in the current studies. The following section presents cryo-EM images that show the smaller objects observed in the DLS traces have distinct, bilayer structures with an aqueous buffer interior, suggesting that they are neither micelles nor disordered aggregates. Instead, the smaller structures share many features in common with niosomes, small bilayer objects composed of nonionic surfactants and other amphiphilic constituents including cholesterol.[170] Niosomes have attracted considerable interest as drug delivery vehicles.[171, 172]

Table 3.4. Temperature dependent changes of DPPC vesicles in the absence of PFOA and in 100 nM PFOA solutions, d_2 and Δ_2 refer to vesicle sizes. d_1 and Δ_1 refer to the niosome-like structures induced by PFOA.

	Temperature (°C)	d_1 (nm)	Δ_1 (nm)	d_2 (nm)	Δ_2 (nm)
Pure DPPC	25	-	-	115	6
	50	-	-	133	12
	25, post heat	-	-	129	11
DPPC + 100 nM PFOA	25	35	5	112	32
	50	-	-	124	25
	25, post heat	52	9	127	38

Cryo-EM.

Figure 3.3 shows representative cryo-EM images of DPPC vesicles created from PFOA-free solutions and solutions containing 100 nM PFOA. Additional images are included in Appendix B. Figure 3.3A (pure DPPC, no PFOA) shows a representative single unilamellar vesicle having a 121 nm diameter. Across 8 separate images, the average vesicle diameter measured 117 ± 20 nm, consistent with the DLS measurements reported in Figure 3.3 and Table 3.3. Careful measurements of bilayer dimensions result in an average thickness of 7.3 ± 0.4 nm. Experimental and MD simulations report DPPC vesicles with bilayer thickness ranging from 6.7 – 7.7 nm.[173, 174]

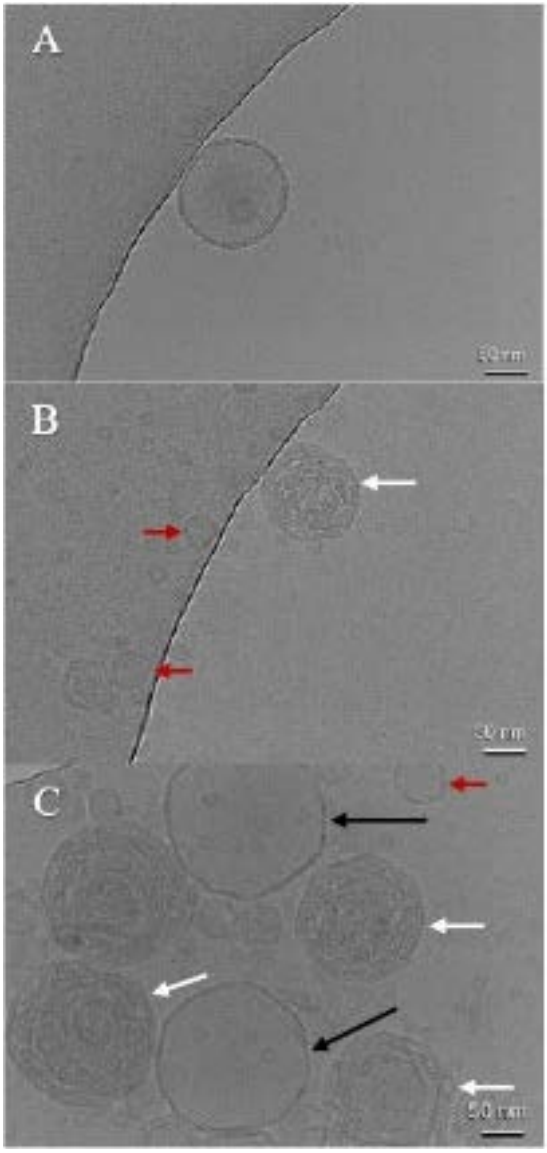

Figure 3.3. Representative cryo-EM images of DPPC vesicles prepared in a 10 mM carbonate buffer solution. A) DPPC vesicle prepared in the absence of PFOA. B and C both show images of DPPC vesicles prepared in the presence of 100 nM PFOA. Representative niosomes are indicated with the short red arrows. Medium white arrows show multilamellar structures in vesicles formed in PFOA solutions. The long black arrows show faceted vesicles.

PFOA-induced structural changes in the lipid bilayer are self-evident in Figures 3.3B and 3.3C. First, the vesicles in the PFOA solution are less round and appear faceted. This phenomenon is ascribed to curvature strain caused by PFOA being integrated into the bilayer during vesicle preparation.[124] Bilayer strain will cause the membranes to become thinner and

more flexible due to the bilayer being unable to accommodate for the difference in sizes of the DPPC and PFOA polar head groups and non-polar tails.[124] Membrane thickness was again measured. Results showed that vesicles created in 100 nM PFOA solutions had an average size slightly larger than pure DPPC vesicles (124 nm vs. 117 nm) and with a broader size distribution (±36 nm vs. ±20 nm). Again, these observations are qualitatively consistent with results from DLS measurements reported in Figure 3.2 and Table 3.3. In addition, vesicles containing PFOA had more narrow bilayers (6.2 ± 0.5 nm).

Vesicles created in the presence of PFOA frequently contained dense, nested multi-lamellar structures. We note that in instances where multilamellar structures, the images do not allow us to assess *a priori* if the different objects are nested or simply show a 2-dimensional projection of objects separated in three dimensions. We expect that conformal, multilamellar structures are nested but proof of this assertion will require 3-dimensional, tomographic imaging of structures such as those shown in Figure 3.3. The mechanism responsible for creating these complex structures remains unknown but the interior lamellae having smaller radii are consistent with the notion of bilayer strain described above.

Another effect of PFOA on vesicle formation is the appearance of objects having smaller diameters but retaining a bilayer structure. The appearance of smaller structures is consistent with niosome formation. Niosomes are vesicle-like structures typically generated from nonionic surfactants and cholesterol for drug delivery purposes.[170] A surprising observation in the results presented here is that while most niosomes are made with ratios of 1:1 surfactant: cholesterol, the DPPC/PFOA solutions used to create the cryo-EM images shown in Figure 3.3 have a DPPC:PFOA ratio of 15,000:1. These findings emphasize PFOA's distinctive properties that fall outside of what one expects for traditional (non-fluorinated) surfactants.[116] Again, when the

niosome-like structures are superimposed on larger vesicles, we cannot determine if the niosomes are inside of or external to the larger vesicles, but we expect that the niosomes are outside of the uni- and multilamellar structures. Overall, sub-nM PFOA concentrations have several effects on DPPC liposomes: i) PFOA induces a more heterogeneous distribution of liposomes including many having multilamellar structures, ii) vesicles formed when PFOA is present appear less faceted, and iii) PFOA enables the creation of bilayer structures resembling niosomes that have diameters ~3-4 times smaller than the uni- or multilamellar DPPC vesicles.

PFOA effects on secondary solute partitioning.

Results from DSC, DLS, and cryo-EM measurements shown in Figures 3.1-3.3 illustrate that sub-μM PFOA concentrations affect DPPC bilayer structure and properties. From these data we have inferred that PFOA disrupts domain formation within the lipid bilayer's gel phase and creates smaller structures adjacent to the vesicles. We expect these changes to impact lipid membrane function including the ability of membranes to accommodate secondary solutes from bulk solution. Such secondary solute partitioning is foundational to bioconcentration mechanisms.[175-179]

To understand the effects of PFOA on secondary solute partitioning into DPPC bilayers, we measured the time resolved fluorescence emission from a coumarin dye, Coumarin 152 (C152), in solutions containing DPPC vesicles as well as solutions containing both DPPC vesicles and 100 nM PFOA. C152 is a useful probe of membrane partitioning given that its time resolved emission is largely single exponential and lifetimes depend on solvent polarity and proticity. Previous studies have shown that C152 (LogP =2.7) is particularly sensitive to changes in solvation environment in lipid vesicle solutions and that C152 emission can serve as a sensitive measure of lipid membrane hydration.[180]

Figure 3.4 shows the time resolved emission from C152 in a DPPC vesicle solution containing 100 nM PFOA as a function of temperature. The decay traces are multi-exponential, and a minimum of three lifetimes are required to fit the time resolved data. The lifetimes include a sub-ns contribution that coincides with C152 in bulk aqueous buffer. The other two lifetimes are 1.5 ns and 4.5 ns at 10˚C. Both lifetimes are sensitive to temperature, falling to 0.7 ns and 3.9 ns, respectively at 70˚C. Previous studies have assigned these short, intermediate, and long C152 lifetimes to C152 solvated in aqueous buffer, C152 that has partitioned into the lipid bilayer's polar, glycerol backbone region, and C152 solvated in the lipid bilayer's hydrophobic core, respectively.[180-182]

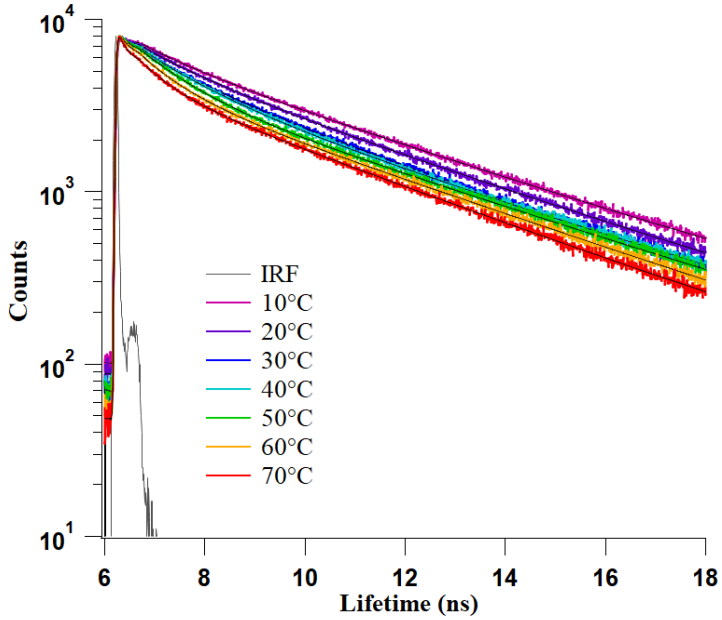

Figure 3.4. TCSPC traces of DPPC vesicle solutions containing 6 μM C152 and 100 nM PFOA as a function of temperature. The multiexponential decay visibly changes with temperature. Data are fit to three independent lifetimes as described in Reference 35. Raw data for the TCSPC traces can be found in Table B-3.1.

Figures 3.5 and 3.6 show how the lifetimes and the corresponding amplitudes change with temperature. Also included on these figures (as dashed lines) are C152 lifetimes and amplitudes in DPPC vesicle solutions with no PFOA present. (TCSPC data for C152 in PFOA-

free DPPC vesicle solutions are reported in Supporting Information.) Several observations stand out. First, C152's intermediate lifetime (τ_2) at low temperatures (10˚C) in the DPPC-PFOA solutions lies between a polar aprotic limit (2.4 ns in acetonitrile) and a polar protic limit (1.1 ns in methanol). We interpret this result as evidence that PFOA disrupts lipid packing, enabling water to penetrate the bilayer and promote protic solvation within the bilayer below $T_{gel\text{-}LC}$. Above $T_{gel\text{-}LC}$, τ_2 converges the polar protic limit indicating complete bilayer hydration in the polar backbone region.[180-182]

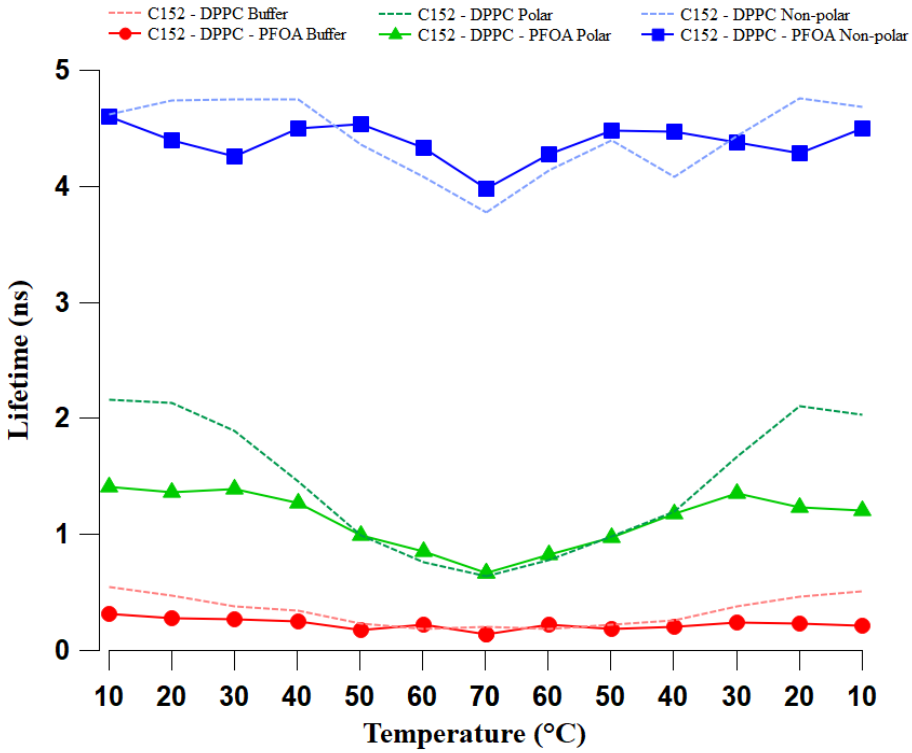

Figure 3.5. A plot of the 3 lifetimes of C152 as a function of temperature from 10-70-10 ˚C. The dotted lines show the lifetime behavior of C152 in a solution of DPPC vesicles without PFOA. The solid lines show lifetimes of C152 in a solution of DPPC vesicles and 100 nM PFOA. The 2nd lifetime of C152 shows the largest change in lifetime when PFOA is present, an effect attributed to PFOA-enabled hydration of the bilayer below $T_{gel\text{-}LC}$.

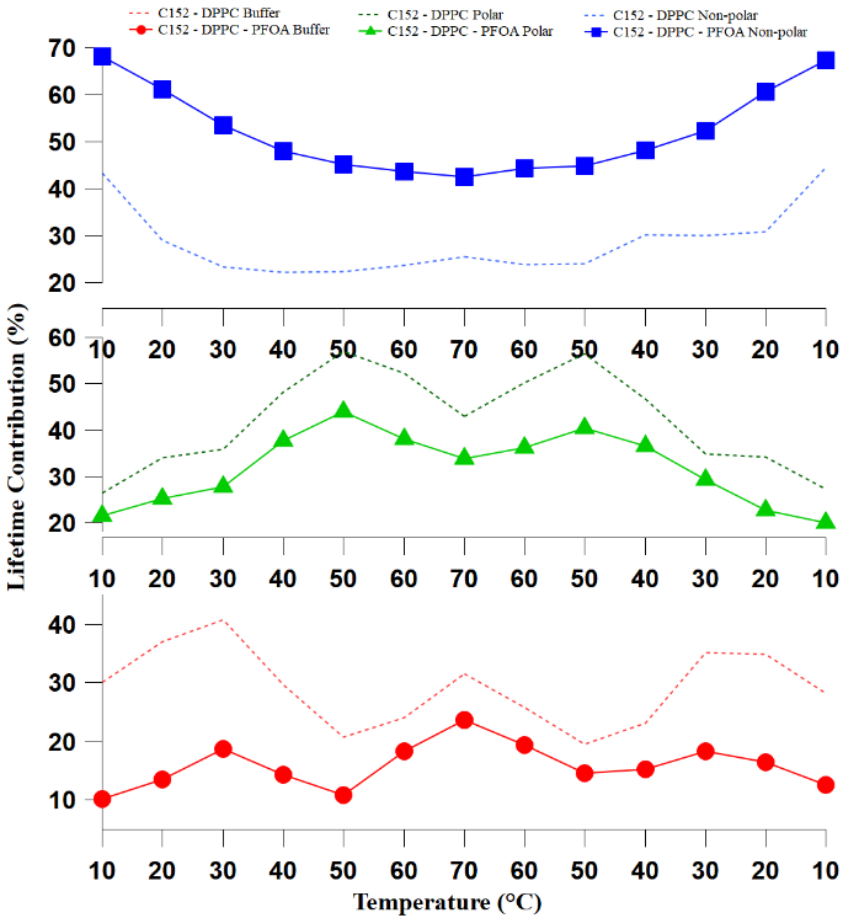

Figure 3.6. A plot of the relative amplitudes of each C152 fluorescence lifetime as a function of temperature. The dotted lines show amplitudes for C152 in pure DPPC vesicle solutions and the symbols show lifetime amplitudes for C152 in DPPC vesicle/100 nM PFOA solutions.

The second observation is that the amount of C152 in the hydrophobic part of the membrane (A_3) is 67% higher in the PFOA containing solution ($A_3 = 0.70$) relative to the PFOA-free solution ($A_3 = 0.42$). This increased partitioning into the hydrophobic region of the bilayer comes at the expense of C152 in aqueous solution ($A_1 = 0.1$ with PFOA; $A_1 = 0.3$ without PFOA). This result is also consistent with PFOA disrupting lipid-lipid interactions within the bilayer and making the nonpolar region more accessible to the hydrophobic C152. We note that PFOA enhances C152 accumulation in the membrane's hydrophobic region regardless of bilayer state. The amplitude of the hydrophobic population remains approximately 2-fold greater when PFOA is present in both the DPPC gel and liquid crystalline states.

Table 3.5. Lifetimes and amplitudes data from fitting TCSPC decay traces of C152 in DPPC vesicle solutions at 10, 50 and 70°C. Shown are results from both PFOA-free and 100 nM PFOA solutions. Lifetimes are reported in nanoseconds and the amplitudes are normalized. Lifetime precision is ± 0.1 ns; amplitude precision is ± 0.05. Lifetimes and amplitudes over all of the temperatures sampled appear in Supporting Information.

Temperature	Sample	τ_1 (A_1)	τ_2 (A_2)	τ_3 (A_3)
10°C	Pure DPPC	0.55 (0.30)	2.16 (0.27)	4.62 (0.43)
	DPPC PFOA	0.32 (0.10)	1.41 (0.22)	4.6 (0.68)
50°C	Pure DPPC	0.23 (0.21)	0.99 (0.57)	4.36 (0.22)
	DPPC PFOA	0.18 (0.11)	0.99 (0.44)	4.54 (0.45)
70°C	Pure DPPC	0.2 (0.32)	0.64 (0.43)	3.78 (0.25)
	DPPC PFOA	0.14 (0.24)	0.67 (0.34)	3.98 (0.42)

The temperature dependent lifetime and amplitude data in Figures 3.5 and 3.6 show that C152 partitioning is reversible with temperature. Furthermore, the data show a similar functional dependence with changing temperature with and without PFOA present. This behavior again suggests that PFOA in the bilayer disrupts chain-chain interactions enabling C152 to access the bilayer's hydrophobic interior more easily. Additional studies examined changes in C152 partitioning behavior at lower PFOA concentrations to discover if similar behaviors were observed. Equivalent experiments indicate that 1 nM PFOA concentrations did enhance lipid membrane hydration below $T_{gel\text{-}LC}$ relative to PFOA-free samples, although the fraction of C152 that partitioned into the membrane did not change measurably. (Appendix B Figures B.1-6 and Tables B.2 and B.3) Taken together, the DSC, DLS, Cryo-EM, and TCSPC data support a mechanism whereby PFOA partitions into biomembranes and fluidizes the membrane hydrophobic interior, enabling access to secondary solutes and lowering collective cohesion within the bilayer. While most studies examining PFOA-lipid interactions have focused on

PFOA concentrations of 100 μM and higher, results presented in this work show that even at the extremely low concentrations currently being considered by regulatory agencies, PFOA effects on lipid membrane structure are profound.

CHAPTER FOUR

PERFLUOROOCTANOIC ACID DESTABALIZES HEMOGLOBIN STRUCTURE AT SUB-MICROMOLAR CONCENTRATIONS

Contributions of Authors and Co-Authors

Manuscript in Chapter 4
Author: Rhys C. Trousdale
Contributions: Collected and analyzed TCSPC data, assisted in sample preparation and data collection for Native mass spec data, wrote manuscript in preparation for publication
Co-Author: Monika Tokmina-Lukaszewska
Contributions: Collected and analyzed experimental native mass spec data, assisted in writing manuscript
Co-Author: Brian Bothner
Contributions: Assisted in data analysis of native mass spec data and manuscript writing and editing
Co-Author: Robert A. Walker
Contributions: Assisted in data analysis of TCSPC data, assisted in manuscript writing and editing

Manuscript Information

Rhys C. Trousdale, Monika Tokmina- Lukaszewska, Brian Bothner, and Robert A. Walker
Journal of Physical Chemistry B
State of Manuscript
_____ Prepared for submission to a peer-reviewed journal
_____ Officially submitted to a peer-reviewed journal
__x__ Accepted by a peer-reviewed journal
_____ Published in a peer-reviewed journal

PERFLUOROOCTANOIC ACID DESTABALIZES HEMOGLOBIN STRUCTURE AT SUB-MICROMOLAR CONCENTRATIONS

Rhys C. Trousdale[a], Monika Tokmina-Lukaszewska[a], Brian Bothner[a] and Robert A. Walker*[a,b].
[a]Chemistry and Biochemistry Department, Montana State University, Bozeman, MT 59717
[b]Montana Materials Science Program, Montana State University, Bozeman, MT 59717

Abstract

Perfluorooctanoic acid's (PFOA) effects on human hemoglobin (Hb) at micromolar and sub-micromolar PFOA concentrations were investigated using time-correlated photon counting (TCSPC) fluorescence, native mass spectrometry (NMS) and ion mobility spectrometry (IMS). TCSPC results show that tryptophan fluorescence quenching mechanisms in Hb change from Förster Resonance Energy Transfer (FRET) with the heme to charge transfer to the peptide backbone as PFOA concentration increases. NMS showed 4 lower and 2 higher affinity sites for PFOA interacting with Hb. At concentrations as low as 10 nM, 2 PFOA molecules bind to Hb leading to destabilization of the complex, loss of an α subunit, and release of heme. Together, these data show that PFOA alters the biophysical properties of human Hb in ways that suggest allosteric inhibition

Introduction

Per- and polyfluorinated alkyl substances, or PFAS, are a class of molecules that threatens community and ecosystem health. PFAS are often called ‘forever chemicals’ because of their environmental persistence and have been linked to reduced vaccine response, high cholesterol, compromised immune system function, and certain types of cancer[93, 95, 96, 183, 184]. Perfluorooctanoic acid (PFOA) is a legacy member of the PFAS family, and despite no longer being manufactured commercially, PFOA is expected to persist in the environment for decades. The U.S. Environmental Protection Agency recently enacted regulatory limits restricting PFOA levels in drinking water to $\leq$ 4ppt.

To date, most PFAS-related research has focused on detection and correlating PFAS levels with various pathologies. Considerably less work has examined the mechanisms underlying how PFAS in general (and PFOA in particular) interact with biological materials. With a log D value of 1.8, PFOA is expected to bioconcentrate in membranes[185] and is expected to show affinity for proteins.

In humans, serum proteins are thought to play a large role in PFOA transport throughout the body[186] while fatty liver proteins may play a role in bioaccumulation[187, 188]. Several studies have examined of PFAS molecules interacting with heme proteins and suggest they may alter protein structure and function by inducing conformational changes to the central heme binding pockets. Hemoglobin is normally associated with oxygen transport. However, Hb is also involved in nitric oxide metabolism, metabolic programming, pH regulation and redox balance[189]. In most vertebrates, Hb is an $\alpha_2\beta_2$ tetramer that is well known as an allosteric protein modulated by homo and heterotropic effectors. Understanding the impact of PFOA on Hb

oxygen binding properties and regulatory functions has direct ramifications to human health and long-term consequences for PFOA remediation strategies.

In 2011, based on optical spectroscopy studies, Qin et. al. reported that 30-160 μM PFOA seemingly had little effect on bovine hemoglobin (Hb) and myoglobin (Mb) fluorescence, but did report that perfluorodecanoic acid (PFDA) influenced the protein optical absorbance and fluorescence.[190] More recently Yang et. al. claimed that PFOA had very little effect on Hb and Mb structures and hemin release at concentrations of ≤100 μM, in contrast to PFOS, a molecule structurally very similar to PFOA.[191] (PFOS is identical to PFOA except for having a sulfonate headgroup rather than a carboxylate group.) These authors reported that PFOS concentrations as low as 50 μM resulted in very small but measurable increase in Hb steady state fluorescence. This increase was attributed to PFOS monomers disrupting interactions between Hb's native fluorescent residues and the heme units. These authors also performed a molecular docking study to predict the number of PFOA binding sites on Hb and Mb. Similar studies with serum albumin and PFOA led to a prediction of one binding site[192] while the crystal structure revealed four distinct sites[193]. Another direct method of stoichiometry confirmation, electrospray ionization mass spectrometry, revealed concentration dependent PFOA and PFOS binding to human and bovine serum albumins. Perera. et. al. used spectroscopic methods to confirm PFOA binds to Hb at low micro-molar concentrations, and inferred that binding alters ligand binding. At 50 μM PFOA, these authors used circular dichroism to observe structural changes attributed to protein unfolding.[194] In addition, they concluded that there are at least two PFOA binding sites. These detailed investigations are instructive, but often provide conflicting accounts describing how many Hb bind to Hb (and other proteins), and *none* of these reports consider PFOA effects

on Hb stability at concentrations approaching regulatory limits. Furthermore, specific mechanisms describing *how* PFOA associates with Hb remain unresolved. Given the important role of allostery in Hb function, this last issue – PFOA binding mechanisms - represents a significant knowledge gap in our understanding of how this regulated analyte affects biomolecular structure.

In this work, we report that sub-micromolar and micromolar PFOA concentrations affect human Hb stability and impact natural fluorescence mechanisms. Native mass spectrometry experiments reveal multiple PFOA molecules binding at concentrations as low as 10 nM, and show significant structural defects occurring when stoichiometric ratios of Hb and PFOA are matched. NMS also shows that when Hb and PFOA are at a 1:1 stoichiometric ratio, PFOA induces heme loss from the α subunit and α subunit loss from the quaternary Hb structure. Time-resolved emission studies used Hb's natural fluorescence from its 6 native Trp residues and uncovered detailed mechanistic consequences of PFOA binding at micromolar concentrations. Specifically, Trp quenching changed as PFOA concentration increased indicating weakened interactions between Hb heme units and the protein chain.

Materials and Methods

PFOA and lyophilized human Hb were purchased from Sigma, PFOA was used as received. Human Hb Samples were prepared in a 100 mM ammonium acetate solution buffered to pH 7.5. Human Hb concentrations were set 5 μM and processed differently for time-resolved studies and mass spectrometry studies described below.

UV-Vis experiments were performed on a Shimadzu UV-2101PC scanning spectrophotometer at a medium scan speed. Hb samples were made in a pH 7.5 100 mM ammonium acetate solution o maintain consistency with NMS and TCSPC experiments.

Time-Correlated Single-Photon Counting Spectroscopy

Fluorescence lifetime experiments were measured following Trp excitation by pulses from a Ti:sapphaire oscillator (Coherent Chameleon, 80 MHz, 85 fs pulse duration, 680-1040 nm wavelength range) coupled with an APE autotracker harmonic generator used to frequency triple the fundamental wavelength. Samples were excited at 290 nm to minimize excitation of/emission from Hb's other naturally occurring fluorescent residues, Phenylalanine (Phe) and Tyrosine (Tyr).

A Conoptics model 350-80 modulator was used to reduce the repetition rate to 4 MHz. Picoquant PicoHarp 300 and FluoTime 200 software were used for data collection. Samples were equilibrated at the reported temperatures for 5 minutes using a Quantum Northwest TC125 control (Seattle, WA). A long pass filter (90% transmission >280 nm) was placed after the sample to reduce scattering from the solution due to incident light. Photon emission was collected at 335 nm via a PMT. Additional detail about the time correlated single photon counting (TCSPC) assembly can be found in prior reports.[156, 180]

Time-resolved emission data from Hb/PFOA solutions were fit with a linear combination of independent lifetimes and amplitudes using fitting parameters that are adjusted to minimize residuals and optimize χ^2. fluorescence decay and amplitude expression are shown in Eq. 1, where A_i and τ_i are the amplitude and the lifetime of the i'th component, respectively.

$$I(t) = \int_0^t IRF\ (t') \sum_{i=1}^{n} A_i e^{-\frac{t-t'}{\tau_i}}\, dt' \qquad (1)$$

Each trace was fit independently, without any constraints, for the lifetimes and amplitudes. The typical $\chi 2$ were from 0.9-1.1 when accounting for at most three lifetimes. Typically, uncertainties in lifetimes and amplitudes were ±0.2 ns and ±0.04, respectively. There is an inherent uncertainty in the lifetimes reported of ± 0.3 ns due to the detection limit of the instrument; however, data and error bars presented in this work represent results from at least 3 independently prepared, equivalent trials averaged together with a single population standard deviation of those trials. The average lifetime and amplitudes and their respective standard deviations are reported for each specific temperature and only compared to their respective temperature.

Fluorescence lifetime measurements showed evidence of 3 lifetimes with an average χ^2 of 1.22, corresponding to confidence levels in lifetimes and amplitudes between 97.5 and 99%. Measurements were performed at 40 °C to simulate approximate biological temperatures. Human Hemoglobin solutions were spun in a microcentrifuge at 10,000 RPM for 8 minutes to remove large hemoglobin aggregates before beginning fluorescence studies. For each PFOA concentration, a new sample was mixed and allowed to equilibrate for ~30 minutes before measurement.

TCSPC data for Hb/PFOA solutions with PFOA concentrations between 0 M and 500 mM are shown in Appendix C and reported in Table B-1.1.

Native Mass Spectrometry

PFOA's impact on hemoglobin structure was also investigated using native mass spectrometry (NMS) and ion mobility spectroscopy (IMS). Briefly, hemoglobin and PFOA stock

solutions were prepared in 100 mM ammonium acetate pH 7.5 (Sigma). The hemoglobin sample at a protein concentration of 5 μM was washed with 100 mM ammonium acetate solution, pH 7.5 using 30-kDa molecular weight cutoff spin filters (Pall Corporation) and then incubated for 5 minutes and one hour at room temperature with following protein to PFOA molar ratios: 1 : 0, 1 : 0.002, 1 : 1 and 1 : 4. The resulting samples were immediately infused from in-house prepared gold-coated borosilicate glass capillaries to the electrospray source (positive polarity) and analyzed in TOF and Ion Mobility modes. The instrument was tuned to optimize performance in the high mass-to-charge range with the following settings: source temperature 30 °C, capillary voltage 1.1-1.4 kV, trap bias voltage 16 V and argon flow in collision cell (trap) 7 mL/min. Transfer collision energy was held at 2 eV while trap energy varied between 5 and 160 eV. In addition, the MSMS experiment was performed on 4,032.46 m/z (16+ ion of the holo hemoglobin tetramer) ramping trap energy between 10 and 105 eV. Data analysis was performed in MassLynx software version 4.1 (Waters). In the Ion Mobility mode, the similar instrument setup was used except the trap bias voltage set to 45 V. In addition, wave velocity and height were, respectively, 300 m/s and 6.1 V in the trap, 800 m/s and 25 V in the IMS cell, and 434 m/s and 5 V in the transfer. IMS gas was nitrogen with a flow of 35 mL/min. Data processing was performed in DriftScope v 2.9 (Waters) and MassLynx v 4.1 (Waters).

Results and Discussion

TCSPC

Time-resolved fluorescence-emission of native Trp residues is an instructive method to follow protein dynamics and conformational changes.[195] In the case of heme-based proteins,

Förster resonance energy transfer (FRET) from Trp to the Hb hemes results in rapid fluorescence quenching and an ultrafast picosecond lifetime.[30, 196, 197] While this lifetime is shorter than what TCSPC can reliably measure, the presence of such a short lifetime is a useful diagnostic of Trp-heme proximity (Fig. 4.1).

Fluorescence quenching can also occur between Trp and the protein's amide backbone resulting in a fluorescence lifetime of ~0.5 ns.[29] In the absence of these quenching mechanisms, Trp rotamer states in peptides have a ~2.5 ns lifetime similar to that of Trp monomers in aqueous solution.[28] These three Trp relaxation pathways – FRET to the heme, energy transfer to amide backbone, and unperturbed radiative decay – result in a time resolved fluorescence emission comprised of three distinct lifetimes. Changes in the relative amplitudes of these lifetimes report on how Hb structure changes in the presence of PFOA.

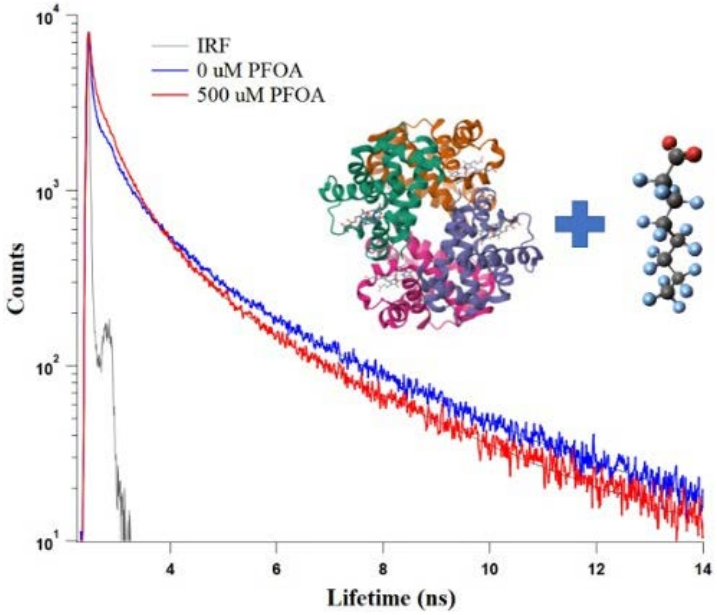

Figure 4.1. Time resolved fluorescence emission of hemoglobin with 500 □M PFOA. The addition of PFOA alters the time resolved emission of Trp residues. Fits to the data are included on the emission decay traces.

Fitting the fluorescence decay traces to three independent decay pathways results in three lifetimes (τ_i) and their corresponding amplitudes (A_i) (Fig. 4.2). A table containing all of the fitting data used to create Figure 4.2 is included in appendix C. Fitting the decay traces requires a minimum of three lifetimes to obtain a statistically reasonable χ^2 and accurately reproduce the data. This finding supports the anticipated three radiative decay pathways available to Trp noted above.

The shortest lifetime (τ_1) does not change significantly with increasing PFOA concentration. The intermediate lifetime, τ_2, begins to lengthen, and the longest lifetime, τ_3, begins to shorten for PFOA concentrations $\geq$ ~300μM. These results are consistent with PFOA induced conformational changes to the protein that alter the microenvironment(s) surrounding Trp residues. The shortest lifetime, τ_1, is too short for TCSPC to measure reliably but serves as an indicator of Trp-heme quenching. An important note is that this ultrafast lifetime remains present through increasing PFOA concentrations, meaning some population of Hb's native Trp residues continues to experience heme-based quenching.

The τ_3 amplitude (A_3) remains largely unchanged and very small (~0.05) as PFOA concentration increases, indicating that the relative fraction of solvent accessible Trp is insensitive to PFOA concentration. The two shorter lifetimes, τ_1 and τ_2, contribute to the time resolved emission in opposite manners when PFOA concentrations rise above ~300 μM. Specifically, the shortest lifetime, τ_1, contributes less to the emission decay while contributions from the intermediate lifetime, τ_2, begin to grow.

The increase in A_2 is correlated to an increase in Trp quenching by the amide backbone. The decrease in τ_1 indicates that Trp FRET to the heme is becoming less important as PFOA

concentration increases. Both effects imply Hb conformational changes. These changes in emission represent the first direct evidence that PFOA alters Hb's internal photophysical behavior by shifting the relative importance of different quenching mechanisms. The data, however, cannot quantify *how* PFOA is changing Hb structure.

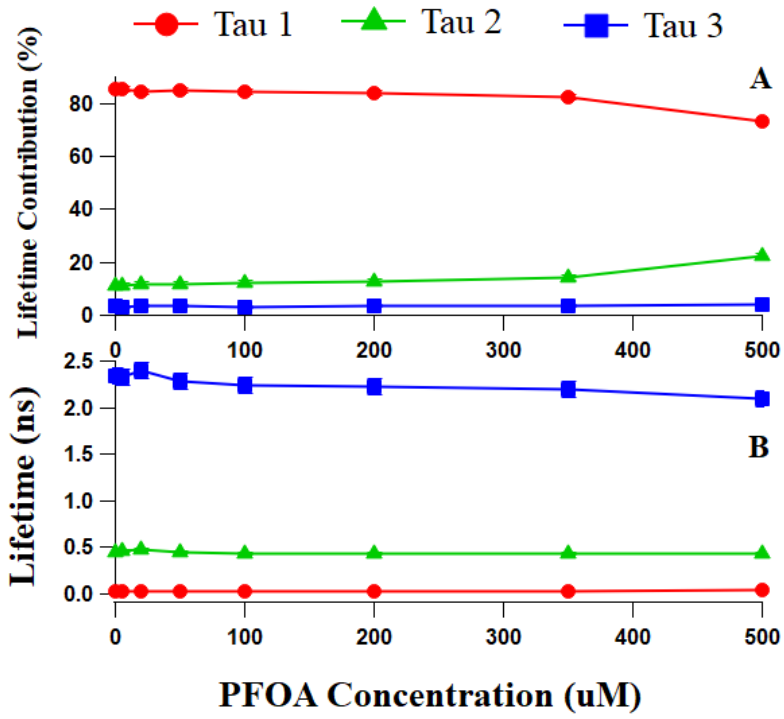

Figure 4.2. Trp Fluorescence lifetimes depend on PFOA concentration and temperature. (A) Fluorescent lifetimes (y-axis) versus PFOA concentration (x-axis) at 40 °C shows how the long lifetime, τ_3, decreases as PFOA concentration increase, and the intermediate lifetime, τ_2, increases. Both effects indicate changes in Hb structure. (B) Fluorescent lifetime contributions for each τ (y-axis) as a function of PFOA concentration (x-axis) at 40 °C. τ_1 and τ_2 show a noticeable difference in percent contribution as PFOA concentration increases illustrating changes in the relative importance of quenching mechanisms.

We note that Yang, *et al.'s* study of PFOS binding to bovine Hb reported changes in the protein's optical properties for surfactant concentrations of 50 μM, ~6-fold lower than where we

observe PFOA effects on *human* Hb's optical emission. This difference could arise from differences in protein concentrations used in the two studies. Results from Yang, *et al*. used solutions containing 20 μM Hb endowing those experiments with intrinsically better detection limits compared to the 5 μM Hb solutions used in the current studies. Furthermore, Fronticelli, *et al.* has reported that bovine Hb is more hydrophobic than human Hb.[203] Increased hydrophobicity is likely to enhance PFOS (and, presumably, PFOA) affinity for protein interiors. If a more general sense, if relatively small changes in hydrophobicity result in measurable changes in PFOS affinity for the closely related human Hb and bovine Hb, then PFAS effects on proteins are likely to be very specific to individual PFAS-protein pairings.

Native Mass Spectrometry

To investigate PFOA binding and its impact on hemoglobin structure directly, we performed NMS and ion mobility measurements. First, we examined a higher mass region (3,500 – 4,500 m/z) to observe PFOA-induced changes to the intact hemoglobin tetramer with all four heme cofactors bound (Fig. 4.3). Between m/z values of 3,800 and 4,300, Hb shows three sharp, distinctive peaks corresponding to Hb charges of +15, +16, and +17 (Fig. 4.3A). In the presence of PFOA peaks broaden and shift in charge state distribution (Fig. 4.3B and 4.3C). Signal deconvolution revealed that at the lower PFOA concentrations (10 nM, or 1 : 0.002 protein ratio to PFOA), the sample contained Hb-bound with two PFOA , while at a Hb:PFOA stoichiometric ratio (1 : 4 ratio) we detected multiple, PFOA-bound Hb species. In addition, at 20 μM PFOA concentration, we observed increased in number of charges going from (15-17)+ to (16-18)+ in both unbound and PFOA-bound Hb forms. This observation indicates that even unbound PFOA

affects a protein solvation layer causing some degree of change to Hb folding. The lower concentration data confirm a proposal made by Perera, *et al.* that inferred (at least) two PFOA binding sites in Hb based on optical absorption titration measurements.[194]

The shift in charge state distribution implies that the protein conformation has changed. To explore this effect further, we collected ion mobility profiles to examine the Hb conformational ensemble (Fig. 3C inset). In a typical ion mobility mass spectrometry experiment (IMS), the time required for the biomolecule to progress through the ion mobility cell is measured. Flight time depends on the molecule's mass, charge, and shape.[203] For example, small, well-folded proteins travel faster than large complexes or denatured proteins. IMS is extremely sensitive to differences in shape and allows for detection of changes from large movements (rigid body motions) to very subtle alterations to protein structure. Comparison of the mobility patterns of unbound and Hb-bound to 6 PFOA monomers revealed at least two distinct drift times for charge state 17+, dt_1 and dt_2, indicating (at least) two distinct conformations. The dt_1 PFOA-bound form is more compact and travels faster through the mobility cell. In fact, the PFOA-bound form travels even faster than unbound Hb. The conformation corresponding to dt_2 travels more slowly due to larger overall size ("shape"). That means PFOA has heterogenous impacts on Hb structure, ranging from partially collapsed structures (smaller size) to partially (locally) unfolded (larger size).

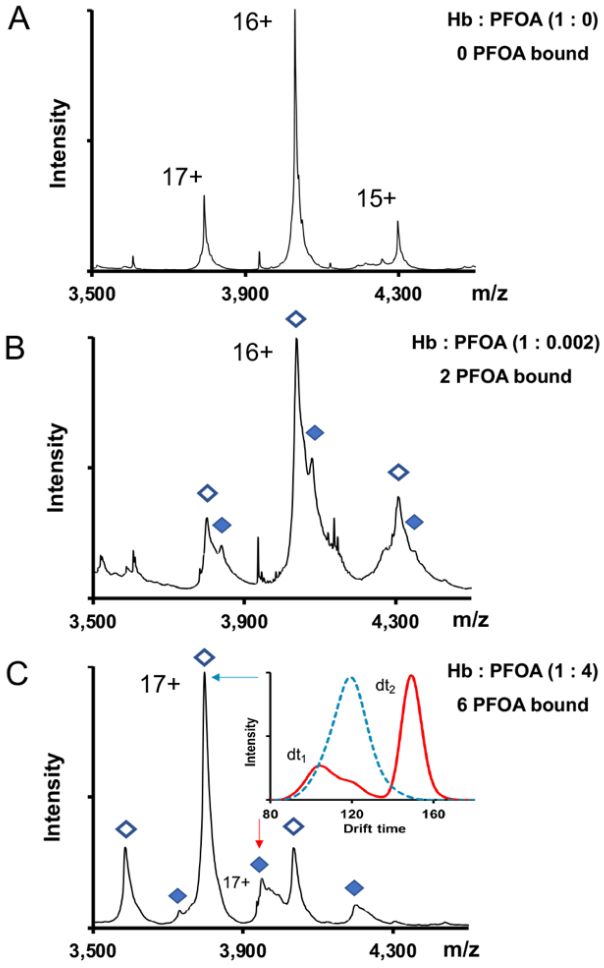

Figure 4.3. Native mass spectra of PFOA-treated human Hb. Mass spectra were recorded in the absence (A) or in the presence of (B) 10 nM or (C) 20 μM PFOA. At the lower PFOA concentration (1 : 0.002 protein ratio to PFOA) Hb binds 2 PFOA monomers while at the stoichiometric amount (1 : 4 ratio) several PFOA-bound Hb species are present. The open vs close symbols represent (PFOA) unbound vs (PFOA) bound Hb. In panel (C) the blue and red arrows point at the charge state 17+ of unbound Hb and Hb binding 6 PFOAs, respectively. Mobilogram of PFOA-bound Hb (red line) in the panel (C) inset shows at least two distinct drift times for charge state 17+, dt1 and dt2, indicating multiple conformations of PFOA-bound Hb. The blue dashed line represents charge state 17+ of (PFOA) unbound intact (holo) Hb.

Motivated by findings from Yang, *et al.*[191] showing PFOS-induced heme loss from Hb at 100 μM concentrations, we performed additional analyses. We focused our attention on the lower

mass region (500 – 3,500 m/z) to examine the α and β subunit spectral features. In the presence of 10 nM PFOA (1 : 0.002 protein ratio to PFOA) NMS data showed an increase in free heme (616.12 m/z) as well as a broader charge state distribution for the α subunit (with and without heme) in comparison to free Hb (Fig. 4.4A and 4.4B). These effects are observed at concentrations that are *4 orders of magnitude* lower than optical studies of PFOS interacting with Hb and 500-fold lower than reports from Perera *et al.*'s studies of PFOA indicating that 5 mM PFOA introduced conformational heterogeneity near Hb's heme units.[194]

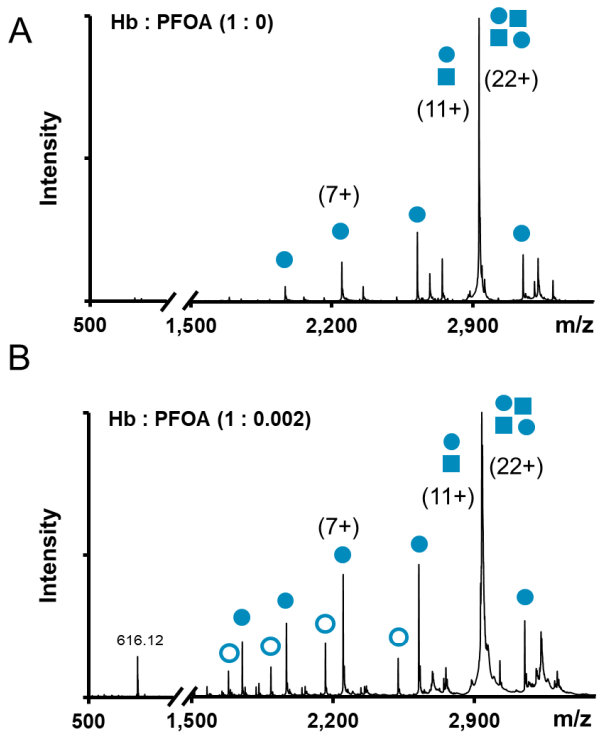

Figure 4.4. Native Mass Spectrometry analysis of PFOA binding on Hb structure and stability. Mass spectra were recorded in the absence (A) or in the presence of (B) 10 nM PFOA (as in Fig. 4.3). α and β subunits are indicated with circles and squares, respectively. Open vs closed symbols represent apo vs heme-bound Hb species. Multiple circle/square blocks represent Hb oligomeric states. Numbers in parenthesis indicate selected charge states. 616.12 m/z is heme.

In addition, we compared the mobilograms of α and β subunits ejected from the tetramer when the complex was activated by increasing the transfer energy (Fig. 4.5A). Interestingly, stoichiometric quantities of PFOA (1 : 4 protein ratio to PFOA or 20 μM PFOA) induced significant changes to α subunit structure as reflected in the presence of multiple conformations, (Fig. 4.5B). Under these same conditions, the β subunits seemed unaffected.

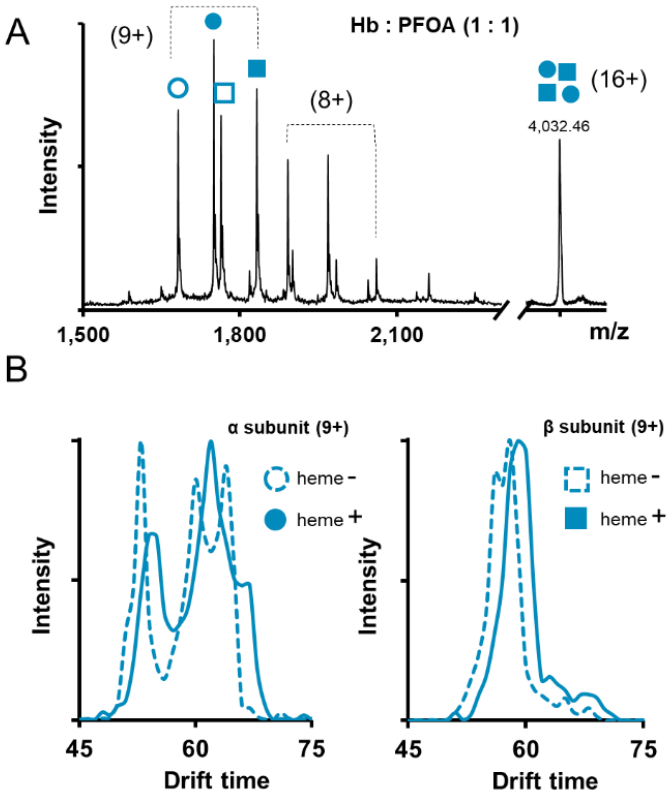

Figure 4.5. Hb conformational ensemble in a presence of PFOA. Panel (A) shows the MSMS spectrum performed on 4,032.46 m/z which represents 16+ charge state of intact, heme-bound Hb tetramer in presence of PFOA (1 : 1 ratio, 5μM). Panel (B) shows mobilograms of α and β subunits (charge state 9+ only) generated during fragmentation of 4,032.46 m/z parent ion (panel A). α and β subunits are presented as circles and squares, respectively. Open vs closed symbols represent apo form vs heme-bound Hb species. Multiple circle/square blocks represent Hb oligomeric states. Numbers in parenthesis indicate selected charge states. Holo and apo forms are denoted by solid and dash line, respectively.

Conclusions

As the adverse effects of PFOA and other members of the PFAS family on human health become increasingly clear, regulatory agencies around the world are enacting stringent limits to allowable amounts of PFOA in drinking water and manufactured goods. Furthermore, a growing body of literature highlights PFOA's bioconcentration tendencies. Missing in these studies is mechanistic information about *how* PFOA affects the structure and function of the biological materials it is thought to impact *at concentrations approaching regulatory limits*. Findings reported in this study show unambiguously that PFOA destabilizes and induces conformational changes in Hb. Time resolved emission from Hb's native Trp residues begins changing at PFOA concentrations ≥ 100 μM and indicates a change in Trp radiative decay mechanisms. NMS experiments push the PFOA concentration limit lower (by 4 orders of magnitude). These measurements show that PFOA to preferentially targets Hb's α subunit and heme cofactor environments, and alters the global structure of Hb at PFOA concentrations of 10 nM and 20 μM Binding of two PFOA molecules is observed when at 10 nM concentrations and binding of 6 PFOA molecules is observed when at 20μM concentrations. Whether PFOA competes with heme for binding to an α subunit or PFOA binding to the tetramer causes structural changes propagated throughout the complex, weakening cofactor affinity, is a question that remains to be answered. The second scenario implies that PFOA binding to Hb and its subsequent effects on interactions within the complex are allosteric in nature. Since the legacy of forever chemicals will last for decades, identifying the mechanisms of biochemical activity are critical. The work presented here certainly raises the question: what other proteins might be allosterically impacted by this class of compounds? Likewise, might energy transfer to PFOA, as seen in our fluorescence

quenching experiments, alter electron transfer in proteins such as Cytochrome C which rely on electron transfer dynamics to perform their overall function.

CHAPTER FIVE

CONCLUSIONS AND FUTURE DIRECTIONS

Summary

The experiments described in this dissertation analyzed specific chemical interactions that occur when a solute is introduced to a system containing biological materials such as lipid membranes and proteins. Time-resolved fluorescence emission, combined with steady state spectroscopy, differential scanning calorimetry (DSC), dynamic light scattering (DLS) and native mass spectrometry were used to assess the following questions:

1. Do specific solutes partition into model biological membranes and/or bind to native proteins?
2. If so, where in the membrane do solutes accumulate?
3. Do partitioned solutes alter membrane/protein properties?
4. What is the quantitative distribution of solutes within membranes and proteins?

Each chapter in this dissertation analyzed either different solutes, or different biological targets to better understand the mechanisms of bioconcentration. L-phenylalanine affinity for phosphocholine lipid bilayers, and PFOA affinity for both lipid bilayers and the protein human hemoglobin were quantitatively characterized to better understand specific chemical interactions and solute affinity effects on biological material properties. A variety of experimental techniques were deployed to examine the photophysical behavior of these solutes, either directly using solute fluorescence, or leveraging the natural fluorescence of the biological material itself. Paired with time resolved emission, data from other analytical techniques including differential scanning calorimetry and dynamic light scattering provided insight into how solutes affected

structural and thermodynamic properties of both membrane vesicles and native proteins. Cryo-EM and native mass spectrometry experiments further expanded our understanding of these solute-biological material interactions.

Research presented in Chapter 2 analyzed the effects of the understudied amino acid L-Phenylalanine on model biological membranes comprised of phosphocholine lipids, as well as the photophysical behavior L-Phe displays when in a solution containing lipid vesicles. In the presence of a lipid vesicles, results showed that ~70% of the L-Phe population remains in the bulk buffer solution, while ~30% display a lifetime of 1.8 ns that does not match L-Phe emission in any of the bulk solvents used to model different biological solvation environments. This second lifetime appears at temperatures approaching the $T_{gel\text{-}lc}$ transition of DPPC lipid bilayers and is assigned to L-Phe integration into the glycero-chain backbone region of the lipid bilayer. Based on these findings and literature descriptions of L-Phe photophysical behavior, we proposed that L-Phe monomers in the lipid bilayer only become optically observable after water has begun to hydrate the lipid backbone. Literature reports a similar lifetime of L-Phe when in a conformationally/rotationally restricted polypeptide [84], we assign this lifetime to L-Phe being in a restrictive environment within the polar headgroups of the bilayer. The backbone region of the bilayer is intrinsically polar and aprotic until membrane hydration begins. Membrane hydration leads to this region of the bilayer becoming a polar, protic solvation environment similar to that of bulk methanol. This switch in the local solvation environment causes a 5.5-fold increase in L-Phe's quantum yield rendering these amino acids optically observable. The generality of this effect was tested by performing similar experiments with other lipid vesicle systems, being DMPC (14:0), DSPC (18:0) and DLPC (12:0) measuring the appearance of the lifetime around

$T_{gel\text{-}lc}$ for each lipid. The behavior observed was general: L-Phe's rotamer lifetime in both DMPC and DSPC bilayers began contributing to the emission decay near each lipid's $T_{gel\text{-}lc}$. For the shortest lipid tested, DLPC, experiments detected no affinity of L-Phe for DLPC bilayers although these experiments were complicated by DLPC's low $T_{gel\text{-}LC}$ (-2˚C).

Chapter 3 described experiments examining how low concentrations of PFOA, a regulated 'forever chemical' and environmental pollutant, impacts the structure and function of lipid bilayer vesicles. Due to recent EPA regulatory limits set in 2024 putting the maximum allowable amount of PFAS in drinking water at 4ppt (~4 nM), this study focused on solutions having low PFOA concentrations. Results were consistent and reliable for 100 nM PFOA solutions, and while this concentration is still 25x higher than regulatory limits, it is ~2-4 *orders of magnitude* lower than concentrations used in most literature studies [148, 150]. Results from several analytical techniques including DSC, DLS, Cryo-EM, and TCSPC showed the drastic effects that PFOA can cause to DPPC vesicles. DSC measurements showed that PFOA lowered the enthalpy of the lipid bilayer gel-liquid crystalline transition at concentrations as low as *100 pM*. At micromolar PFOA concentrations, $\Delta H_{gel\text{-}LC}$ was diminished by 25% from its original value. DLS studies revealed that the lipid vesicles undergo a size increase with the presence of 100 nM PFOA, and also revealed unknown structures which having 50 nm diameters compared to the ~115 nm vesicles. Cryo-EM confirmed the DLS measurements of increasing average vesicle size, and confirmed the presence of the ~50 nm size particles that were determined to be structurally similar to niosomes. Niosomes are typically comprised of a lipid, cholesterol, and a surfactant, but with surfactant concentrations that are much higher than the 100nM PFOA concentrations used in these experiments. Cryo-EM results also showed that the 100 nM PFOA

induces structural changes in unilamellar DPPC vesicles with more facets, larger sizes, and thinner bilayers, as well as an increase in the presence of multilamellar vesicles when 100 nM PFOA is present. TCSPC experiments examined the effect of secondary solute partitioning in PFOA-containing DPPC vesicle solutions. Results showed that 100 nM PFOA caused membrane hydration well below $T_{gel\text{-}lc}$, and PFOA also increased in secondary solute partitioning into the bilayer's hydrophobic acyl chain interior by ~30% compared to the PFOA-free control.

Chapter 4 of this dissertation expanded the bioconcentration targets for PFOA, and considered the protein Human Hemoglobin (Hb) as a target for PFOA to accumulate and be transported throughout the human body. PFOA affinity for other proteins such as Bovine Serum Albumin and Human Serum Albumin has been examined in literature, [186-188] but very little information was known about how PFOA interacted with and affected Hb. Studies that did examine Hb as a target failed to quantify the number of PFOA molecules bound to the protein. Chapter 4 in this dissertation shows how TCSPC was able to determine structural changes to the protein when PFOA concentrations reached ~300 μM based on changes to the native Trp fluorescence quenching mechanism. As increasing amounts of PFOA is titrated into a Hb solution, time resolved emission shows a switch from Förster Resonance Energy Transfer to fluorescence quenching via the peptide backbone. Native mass spectrometry experiments were performed to identify the conformation and stability of the protein with PFOA present. Data showed that at concentrations as low as 10 nM, two PFOA molecules are bound to the protein with small changes apparent in the protein conformation. At a molar ratio of 1:4 PFOA to Hb, upwards of six PFOA molecules are bound, and significant structural changes are taking place. Specifically, there are two distinct conformations uncovered by drift-time experiments, as well as

loss of alpha subunits and heme ejection from the protein. These structural changes confirm the TCSPC results, because if heme is being lost from the protein, some Trp residues must fluorescence through different mechanisms other that FRET. This study confirms that Hb is a bioconcentration target for PFOA even at low PFOA concentrations, and the changes PFOA induces in Hb are likely to impact Hb function.

Future Directions

The work described in Chapter 2 studied the effect of L-Phe partitioning into lipid bilayer vesicles, and displaying fluorescence of a rotamer state not previously characterized. The idea behind this study was to analyze the partitioning behavior of biologically relevant solutes and to increase the complexity of membranes so that they are more akin to actual biological cells containing membrane proteins. This intent sparked a study that began analyzing various dipeptide and polypeptides containing L-Phe as a residue. Our proposed experiments entail characterizing three polypeptides being Isoleucine-Phenylalanine (Iso-Phe), Phenylalanine-phenylalanine (Phe-Phe), and Isoleucine-Phenylalanine-Isoleucine (Iso-Phe-Iso). The purpose of these studies will be to analyze the partitioning behavior of the polypeptides with lipid bilayer vesicles as described in Chapter 2, to understand how linking Phe – a hydrophilic residue – to Iso – a hydrophobic residue – changes the distribution of the peptide within a membrane and rotamer states of Phe when conformationally restricted by both the lipid bilayer interior *and* other peptides. Preliminary TCSPC experiments in both bulk solvents and a DPPC vesicle solution displayed a fluorescence decay that can be described with two lifetimes, one short referred to as τ_1, and one long referred to as τ_2 and can be visibly seen in Figures 5.1-5.3.

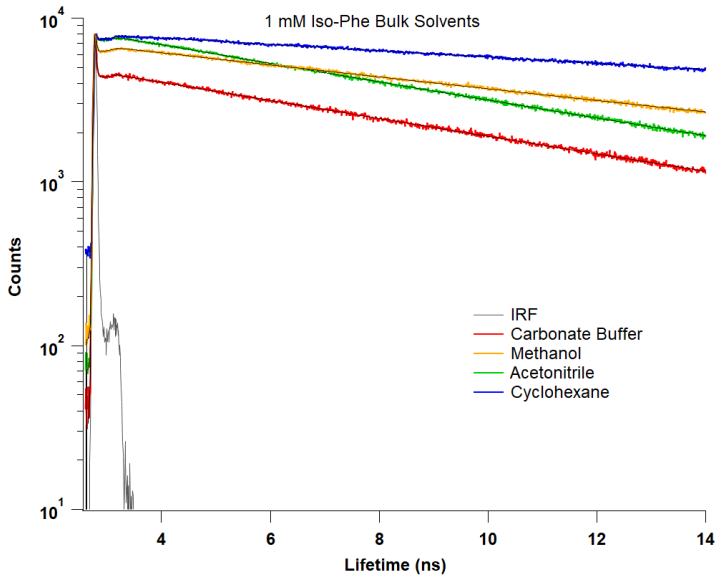

Figure 5.5. TCPSC fluorescence decay of 1 mM Iso-Phe in bulk solvents. An early decay can be seen, typically associated with fluorescence quenching, followed by a long lifetime reminiscent of free L-Phe.

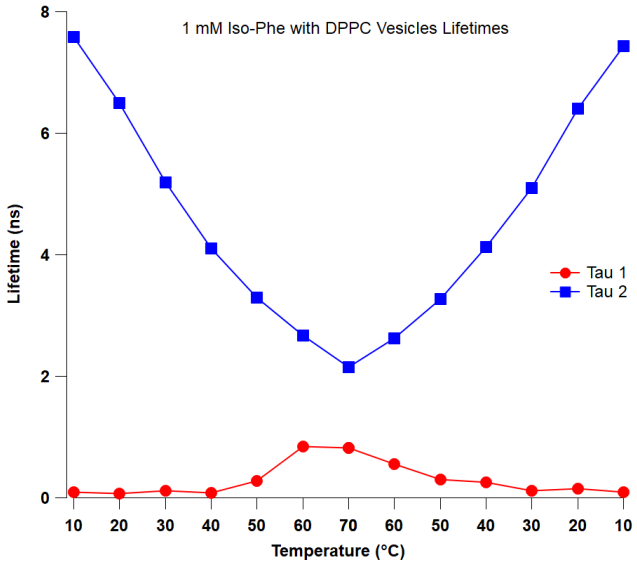

Figure 5.6. Results from fitting TCPSC decay traces from 1 mM Iso-Phe in a carbonate buffer solution containing DPPC Vesicles varying the temperature from 10-70-10°C. The short lifetime is present like it would be in a carbonate buffer, however this lifetime rises as temperature is

increased passed T_{gel-lc}, and becomes similair to the ~1.8 ns lifetime displayed in free L-Phe – DPPC solutions.

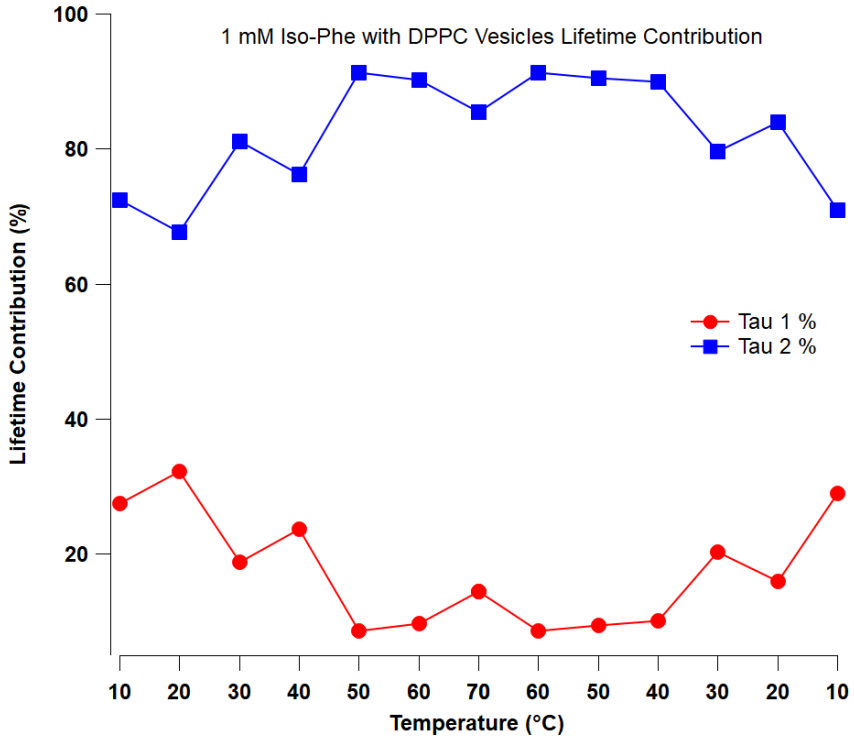

Figure 5.7. Lifetime contributions from the experiment described above. The short lifetime τ_1 begins at a relatively high percent contribution to the fluorescence at ~30%. As temperature is increased, and around T_{gel-lc}, the lifetime comprises less of the overall fluorescence as it switches to a longer lifetime.

Results from preliminary experiments show that simply attaching an Isoleucine to a Phenylalanine changes the fluorescence behavior as reflected in the bulk solvent data (Fig. 5.1-5.3). In DPPC vesicles solutions, Iso-Phe emission is described by two lifetimes: the long lifetime (τ_2) is attributed to L-Phe and is similar to free L-Phe discussed in Chapter 2. The short lifetime (τ_1) is present throughout the entire temperature range, as opposed to a solution with free L-Phe, in which the shorter lifetime doesn't appear until membrane hydration can take place. This lifetime could be due to free Iso-Phe in the surrounding aqueous environment. However, as

the temperature passes $T_{gel\text{-}lc}$, the lifetime begins to rise to ~1.5 ns, reminiscent of free L-Phe becoming optically visible. At the same time, the lifetime contribution from τ_1 begins at around 30% at low temperatures and only rises above $T_{gel\text{-}lc}$. A preliminary explanation for this behavior is that the Iso-Phe free in solution begins to partition into the bilayers after $T_{gel\text{-}LC}$. Experiments following the same procedure but using Phe-Phe and Iso-Phe-Iso may shed more light into this phenomenon.

Following the Chapter 3 work describing low concentration PFOA effects on lipid bilayer vesicles, experiments exploring the effects of other PFAS chemicals would give insight into the compiled effects of PFAS on biological cells. The EPA has defined the PFAS family with a broad definition of “a molecule with two adjacent carbon atoms one of which is fully fluorinated while the other is at least partially fluorinated”. Given the size of the PFAS family (>12,000 distinct species) assuming that all PFAS have the same effects on biological membranes is naïve. In this study, we would test how chain length and head group impact DPPC bilayer behavior and secondary solute partitioning into DPPC vesicles. Perfluorobutane sulfonic acid (PFBS) and perfluorooctane sulfatonic acid (PFOS) would be the appropriate candidates to expand the original work that focused on PFOA. PFBS is a fully fluorinated four-carbon chain PFAS molecule with a sulfonate headgroup, while PFOS is a fully fluorinated eight-carbon chain with a sulfonate headgroup. PFOS, like PFOA, is now considered a legacy PFAS molecule, no longer being manufactured for commercial use, while PFBS is a replacement molecule and still used worldwide. Experiments described in Chapter 3 attribute PFOA’s large effects on lipid bilayers to PFOA being integrated into the membrane when formation takes place, due to its similar

structure to the lipid, allowing to be part of the membrane during formation and disrupting the chain-chain interactions which would normally stabilize the membrane.

Recent studies done by our group have examined how both PFBS and PFOS (at 100 nM concentrations) impact $T_{gel\text{-}lc}$ and $\Delta H_{gel\text{-}lc}$, of lipid bilayers. Both sulfonate PFAS lower the transition enthalpy but do not change the transition temperature. In this respect, both solutes behave similarly to PFOA. Further work would set out to test if PFBS and PFOS follow the same mechanism of bioconcentration and effects on secondary solute partitioning, using the well-established Coumarin 152 as a fluorescent probe in experiments similar to those described in Chapter 3.

Results of fluorescence lifetime experiments with PFBS and DPPC vesicles using C152 as a probe can be described by Figs 5.4 & 5.5. Referencing the TCSPC experiments Chapter 3, the lifetimes and lifetime contributions give information about not only where within the bilayer C152 is, but also how much of the C152 is within a given local solvation environment, surrounding aqueous, polar headgroups, or non-polar tails. Tau (τ) 1, 2, and 3 are representative of C152 in the aqueous environment, polar headgroup, and non-polar acyl chains respectively. T_2 is slightly more complicated due to the phase transition $T_{gel\text{-}lc}$, where a lifetime of 2.2 ns represents a polar aprotic headgroup and a lifetime of 1.1 is attributed to polar protic headgroups.

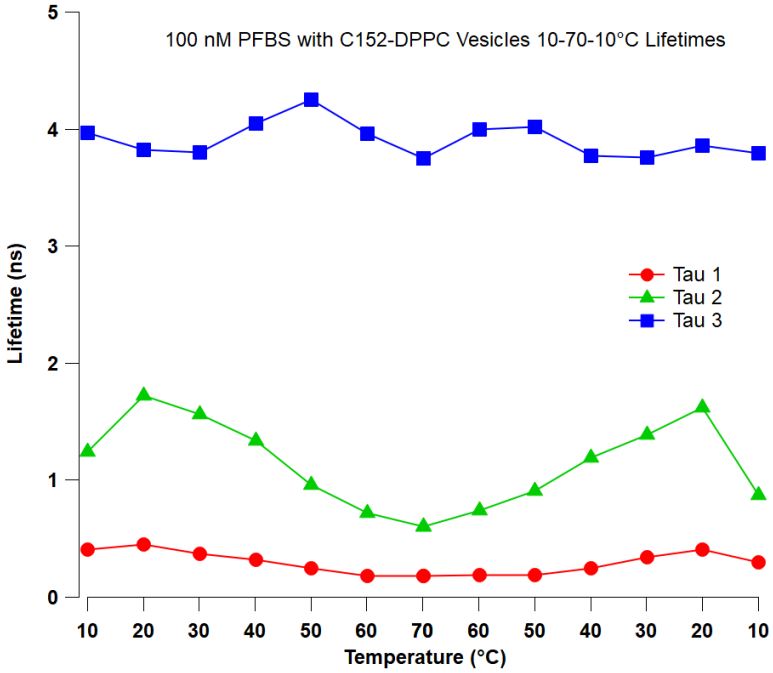

Figure 5.8. Lifetimes fit from TCSPC decay traces of a solution containing DPPC vesicles, C152, and 100 nM PFBS. Compared to a solution with just C152-DPPC, τ_2, an indicator of membrane hydration, shows a polar protic lifetime suggesting PFBS is causing membrane hydration at temperature below $T_{gel\text{-}lc}$, similar to the behavior of PFOA.

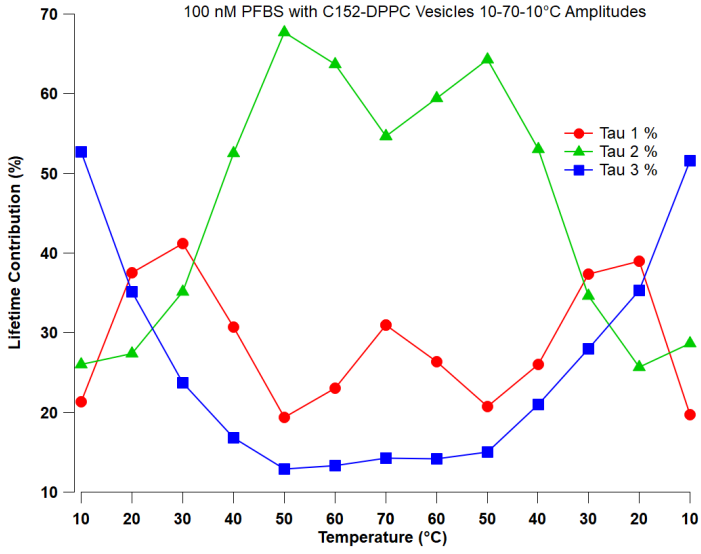

Figure 5.9. Lifetime contributions from the experiment described above. Initially, τ_3, which is attributed to C152 in a non-polar environment comprises a majority of the fluorescence, while τ_1

and τ_2 are both lower. However, as temperature increases, the contribution from τ_3 quickly decreases, while τ_2 increases.

Similar to PFOA, PFBS appears to induce membrane hydration at temperature well below $T_{gel\text{-}lc}$ according to the ~1.2 ns lifetime at 10°C, but raises to a 1.8 ns lifetime at 20°C. From there τ_2 follows the trend of just C152 with DPPC vesicles. The τ_3 lifetime contribution shows that a majority of the C152 is within the non-polar tails of the DPPC bilayer at 10°C, but thischanges rapidly as the temperature increases. Interestingly, this rapid drop is paired with a modest increase in the τ_2 lifetime contribution before $T_{gel\text{-}Lc}$, suggesting that the C152 is migrating into the polar backbone region as opposed to staying in the non-polar solvation environment created by DPPC's acyl tails. In this respect, PFBS effects appear very similar to those of PFOA described in Chapter 3. Since PFBS is a smaller chain molecule, this behavior can be explained by the size of the PFAS molecule. While PFBS might initially integrate with the membrane in a similar manner to PFOA and associate with the polar headgroups, the length of the molecule will reduce the impact it has on the bilayer, as PFBS will have less access to associate with the lipids acyl chains. At lower temperatures, in the gel state of the lipid, it is more likely that PFBS will associate closer to the polar headgroups with the sulfonate headgroup altering membrane hydration at lower temperatures. As temperature increases and DPPC begin to melt, PFBS become less likely to be associated with the headgroups or acyl chains, and would free itself into the surrounding environment. However, the PFBS that does remain causes C152 to associate with the polar headgroups at a temperature lower than $T_{gel\text{-}lc}$, where this transition would normally occur. [77]

Similar experiments have been tested using PFOS instead of PFBS, however the spectra acquired resembles a pure C152-DPPC spectra, with hardly any significant changes to the

lifetimes and amplitudes of C152 in the local solvation environments. While it is seemingly unlikely, this could be attributed to PFOS not being integrated into the lipid bilayer as assembly occurs, due to the head group or tail length. Additional work also should consider experiments containing just C152 and higher concentrations of PFAS in a buffer to see if the fluorinated compounds associate with C152 freely in solution.

Inspired by the changes in fluorescence of Human Hemoglobin discussed in Chapter 4, a logical next study would analyze the fluorescence behavior of a simpler protein, Cytochrome C (Cyt C) at low PFOA concentrations. Cytochrome C is a heme-based protein and plays an important role in biological electron transfer [198, 199]. Multiple reports have shown that ionic surfactants interact very strongly with oppositely charged proteins when performed using sodium dodecyl sulfate (SDS) being one of the most common surfactants used [200, 201]. Studies have looked into the harmful effects of PFAS surfactants on total cells, and one paper found that PFOS exposure can lead to mitochondrial membrane damage, CytC release and collapse of the mitochondrial membrane potential [202]. However, direct observation of CytC with PFAS has very little information. Due to the importance of electron-transfer in biological systems, CytC, becomes an important target for analysis with the PFAS family as a possible bioconcentration target, and can also give more information about the fluorescence quenching behavior discussed in chapter 4. A series of experiments similar to those described in Chapter 4 would further clarify how Trp fluorescence changes in the presence of PFOA, PFBS, and PFOS and identify how these forever chemicals impact the structure and, inferentially, function of biologically important proteins. Additional experiments using CD spectroscopy would be helpful for determining changes to the protein backbone with increasing PFAS concentrations.

REFERENCES CITED

(1) Chiou, C. T. F., V. H.; Schmedding, D. W.;Kohnert, R. L. Partition Coeffecient and Bioaccumulation of Selected Organic Chemicals. Enironmental Science and Technology 1977, 11 (5), 475-478.

(2) Alengebawy, A.; Abdelkhalek, S. T.; Qureshi, S. R.; Wang, M. Q. Heavy Metals and Pesticides Toxicity in Agricultural Soil and Plants: Ecological Risks and Human Health Implications. *Toxics* **2021**, *9* (3). DOI: 10.3390/toxics9030042 From NLM PubMed-not-MEDLINE.

(3) Gupta, N.; Yadav, K. K.; Kumar, V.; Kumar, S.; Chadd, R. P.; Kumar, A. Trace elements in soil-vegetables interface: Translocation, bioaccumulation, toxicity and amelioration - A review. *Sci Total Environ* **2019**, *651* (Pt 2), 2927-2942. DOI: 10.1016/j.scitotenv.2018.10.047 From NLM Medline.

(4) Klunemann, M.; Andrejev, S.; Blasche, S.; Mateus, A.; Phapale, P.; Devendran, S.; Vappiani, J.; Simon, B.; Scott, T. A.; Kafkia, E.; et al. Bioaccumulation of therapeutic drugs by human gut bacteria. *Nature* **2021**, *597* (7877), 533-538. DOI: 10.1038/s41586-021-03891-8 From NLM Medline.

(5) Arnot, J. A.; Gobas, F. A. P. C. A review of bioconcentration factor (BCF) and bioaccumulation factor (BAF) assessments for organic chemicals in aquatic organisms. *Environmental Reviews* **2006**, *14* (4), 257-297. DOI: 10.1139/a06-005.

(6) Hoffman, D. J. R. B., A; Burton Jr., G. Allen; Cairns Jr., John. *Handbook of Exotoxicology*; Lewis Publishers, 2003.

(7) Gobas, F. A.; Lahittete, J. M.; Garofalo, G.; Wan, Y. S.; Mackay, D. A Novel Method for Measuring Membrane-Water Partition-Coefficients of Hydrophobic Organic Chemicals - Comparison with 1-Octanol-Water Partitioning. *Journal of Pharmaceutical Sciences* **1988**, *77* (3), 265-272. DOI: 10.1002/jps.2600770317.

(8) Chamberlain, K.; Evans, A. A.; Bromilow, R. H. 1-Octanol/Water Partition Coefficient (Kow) and pKafor Ionisable Pesticides Measured by apH-Metric Method. *Pesticide Science* **1996**, *47* (3), 265-271. DOI: 10.1002/(sici)1096-9063(199607)47:3<265::Aid-ps416>3.0.Co;2-f.

(9) Krishnamoorthy, G.; Alluvada, P.; Alemayehu, E.; Mohammed Sherieff, S. H.; Addi, W. A.; Kwa, T.; Krishnamoorthy, J. Log D analysis using dynamic approach. *Biochem Biophys Rep* **2018**, *16*, 1-11. DOI: 10.1016/j.bbrep.2018.07.006 From NLM PubMed-not-MEDLINE.

(10) J;, D. W. J. G. H. A. Solubility and Micelle-water Partitioning of Polyschlorinated Biphenyls in Solutions of Bile Salt Micelles. *Chemosphere* **1994**, *30* (2), 293-306.

(11) Droge, S. T. J.; Hodges, G.; Bonnell, M.; Gutsell, S.; Roberts, J.; Teixeira, A.; Barrett, E. L. Using membrane-water partition coefficients in a critical membrane burden approach to aid the identification of neutral and ionizable chemicals that induce acute toxicity below narcosis levels.

Environ Sci Process Impacts **2023**, *25* (3), 621-647. DOI: 10.1039/d2em00391k From NLM Medline.

(12) Lipinski, C. A.; Lombardo, F.; Dominy, B. W.; Feeney, P. J. Experimental and computational approaches to estimate solubility and permeability in drug discovery and development settings. *Adv. Drug Deliv. Rev.* **2001**, *46* (1-3), 3-26. DOI: 10.1016/s0169-409x(00)00129-0.

(13) Sun, Y.; Hou, T.; He, X.; Man, V. H.; Wang, J. Development and test of highly accurate endpoint free energy methods. 2: Prediction of logarithm of n-octanol-water partition coefficient (logP) for druglike molecules using MM-PBSA method. *J Comput Chem* **2023**, *44* (13), 1300-1311. DOI: 10.1002/jcc.27086 From NLM PubMed-not-MEDLINE.

(14) Zhang, Y.; Chen, Y.; Chen, H.; Zhang, Y.; Yang, L.; Zhong, W.; Zhu, L. Direct evidence of the important role of proteins in bioconcentration and biomagnification of PFASs in benthic organisms based on comparison with OPEs. *Sci Total Environ* **2023**, *863*, 161012. DOI: 10.1016/j.scitotenv.2022.161012 From NLM Medline.

(15) Tanee, T.; Chaveerach, A.; Sudmoon, R.; Teanma, J.; Ragsasilp, A.; Sirikhansaeng, P. Heavy Metal Accumulation and DNA Changes in Plants Around an Electronic Waste Dumpsite Suggested Environmental Management Plan. *Environmental Claims Journal* **2018**, *30* (2), 131-141. DOI: 10.1080/10406026.2018.1427961.

(16) Alhankawi, A. R.; Al-Husseini, J. K.; Spindler, A.; Baker, C.; Shoniwa, T. T.; Ahmed, M.; Chiarelli, P. A.; Johal, M. S. The Relationship between Hydrophobicity and Drug-Protein Binding in Human Serum Albumin: A Quartz Crystal Microbalance Study. *Biophysica* **2022**, *2* (2), 113-120. DOI: 10.3390/biophysica2020012.

(17) Fasano, M.; Curry, S.; Terreno, E.; Galliano, M.; Fanali, G.; Narciso, P.; Notari, S.; Ascenzi, P. The extraordinary ligand binding properties of human serum albumin. *IUBMB Life* **2005**, *57* (12), 787-796. DOI: 10.1080/15216540500404093 From NLM Medline.

(18) J-P., S. B. Z. R. M. C.-V. T. N. T. Separation procedures used to reveal and follow drug-protein binding. *Journal of Chromatography* **1990**, *531*, 51-77.

(19) Nicolson, G. L. The Fluid-Mosaic Model of Membrane Structure: still relevant to understanding the structure, function and dynamics of biological membranes after more than 40 years. *Biochim. Biophys. Acta* **2014**, *1838* (6), 1451-1466. DOI: 10.1016/j.bbamem.2013.10.019.

(20) Nickels, J. D.; Smith, M. D.; Alsop, R. J.; Himbert, S.; Yahya, A.; Cordner, D.; Zolnierczuk, P.; Stanley, C. B.; Katsaras, J.; Cheng, X.; et al. Lipid Rafts: Buffers of Cell Membrane Physical Properties. *J Phys Chem B* **2019**, *123* (9), 2050-2056. DOI: 10.1021/acs.jpcb.8b12126 From NLM Medline.

(21) Ricchelli, F. J. G. G. S. T. M. Liposomes as models to study the distribution of porphyrins in cell membranes. *Biochimica et Biophysica Acta (BBA) - Biomembranes* **1991**, *1065* (1).

(22) Drabik, D.; Chodaczek, G.; Kraszewski, S.; Langner, M. Mechanical Properties Determination of DMPC, DPPC, DSPC, and HSPC Solid-Ordered Bilayers. *Langmuir* **2020**, *36* (14), 3826-3835. DOI: 10.1021/acs.langmuir.0c00475 From NLM PubMed-not-MEDLINE.

(23) Akbarzadeh. A.; Rezaei-Sabady. R.; Davaran, S. J. S. W. Z. N. H. Y. S. M. K., M.; Nejati-Koshki. K. Liposome: classification, preparation, and applications. *Nanoscale Research Letters* **2013**, *8* (102).

(24) Leekumjorn, S.; Sum, A. K. Molecular studies of the gel to liquid-crystalline phase transition for fully hydrated DPPC and DPPE bilayers. *Biochim Biophys Acta* **2007**, *1768* (2), 354-365. DOI: 10.1016/j.bbamem.2006.11.003 From NLM Medline.

(25) Leroy, E.; Lami, H.; Laustria.G. Fluorescence Lifetime and Quantum Yield of Phenylalanine Aqueous Solutions. Temperature and Concentration Effects. *Photochem Photobiol* **1971**, *13* (5), 411-421. DOI: DOI 10.1111/j.1751-1097.1971.tb06132.x.

(26) Chen, R. F. Fluorescence Quantum Yields of Tryptophan and Tyrosine. *Anal. Lett.* **1967**, *1* (1), 35-42. DOI: 10.1080/00032716708051097.

(27) Dahiya, P.; Kumbhakar, M.; Mukherjee, T.; Pal, H. Effect of protic solvents on twisted intramolecular charge transfer state formation in coumarin-152 and coumarin-481 dyes. *Chemical Physics Letters* **2005**, *414* (1-3), 148-154. DOI: 10.1016/j.cplett.2005.08.051.

(28) Chen, J.; Toptygin, D.; Brand, L.; King, J. Mechanism of the Efficient Tryptophan Fluorescence Quenching in Human γD-Crystallin Studied by Time-Resolved Fluorescence†. *Biochemistry* **2008**, *47*, 10705-10721. DOI: 10.1021/bi800499k.

(29) Osysko, A. P.; Muíño, P. L. Fluorescence quenching of tryptophan and tryptophanyl dipeptides in solution. *Journal of Biophysical Chemistry* **2011**, *02* (03), 316-321. DOI: 10.4236/jbpc.2011.23036.

(30) Carolina Bosch Cabral , H. I., Jose Cesar Rosa , Helen Julie Laure ,´Carlos Henrique Tomich de Paula da Silva , Marcel Tabak , Richard Charles Garratt , Lewis Joel Greene. Fluorescence properties of tryptophan residues in the monomeric d-chain of Glossoscolex paulistus hemoglobin: an interpretation based on a comparative molecular model. *Biophysical Chemistry* **2002**, *97*, 139-157.

(31) Jenkins, A.; Andreasen, A.; Trudell, J. R.; Harrison, N. L. Tryptophan scanning mutagenesis in TM4 of the GABA(A) receptor alpha 1 subunit: implications for modulation by inhaled anesthetics and ion channel structure. *Neuropharmacology* **2002**, *43* (4), 669-678. DOI: 10.1016/s0028-3908(02)00175-2.

(32) Patel, A. J.; Honore, E.; Lesage, F.; Fink, M.; Romey, G.; Lazdunski, M. Inhalational anesthetics activate two-pore-domain background K+ channels. *Nature Neuroscience* **1999**, *2* (5), 422-426. DOI: 10.1038/8084.

(33) Choucair, A.; Chakrapani, M.; Chakravarthy, B.; Katsaras, J.; Johnston, L. J. Preferential accumulation of A beta(1-42) on gel phase domains of lipid bilayers: An AFM and fluorescence study. *Biochimica Et Biophysica Acta-Biomembranes* **2007**, *1768* (1), 146-154. DOI: 10.1016/j.bbamem.2006.09.005.

(34) Gaschler, M. M.; Stockwell, B. R. Lipid peroxidation in cell death. *Biochemical and Biophysical Research Communications* **2017**, *482* (3), 419-425. DOI: 10.1016/j.bbrc.2016.10.086.

(35) Rochette, L.; Dogon, G.; Rigal, E.; Zeller, M.; Cottin, Y.; Vergely, C. Lipid Peroxidation and Iron Metabolism: Two Corner Stones in the Homeostasis Control of Ferroptosis. *International Journal of Molecular Sciences* **2023**, *24* (1). DOI: 10.3390/ijms24010449.

(36) Xie, Y.; Hou, W.; Song, X.; Yu, Y.; Huang, J.; Sun, X.; Kang, R.; Tang, D. Ferroptosis: process and function. *Cell Death and Differentiation* **2016**, *23* (3), 369-379. DOI: 10.1038/cdd.2015.158.

(37) Leo, A.; Hansch, C.; Elkins, D. Partition coefficients and their uses. *Chem. Rev.* **1971**, *71* (6), 525-616. DOI: 10.1021/cr60274a001.

(38) Lipinski, C. A. Drug-like properties and the causes of poor solubility and poor permeability. *J Pharmacol Toxicol Methods* **2000**, *44* (1), 235-249. DOI: 10.1016/s1056-8719(00)00107-6.

(39) Ginex, T.; Vazquez, J.; Gilbert, E.; Herrero, E.; Luque, F. J. Lipophilicity in drug design: an overview of lipophilicity descriptors in 3D-QSAR studies. *Future Medicinal Chemistry* **2019**, *11* (10), 1177-1193. DOI: 10.4155/fmc-2018-0435.

(40) Hilal, S. H.; Karickhoff, S. W.; Carreira, L. A. Prediction of the solubility, activity coefficient and liquid/liquid partition coefficient of organic compounds. *Qsar & Combinatorial Science* **2004**, *23* (9), 709-720. DOI: 10.1002/qsar.200430866.

(41) Labute, P. A widely applicable set of descriptors. *Journal of Molecular Graphics & Modelling* **2000**, *18* (4-5), 464-477. DOI: 10.1016/s1093-3263(00)00068-1.

(42) Liang, Y. Z.; Kuo, D. T. F.; Allen, H. E.; Di Toro, D. M. Experimental determination of solvent-water partition coefficients and Abraham parameters for munition constituents. *Chemosphere* **2016**, *161*, 429-437. DOI: 10.1016/j.chemosphere.2016.07.028.

(43) Singer, S. J. N., G.L. The Fluid Mosaid Model of the Structure of Cell Membranes. *Science* **1972**, *175*, 720-731.

(44) Gleason, N. J.; Vostrikov, V. V.; Greathouse, D. V.; Koeppe, R. E. Buried lysine, but not arginine, titrates and alters transmembrane helix tilt. *Proceedings of the National Academy of Sciences of the United States of America* **2013**, *110* (5), 1692-1695. DOI: 10.1073/pnas.1215400110.

(45) Hong, H.; Rinehart, D.; Tamm, L. K. Membrane Depth-Dependent Energetic Contribution of the Tryptophan Side Chain to the Stability of Integral Membrane Proteins. *Biochemistry* **2013**, *52* (25), 4413-4421. DOI: 10.1021/bi400344b.

(46) Vostrikov, V. V.; Hall, B. A.; Sansom, M. S. P.; Koeppe, R. E. Accommodation of a Central Arginine in a Transmembrane Peptide by Changing the Placement of Anchor Residues. *Journal of Physical Chemistry B* **2012**, *116* (43), 12980-12990. DOI: 10.1021/jp308182b.

(47) Piotto, S.; Di Biasi, L.; Sessa, L.; Concilio, S. Transmembrane Peptides as Sensors of the Membrane Physical State. *Frontiers in Physics* **2018**, *6*. DOI: 10.3389/fphy.2018.00048.

(48) Zeno, W. F.; Thatte, A. S.; Wang, L. P.; Snead, W. T.; Lafer, E. M.; Stachowiak, J. C. Molecular Mechanisms of Membrane Curvature Sensing by a Disordered Protein. *Journal of the American Chemical Society* **2019**, *141* (26), 10361-10371. DOI: 10.1021/jacs.9b03927.

(49) Perkins, R.; Vaida, V. Phenylalanine Increases Membrane Permeability. *J. Am. Chem. Soc.* **2017**, *139* (41), 14388-14391. DOI: 10.1021/jacs.7b09219.

(50) Nandi, S.; Pyne, A.; Ghosh, M.; Banerjee, P.; Ghosh, B.; Sarkar, N. Antagonist Effects of l-Phenylalanine and the Enantiomeric Mixture Containing d-Phenylalanine on Phospholipid Vesicle Membrane. *Langmuir* **2020**, *36* (9), 2459-2473. DOI: 10.1021/acs.langmuir.9b03543.

(51) Nandi, S.; Ghosh, B.; Ghosh, M.; Layek, S.; Nandi, P. K.; Sarkar, N. Phenylalanine Interacts with Oleic Acid-Based Vesicle Membrane. Understanding the Molecular Role of Fibril-Vesicle Interaction under the Context of Phenylketonuria. *J. Phys. Chem. B* **2021**, *125* (34), 9776-9793. DOI: 10.1021/acs.jpcb.1c05592.

(52) Griffith, E. C.; Perkins, R. J.; Telesford, D. M.; Adams, E. M.; Cwiklik, L.; Allen, H. C.; Roeselova, M.; Vaida, V. Interaction of L-Phenylalanine with a Phospholipid Monolayer at the Water-Air Interface. *J. Phys. Chem. B* **2015**, *119* (29), 9038-9048. DOI: 10.1021/jp508473w.

(53) Duncan, K. M.; Steel, W. H.; Walker, R. A. Amino acids change solute affinity for lipid bilayers. *Biophys. J.* **2021**, *120* (17), 3676-3687. DOI: 10.1016/j.bpj.2021.07.021.

(54) Cutro, A. C.; Disalvo, E. A. Phenylalanine Blocks Defects Induced in Gel Lipid Membranes by Osmotic Stress. *J. Phys. Chem. B* **2015**, *119* (31), 10060-10065. DOI: 10.1021/acs.jpcb.5b05590.

(55) Chakrabarti, A. C. Permeability of membranes to amino acids and modified amino acids: Mechanisms involved in translocation. *J. Amino Acids* **1994**, *6*, 213-229.

(56) Chakrabarti, A. C. D., D.W. Permeability of lipid bilayers to amino acids and phosphate. *Biochim. Biophys. Acta* **1992**, *1111*, 171-177.

(57) Cutro, A. C.; Disalvo, E. A.; Frias, M. A. Effects of Phenylalanine on the Liquid-Expanded and Liquid-Condensed States of Phosphatidylcholine Monolayers. *Lipid Insights* **2019**, *12*, 1-9. DOI: 10.1177/1178635318820923.

(58) Johansson, A. C.; Lindahl, E. The role of lipid composition for insertion and stabilization of amino acids in membranes. *J. Chem. Phys.* **2009**, *130* (18), 185101. DOI: 10.1063/1.3129863.

(59) MacCallum, J. L.; Bennett, W. F.; Tieleman, D. P. Distribution of amino acids in a lipid bilayer from computer simulations. *Biophys. J.* **2008**, *94* (9), 3393-3404. DOI: 10.1529/biophysj.107.112805.

(60) Rosa, A. S.; Cutro, A. C.; Frias, M. A.; Disalvo, E. A. Interaction of Phenylalanine with DPPC Model Membranes: More Than a Hydrophobic Interaction. *J. Phys. Chem. B* **2015**, *119* (52), 15844-15847. DOI: 10.1021/acs.jpcb.5b08490.

(61) White, S. H. W., W, C. Hydrophobic interactions of peptides with membarne interfaces. *Biochim. Biophys. Acta* **1998**, *1376*, 339-352.

(62) Bent, D. V. H., E. Excited State Chemistry of Aromatic Amino Acids and Related Peptides. II. Phenylanine. *J. Am. Chem. Soc.* **1974**, *97(10)*, 2606-2612.

(63) Mittal, L. J.; Mittal, J. P.; Hayon, E. Primary processes in the photochemistry of phenylalanine and derivatives in aqueous solution. Biphotonic photoionization and photodissociation reactions. *J. Am. Chem. Soc.* **2002**, *95* (19), 6203-6210. DOI: 10.1021/ja00800a009.

(64) Mittal, L. J. M., J.P.; Hayon, E. Biphotonic photodissociation of phenylalanine in aqueous solutions at 20 °C. *Chem. Phys. Lett.* **1973**, *18*, 319-322.

(65) Chin, K. K. T.-S., C.C.; McCallum, J.; Jockusch, S.; Turro, N.J.; Scaiano, J.C.; Foote, C.S.; Garcia-Garibay, M.A. Quantitative Determination of Singlet Oxygen Generate4d by Excited State Aromatic Amino Acids, Proteins, and Immunoglobulins. *J. Am. Chem. Soc.* **2008**, *130*, 6912-6913.

(66) Gally, J. A. E., G.M. The Effect of Temperature on the Fluorescence of Some Aromatic Amino Acids and Proteins. *Biochim. Biophys. Acta* **1962**, *60*, 499-509.

(67) Lorenz, U. J.; Rizzo, T. R. Structural melting of an amino acid dimer upon intersystem crossing. *J. Am. Chem. Soc.* **2014**, *136* (42), 14974-14980. DOI: 10.1021/ja507981p.

(68) Omidyan, R.; Ataelahi, M.; Azimi, G. Excited-state deactivation mechanisms of protonated and neutral phenylalanine: a theoretical study. *RSC Adv.* **2015**, *5* (37), 29032-29039. DOI: 10.1039/c5ra00630a.

(69) Tournon, J. E.-B. A. Intramolecular Charge-Transfer Interactions in Benzyl Derivatives. *J. Chem. Phys.* **2015**, *56*, 5128-5134. DOI: 10.1063/1.4926998.

(70) Rzeska, A.; Stachowiak, K.; Malicka, J.; Lankiewicz, L.; Wiczk, W. Photophysics of phenylalanine analogues - Part 1. Constrained analogues of phenylalanine modified at phenyl ring. *J Photoch Photobio A* **2000**, *133* (1-2), 33-38. DOI: Doi 10.1016/S1010-6030(00)00229-X.

(71) Rzeska, A. M., J.; Stachowiak, K; ; Szymariska, A.; Lankiewicz, L.; Wiczk, W. Photophysics of phenylalanine analogues Part 2. Linear analogues of phenylalanine. *J Photoch Photobio A* **2001**, *140* (1), 21-26. DOI: Doi 10.1016/S1010-6030(01)00394-X.

(72) MacCallum, J. L.; Bennett, W. F. D.; Tieleman, D. P. Distribution of amino acids in a lipid bilayer from computer simulations. *Biophysical Journal* **2008**, *94* (9), 3393-3404. DOI: 10.1529/biophysj.107.112805.

(73) Alanso, A. G., Felix M. Effect of Detergents and Fusogenic Lipids on Phospholipid Phase Transitions. *J. Membr. Biol.* **1983**, *71*, 183-187.

(74) Chapman, D. U., J.; Keough, K.M. Biomembrane Phase Transitions. *J. Biol. Chem.* **1974**, *249*, 2512-2521.

(75) Jain, M. K. W., Nora Min. Effect of Small Molecules on the Dipalmitoyl Lecthin Liposomal Bilayer: III. Phase Transition in Lipid Bilayer. *J. Membrane Biol.* **1977**, *34*, 157-201.

(76) Link, K. A.; Spurzem, G. N.; Tuladhar, A.; Chase, Z.; Wang, Z.; Wang, H.; Walker, R. A. Cooperative Adsorption of Trehalose to DPPC Monolayers at the Water-Air Interface Studied with Vibrational Sum Frequency Generation. *J Phys Chem B* **2019**, *123* (42), 8931-8938. DOI: 10.1021/acs.jpcb.9b07770.

(77) Duncan, K. M.; Casey, A.; Gobrogge, C. A.; Trousdale, R. C.; Piontek, S. M.; Cook, M. J.; Steel, W. H.; Walker, R. A. Coumarin Partitioning in Model Biological Membranes: Limitations of logP as a Predictor. *J. Phys. Chem. B* **2020**, *124* (38), 8299-8308. DOI: 10.1021/acs.jpcb.0c06109.

(78) Gobrogge, C. A.; Blanchard, H. S.; Walker, R. A. Temperature-Dependent Partitioning of Coumarin 152 in Phosphatidylcholine Lipid Bilayers. *J. Phys. Chem. B* **2017**, *121* (16), 4061-4070. DOI: 10.1021/acs.jpcb.6b10893.

(79) Gobrogge, C. A.; Walker, R. A. Quantifying Solute Partitioning in Phosphatidylcholine Membranes. *Analytical Chemistry* **2017**, *89* (22), 12587-12595. DOI: 10.1021/acs.analchem.7b03964.

(80) de Vries, A. H.; Yefimov, S.; Mark, A. E.; Marrink, S. J. Molecular structure of the lecithin ripple phase. *Proc. Natl. Acad. Sci. U.S.A.* **2005**, *102* (15), 5392-5396. DOI: 10.1073/pnas.0408249102.

(81) Chen, W.; Dusa, F.; Witos, J.; Ruokonen, S. K.; Wiedmer, S. K. Determination of the Main Phase Transition Temperature of Phospholipids by Nanoplasmonic Sensing. *Sci. Rep.* **2018**, *8* (1), 14815. DOI: 10.1038/s41598-018-33107-5.

(82) Lentz, B. R.; Freire, E.; Biltonen, R. L. Fluorescence and calorimetric studies of phase transitions in phosphatidylcholine multilayers: kinetics of the pretransition. *Biochem.* **1978**, *17* (21), 4475-4480. DOI: 10.1021/bi00614a018.

(83) Leroy, E. L., H.; Laustrait, G. Fluorescence lifetime and quantum yield of phenylalanine aqueous solutions. Temperature and concentration effects. *J. Photochem. Photobiol.* **1971**, *13*, 411-421.

(84) Duneau, J. P. G., N.; Cremel, G.; Nullans, G.; Hubert, P.; Genest, D.; Vincent, M.; Gallay, J.; Genest, M. Time resolved fluorescence properties of phenylalanine in different environments. Comparison with molecular dynamics simulation. *Biophys. Chem.* **1993**, *73*, 109-119.

(85) Demetzos, C. Differential Scanning Calorimetry (DSC): a tool to study the thermal behavior of lipid bilayers and liposomal stability. *J. Liposome Res.* **2008**, *18* (3), 159-173. DOI: 10.1080/08982100802310261.

(86) Majhi, P. R. B., A. Temperature-Induced Micelle-Vesicle Transitions in DMPC-SDS and DMPC-DTAB Mixtures Studied by Calorimetry and Dynamic Light Scattering. *J. Phys. Chem. B* **2002**, *106*, 10753-10763.

(87) Olsztynska, S. K., M.; Dupuy, N. Influence of Near-Infrared Radiation on the pK_a values of L-Phenylalanine *J. Appl. Spectrosc.* **2006**, *60*, 648-652.

(88) Cavanaugh, J. R. The rotational isomerism of phenylalanine by nuclear magnetic resonance. *J. Am. Chem. Soc.* **1967**, *89* (7), 1558-1564. DOI: 10.1021/ja00983a004.

(89) Stephinewski, M. B., A.; Pasenkiewicz-Gierula, M.; Karttunen, M.; Rog, T. Effects of the Lipid Bilayer Phase State on the Water Membrane Interface. *J. Phys. Chem. B* **2010**, *114*, 11784-11792.

(90) Pasenkiewicz-Gierula, M.; Baczynski, K.; Markiewicz, M.; Murzyn, K. Computer modelling studies of the bilayer/water interface. *Biochim. Biophys. Acta* **2016**, *1858* (10), 2305-2321. DOI: 10.1016/j.bbamem.2016.01.024.

(91) Shinoda, W. Permeability across lipid membranes. *Biochem. Biophys. Acta* **2016**, *1858* (10), 2254-2265. DOI: 10.1016/j.bbamem.2016.03.032.

(92) Kucerka, N.; Nieh, M. P.; Katsaras, J. Fluid phase lipid areas and bilayer thicknesses of commonly used phosphatidylcholines as a function of temperature. *Biochim Biophys Acta* **2011**, *1808* (11), 2761-2771. DOI: 10.1016/j.bbamem.2011.07.022.

(93) Sunderland, E. M.; Hu, X. C.; Dassuncao, C.; Tokranov, A. K.; Wagner, C. C.; Allen, J. G. A review of the pathways of human exposure to poly- and perfluoroalkyl substances (PFASs) and present understanding of health effects. *J Expo Sci Environ Epidemiol* **2019**, *29* (2), 131-147. DOI: 10.1038/s41370-018-0094-1 From NLM Medline.

(94) Key EPA Actions to Address PFAS. https://www.epa.gov/newsreleases/biden-harris-administration-announces-new-steps-protect-communities-pfas-and-other (accessed February 2024).

(95) Brase, R. A.; Mullin, E. J.; Spink, D. C. Legacy and Emerging Per- and Polyfluoroalkyl Substances: Analytical Techniques, Environmental Fate, and Health Effects. *Int J Mol Sci* **2021**, *22* (3). DOI: 10.3390/ijms22030995 From NLM Medline.

(96) Fenton, S. E.; Ducatman, A.; Boobis, A.; DeWitt, J. C.; Lau, C.; Ng, C.; Smith, J. S.; Roberts, S. M. Per- and Polyfluoroalkyl Substance Toxicity and Human Health Review: Current State of Knowledge and Strategies for Informing Future Research. *Environ Toxicol Chem* **2021**, *40* (3), 606-630. DOI: 10.1002/etc.4890 From NLM Medline.

(97) Bell, E. M.; De Guise, S.; McCutcheon, J. R.; Lei, Y.; Levin, M.; Li, B.; Rusling, J. F.; Lawrence, D. A.; Cavallari, J. M.; O'Connell, C.; et al. Exposure, health effects, sensing, and remediation of

the emerging PFAS contaminants - Scientific challenges and potential research directions. *Sci Total Environ* **2021**, *780*, 146399. DOI: 10.1016/j.scitotenv.2021.146399 From NLM PubMed-not-MEDLINE.

(98) Brennan, N. M.; Evans, A. T.; Fritz, M. K.; Peak, S. A.; von Holst, H. E. Trends in the Regulation of Per- and Polyfluoroalkyl Substances (PFAS): A Scoping Review. *Int J Environ Res Public Health* **2021**, *18* (20). DOI: 10.3390/ijerph182010900 From NLM Medline.

(99) Gatz, L. Regulating PFAS Under the Clean Water Act. Service, C. R., Ed.; 2022.

(100) Agency, U. E. P. Biden-Harris Administration Finalizes First-Ever National Drinking Water Standard to Protext 100M People from PFAS Pollution. EPA Press Office 2024.

(101) Ahrens, L.; Bundschuh, M. Fate and effects of poly- and perfluoroalkyl substances in the aquatic environment: a review. *Environmental Toxicology and Chemistry* **2014**, *33* (9), 1921-1929. DOI: 10.1002/etc.2663.

(102) Wee, S. Y.; Aris, A. Z. Revisiting the “forever chemicals”, PFOA and PFOS exposure in drinking water. *npj Clean Water* **2023**, *6* (1). DOI: 10.1038/s41545-023-00274-6.

(103) Daina, A.; Michielin, O.; Zoete, V. SwissADME: a free web tool to evaluate pharmacokinetics, drug-likeness and medicinal chemistry friendliness of small molecules. *Scientific Reports* **2017**, *7*. DOI: 10.1038/srep42717.

(104) *ChemSpider*. Royal Society of Chemistry, 2024. https://www.chemspider.com (accessed September 24, 2024).

(105) Daina, A. M., O.; Zoete, V. SwissADME: a free web tool to evaluate pharmacokinetics, drug-likeness and medicinal chemistry friendliness of small molecules. *Sci. Rep.* **2017**, *7*. DOI: 10.1038/srep42717.

(106) Burns, D. C. E., D.A.; Li, H.; McMurdo, C.J.; Webster, E. . Experimental pKa Determination for Perfluorooctanoic Acid (PFOA) and the Potential Impact of pKa Concentration Dependence on Laboratory-Measured Patitioning Phenomena and Environmental Modeling. *Environ. Sci. Technol.* **2008**, *42*, 9238-9288.

(107) Li, F.; Duan, J.; Tian, S.; Ji, H.; Zhu, Y.; Wei, Z.; Zhao, D. Short-chain per- and polyfluoroalkyl substances in aquatic systems: Occurrence, impacts and treatment. *Chemical Engineering Journal* **2020**, *380*. DOI: 10.1016/j.cej.2019.122506.

(108) Goss, K.-U. The pKa Values of PFOA and Other Highly Fluorinated Carboxylic Acids. *Environ. Sci. Technol.* **2008**, *42*, 456-458.

(109) Brace, N. O. Long chain alkanoic and alkenoic acids with perfluoroalkyl terminal segments. *Journal of Organic Chemistry* **1962**, *27* (12), 4491-&. DOI: 10.1021/jo01059a090.

(110) Goss, K. U. The pKa values of PFOA and other highly fluorinated carboxylic acids (vol 73, pg 2323, 1951). *Environmental Science & Technology* **2008**, *42* (13), 5032-5032. DOI: 10.1021/es8011904.

(111) Goss, K. U. The pKa values of PFOA and other highly fluorinated carboxylic acids. *Environmental Science & Technology* **2008**, *42* (2), 456-458. DOI: 10.1021/es702192c.

(112) Goss, K. U.; Arp, H. P. H. Comment on "Experimental pKa Determination for Perfluorooctanoic Acid (PFOA) and the Potential Impact of pKa Concentration Dependence on Laboratory-Measured Partitioning Phenomena and Envrionmental Modeling". *Environmental Science & Technology* **2009**, *43* (13), 5150-5151. DOI: 10.1021/es900451s.

(113) Moroi, Y.; Yano, H.; Shibata, O.; Yonemitsu, T. Determination of acidity constants of perfluoroalkanoic acids. *Bulletin of the Chemical Society of Japan* **2001**, *74* (4), 667-672. DOI: 10.1246/bcsj.74.667.

(114) Blanco, E.; González-Pérez, A.; Ruso, J. M.; Pedrido, R.; Prieto, G.; Sarmiento, F. A comparative study of the physicochemical properties of perfluorinated and hydrogenated amphiphiles. *Journal of Colloid and Interface Science* **2005**, *288* (1), 247-260. DOI: 10.1016/j.jcis.2005.02.085.

(115) Burns, D. C.; Ellis, D. A.; Webster, E.; McMurdo, C. J. Response to Comment on “Experimental pKa Determination for Ferfluorooctanoic Acid (PFOA) and the Potental Impact of pKa Concentration Dependence on Laboratory-Measured Partitioning Phenomena and Environmental Modeling”. *Environmental Science & Technology* **2009**, *43*, 5152-5154.

(116) Sobolewski, T. N.; Findlay, J. L.; Hemphill, J. E.; Walker, R. A. Aggregation, not micellization: perfluorooctanoic acid, perfluorobutanesulfonic acid, and potassium perfluorooctanesulfonate behavior in aqueous solution. *Langmuir* **2024**. DOI: 10.1021/acs.langmuir.4c02566.

(117) Ebert, A.; Allendorf, F.; Berger, U.; Goss, K. U.; Ulrich, N. Membrane/Water Partitioning and Permeabilities of Perfluoroalkyl Acids and Four of their Alternatives and the Effects on Toxicokinetic Behavior. *Environmental Science & Technology* **2020**, *54* (8), 5051-5061. DOI: 10.1021/acs.est.0c00175.

(118) Droge, S. T. J. Membrane-Water Partition Coefficients to Aid Risk Assessment of Perfluoroalkyl Anions and Alkyl Sulfates. *Environmental Science & Technology* **2019**, *53* (2), 760-770. DOI: 10.1021/acs.est.8b05052.

(119) Xie, W.; Bothun, G. D.; Lehmler, H. J. Partitioning of perfluorooctanoate. into phsphatidylcholine bilayers is chain length-independent. *Chemistry and Physics of Lipids* **2010**, *163* (3), 300-308. DOI: 10.1016/j.chemphyslip.2010.01.003.

(120) Xie, W.; Kania-Korwel, I.; Bummer, P. M.; Lehmler, H. J. Effect of potassium perfluorooetanesulfonate, perfluorooctanoate and octanesulfonate on the phase transition of

dipalmitoylphosphatidylcholine (DPPC) bilayers. *Biochimica Et Biophysica Acta-Biomembranes* **2007**, *1768* (5), 1299-1308. DOI: 10.1016/j.bbamem.2007.02.003.

(121) Ruba Bnyan, I. K., Touraj Ehtezazi, Imran Saleem, Sarah Gordon, Francis O'Neill, Matthew Roberts. Surfactant effects on lipid-based vesicles properties. *Journal of Pharmaceutical Sciences* **2018**, *107* (5), 1237-1246.

(122) Somasundaran, N. D. a. P. Effects of Sodium Dodecyl Sulfate on Mixed Liposome Solubilization. *Langmuir* **2003**, *19*, 7271-7275.

(123) Fessler, M. B.; Summer, R. S. Surfactant Lipids at the Host-Environment Interface. Metabolic Sensors, Suppressors, and Effectors of Inflammatory Lung Disease. *Am J Respir Cell Mol Biol* **2016**, *54* (5), 624-635. DOI: 10.1165/rcmb.2016-0011PS From NLM Medline.

(124) Heerklotz, H. Interactions of surfactants with lipid membranes. *Q Rev Biophys* **2008**, *41* (3-4), 205-264. DOI: 10.1017/S0033583508004721 From NLM Medline.

(125) Borthakur, A.; Cranmer, B. K.; Dooley, G. P.; Blotevogel, J.; Mahendra, S.; Mohanty, S. K. Release of soil colloids during flow interruption increases the pore-water PFAS concentration in saturated soil. *Environ Pollut* **2021**, *286*, 117297. DOI: 10.1016/j.envpol.2021.117297 From NLM Medline.

(126) Silva, J. A. K.; Simunek, J.; McCray, J. E. A Modified HYDRUS Model for Simulating PFAS Transport in the Vadose Zone. *Water* **2020**, *12* (10). DOI: 10.3390/w12102758.

(127) Lyu, X. Y.; Xiao, F.; Shen, C. Y.; Chen, J. J.; Park, C. M.; Sun, Y. Y.; Flury, M.; Wang, D. J. Per- and Polyfluoroalkyl Substances (PFAS) in Subsurface Environments: Occurrence, Fate, Transport, and Research Prospect. *Reviews of Geophysics* **2022**, *60* (3). DOI: 10.1029/2021rg000765.

(128) Radi, A. B.; Noll, K. E.; Oskouie, A. K. Per- and Polyfluoroalkyl Substances: Background Information with Focus on Modeling of Fate and Transport of Per- and Polyfluroalkyl Substances in Air Media. *Journal of Environmental Engineering* **2022**, *148* (6). DOI: 10.1061/(asce)ee.1943-7870.0001989.

(129) Mahmoudnia, A.; Mehrdadi, N.; Baghdadi, M.; Moussavi, G. Change in global PFAS cycling as a response of permafrost degradation to climate change. *Journal of Hazardous Materials Advances* **2022**, *5*. DOI: 10.1016/j.hazadv.2021.100039.

(130) Faust, J. A. PFAS on atmospheric aerosol particles: a review. *Environmental Science-Processes & Impacts* **2023**, *25* (2), 133-150. DOI: 10.1039/d2em00002d.

(131) Dassuncao, C.; Pickard, H.; Pfohl, M.; Tokranov, A. K.; Li, M. L.; Mikkelsen, B.; Slitt, A.; Sunderland, E. M. Phospholipid Levels Predict the Tissue Distribution of Poly- and Perfluoroalkyl Substances in a Marine Mammal. *Environmental Science & Technology Letters* **2019**, *6* (3), 119-125. DOI: 10.1021/acs.estlett.9b00031.

(132) Garcia-Garin, O.; Borrell, A.; Colomer-Vidal, P.; Vighi, M.; Trilla-Prieto, N.; Aguilar, A.; Gazo, M.; Jiménez, B. Biomagnification and temporal trends (1990-2021) of perfluoroalkyl substances in striped dolphins (Stenella coeruleoalba) from the NW Mediterranean sea. *Environmental Pollution* **2023**, *339*. DOI: 10.1016/j.envpol.2023.122738.

(133) Manera, M.; Castaldelli, G.; Giari, L. Perfluorooctanoic Acid Promotes Recruitment and Exocytosis of Rodlet Cells in the Renal Hematopoietic Tissue of Common Carp. *Toxics* **2023**, *11* (10). DOI: 10.3390/toxics11100831.

(134) Dong, H. K.; Lu, G. H.; Yan, Z. H.; Liu, J. C.; Ji, Y. Molecular and phenotypic responses of male crucian carp exposed to perfluorooctanoic acid. *Science of the Total Environment* **2019**, *653*, 1395-1406. DOI: 10.1016/j.scitotenv.2018.11.017.

(135) Ren, J. D.; Point, A. D.; Baygi, S. F.; Fernando, S.; Hopke, P. K.; Holsen, T. M.; Crimmins, B. S. Bioaccumulation of polyfluoroalkyl substances in the Lake Huron aquatic food web. *Science of the Total Environment* **2022**, *819*. DOI: 10.1016/j.scitotenv.2022.152974.

(136) Munoz, G.; Mercier, L.; Duy, S. V.; Liu, J. X.; Sauve, S.; Houde, M. Bioaccumulation and trophic magnification of emerging and legacy per-and polyfluoroalkyl substances (PFAS) in a St. Lawrence River food web. *Environmental Pollution* **2022**, *309*. DOI: 10.1016/j.envpol.2022.119739.

(137) Kannan, K.; Hansen, K. J.; Wade, T. L.; Giesy, J. P. Perfluorooctane sulfonate in oysters, Crassostrea virginica, from the Gulf of Mexico and the Chesapeake Bay, USA. *Arch Environ Contam Toxicol* **2002**, *42* (3), 313-318. DOI: 10.1007/s00244-001-0003-8 From NLM Medline.

(138) Kannan, J. P. G. K. Global Distribution of Perfluorooctane Sulfonate in Wildlife. *Environ. Sci. Technol.* **2001**, *35*, 1339-1342.

(139) Corsolin;, K. K. S.; Giesy, J. F. G. O. S. F. J. P. Perfluorooctanesulfonate and related fluorinated hydrocarbons in marine mammals, fishes, and birds from coats of the Baltic and the Mediterranean seas. *Environ. Sci. Technol.* **2002**, *36*, 3210-3216.

(140) Perez, F.; Nadal, M.; Navarro-Ortega, A.; Fabrega, F.; Domingo, J. L.; Barcelo, D.; Farre, M. Accumulation of perfluoroalkyl substances in human tissues. *Environ Int* **2013**, *59*, 354-362. DOI: 10.1016/j.envint.2013.06.004 From NLM Medline.

(141) Fujii, S.; Polprasert, C.; Tanaka, S.; Hong Lien, N. P.; Qiu, Y. New POPs in the water environment: distribution, bioaccumulation and treatment of perfluorinated compounds – a review paper. *Journal of Water Supply: Research and Technology-Aqua* **2007**, *56* (5), 313-326. DOI: 10.2166/aqua.2007.005.

(142) European Food Safety, A. Perfluorooctane sulfonate (PFOS), perfluorooctanoic acid (PFOA) and their salts Scientific Opinion of the Panel on Contaminants in the Food chain. *EFSA J* **2008**, *6* (7), 653. DOI: 10.2903/j.efsa.2008.653 From NLM PubMed-not-MEDLINE.

(143) Martin, J. W.; Mabury, S. A.; Solomon, K. R.; Muir, D. C. G. Bioconcentration and tissue distribution of perfluorinated acids in rainbow trout (Oncorhynchus mykiss). *Environmental Toxicology and Chemistry* **2003**, *22* (1), 196-204.

(144) Pandelides, Z.; Conder, J.; Choi, Y.; Allmon, E.; Hoskins, T.; Lee, L.; Hoverman, J.; Sepulveda, M. A Critical Review of Amphibian Per- and Polyfluoroalkyl Substance Ecotoxicity Research Studies: Identification of Screening Levels in Water and Other Useful Resources for Site-Specific Ecological Risk Assessments. *Environ Toxicol Chem* **2023**, *42* (10), 2078-2090. DOI: 10.1002/etc.5695 From NLM Medline.

(145) Dai, C.; Peng, L.; Li, Y. J.; Li, Z. D.; Chen, D.; Wang, F.; Lin, N. Distribution of per- and polyfluoroalkyl substances in blood, serum, and urine of patients with liver cancer and associations with liver function biomarkers. *Journal of Environmental Sciences* **2024**, *139*, 418-427. DOI: 10.1016/j.jes.2023.05.026.

(146) Zheng, T.; Kelsey, K.; Zhu, C.; Pennell, K. D.; Yao, Q.; Manz, K. E.; Zheng, Y. F.; Braun, J. M.; Liu, Y.; Papandonatos, G.; et al. Adverse birth outcomes related to concentrations of per- and polyfluoroalkyl substances (PFAS) in maternal blood collected from pregnant women in 1960-1966. *Environ Res* **2024**, *241*, 117010. DOI: 10.1016/j.envres.2023.117010 From NLM Medline.

(147) Phelps, D. W.; Palekar, A. I.; Conley, H. E.; Ferrero, G.; Driggers, J. H.; Linder, K. E.; Kullman, S. W.; Reif, D. M.; Sheats, M. K.; DeWitt, J. C.; et al. Legacy and emerging per- and polyfluoroalkyl substances suppress the neutrophil respiratory burst. *Journal of Immunotoxicology* **2023**, *20* (1). DOI: 10.1080/1547691x.2023.2176953.

(148) De Toni, L.; Radu, C. M.; Sabovic, I.; Di Nisio, A.; Dall'Acqua, S.; Guidolin, D.; Spampinato, S.; Campello, E.; Simioni, P.; Foresta, C. Increased Cardiovascular Risk Associated with Chemical Sensitivity to Perfluoro-Octanoic Acid: Role of Impaired Platelet Aggregation. *International Journal of Molecular Sciences* **2020**, *21* (2). DOI: 10.3390/ijms21020399.

(149) McLachlan, M. S.; Ebert, A.; Armitage, J. M.; Arnot, J. A.; Droge, S. T. J. A framework for understanding the bioconcentration of surfactants in fish. *Environ Sci Process Impacts* **2023**, *25* (7), 1238-1251. DOI: 10.1039/d3em00070b From NLM Medline.

(150) Naumann, A.; Alesio, J.; Poonia, M.; Bothun, G. D. D. PFAS fluidize synthetic and bacterial lipid monolayers based on hydrophobicity and lipid charge. *Journal of Environmental Chemical Engineering* **2022**, *10* (2). DOI: 10.1016/j.jece.2022.107351.

(151) Roy, D.; Liu, S.; Woods, B. L.; Siler, A. R.; Fourkas, J. T.; Weeks, J. D.; Walker, R. A. Nonpolar Adsorption at the Silica/Methanol Interface: Surface Mediated Polarity and Solvent Density across a Strongly Associating Solid/Liquid Boundary. *The Journal of Physical Chemistry C* **2013**, *117* (51), 27052-27061. DOI: 10.1021/jp410756g.

(152) Gobrogge, C. A.; Blanchard, H. S.; Walker, R. A. Temperature-Dependent Partitioning of Coumarin 152 in Phosphatidylcholine Lipid Bilayers. *J Phys Chem B* **2017**, *121* (16), 4061-4070. DOI: 10.1021/acs.jpcb.6b10893 From NLM Medline.

(153) Purnell, G. E.; McNally, M. T.; Callis, P. R.; Walker, R. A. Buried Liquid Interfaces as a Form of Chemistry in Confinement: The Case of 4-Dimethylaminobenzonitrile at the Silica-Aqueous Interface. *J Am Chem Soc* **2020**, *142* (5), 2375-2385. DOI: 10.1021/jacs.9b11662 From NLM PubMed-not-MEDLINE.

(154) Duncan, K. M.; Casey, A.; Gobrogge, C. A.; Trousdale, R. C.; Piontek, S. M.; Cook, M. J.; Steel, W. H.; Walker, R. A. Coumarin Partitioning in Model Biological Membranes: Limitations of log P as a Predictor. *Journal of Physical Chemistry B* **2020**, *124* (38), 8299-8308. DOI: 10.1021/acs.jpcb.0c06109.

(155) Gobrogge, C. A.; Kong, V. A.; Walker, R. A. Temperature-Dependent Partitioning of C152 in Binary Phosphatidylcholine Membranes and Mixed Phosphatidylcholine/Phosphatidylethanolamine Membranes. *Journal of Physical Chemistry B* **2017**, *121* (33), 7889-7898. DOI: 10.1021/acs.jpcb.7b04831.

(156) Duncan, K. M.; Trousdale, R. C.; Gonzales, C. N.; Steel, W. H.; Walker, R. A. l-Phenylalanine Partitioning Mechanisms in Model Biological Membranes. *J Phys Chem B* **2023**, *127* (25), 5633-5644. DOI: 10.1021/acs.jpcb.2c08582 From NLM Medline.

(157) Marc le Maire, P. C., Jesper V. Moller. Interaction of membrane proteins and lipids with solubilizing detergents *Biochimica et Biophysica Acta* **2000**, *1508*, 86-111.

(158) Lichtenberg, D. Characterization of the solubilization of lipid bilayers by surfactants *Biochimica et Biophysica Acta* **1985**, *821*, 470-478.

(159) DOV Lichtenberg, R. J. R., Edward A. Dennis. Solubilization of Phospholipids by Detergents Structural and Kinetic Aspects *Biochimica et Biophysica Acta* **1983**, *737*, 285-304.

(160) Lichtenberg, D. Characterization of the solubilization of lipid bilayers by surfactants. *Biochimica et Biophysica Acta* **1985**, *821*, 470-478.

(161) Bjornestad, V. A.; Lund, R. Pathways of Membrane Solubilization: A Structural Study of Model Lipid Vesicles Exposed to Classical Detergents. *Langmuir* **2023**, *39* (11), 3914-3933. DOI: 10.1021/acs.langmuir.2c03207 From NLM Medline.

(162) Csiszár, Á., Bóta, A., Novák, C. et al. Calorimetric study of the effects of 2,4-dichlorophenol on the thermotropic phase behavior of DPPC liposomes. *Journal of Thermal Analysis and Calorimetry* **2002**, *69*, 53-63. DOI: https://doi.org/10.1023/A:1019977404803.

(163) Morandi, M. I.; Sommer, M.; Kluzek, M.; Thalmann, F.; Schroder, A. P.; Marques, C. M. DPPC Bilayers in Solutions of High Sucrose Content. *Biophys J* **2018**, *114* (9), 2165-2173. DOI: 10.1016/j.bpj.2018.04.003 From NLM Medline.

(164) Sabín, J.; Prieto, G.; Sennato, S.; Blanco, E.; Messina, P. V.; Ruso, J. M.; Angelini, R.; Bordi, F.; Sarmiento, F. Examination of the influence of F6H10 fluorinated diblocks on DPPC liposomes. *Journal of Thermal Analysis and Calorimetry* **2007**, *87* (1), 301-304. DOI: 10.1007/s10973-006-7846-1.

(165) Almeida, P. F. A simple thermodynamic model of the liquid-ordered state and the interactions between phospholipids and cholesterol. *Biophys J* **2011**, *100* (2), 420-429. DOI: 10.1016/j.bpj.2010.12.3694 From NLM Medline.

(166) Ortona, O.; Vitagliano, V.; Fessas, D.; Del Vecchio, P.; D'Errico, G. Inhomogeneities in sodium decylsulfate doped 1,2-dipalmitoylphosphatidylcholine bilayer. *Journal of Colloid and Interface Science* **2010**, *343* (2), 401-407. DOI: 10.1016/j.jcis.2009.11.054.

(167) Shiffer, K.; Hawgood, S.; Haagsman, H. P.; Benson, B.; Clements, J. A.; Goerke, J. Lung surfactant proteins, SP-B and SP-C, alter the thermodynamic properties of phospholipid membranes - a differential calorimetry study. *Biochemistry* **1993**, *32* (2), 590-597. DOI: 10.1021/bi00053a026.

(168) Maiti, B.; Kumar, K.; Datta, S.; Bhattacharya, S. Physical-Chemical Characterization of Bilayer Membranes Derived from (±) α-Tocopherol-Based Gemini Lipids and Their Interaction with Phosphatidylcholine Bilayers and Lipoplex Formation with Plasmid DNA. *Langmuir* **2022**, *38* (1), 36-49. DOI: 10.1021/acs.langmuir.1c01039.

(169) Kudella, P. W.; Preissinger, K.; Morasch, M.; Dirscherl, C. F.; Braun, D.; Wixforth, A.; Westerhausen, C. Fission of Lipid-Vesicles by Membrane Phase Transitions in Thermal Convection. *Sci Rep* **2019**, *9* (1), 18808. DOI: 10.1038/s41598-019-55110-0 From NLM PubMed-not-MEDLINE.

(170) Ijeoma F. Uchegbu, S. P. V. Non-ionic surfactant based vesicles (niosomes) in drug delivery. *Journal of Pharmaceutics* **1998**, *172*, 33-70.

(171) Bhardwaj, P.; Tripathi, P.; Gupta, R.; Pandey, S. Niosomes: A review on niosomal research in the last decade. *Journal of Drug Delivery Science and Technology* **2020**, *56*. DOI: 10.1016/j.jddst.2020.101581.

(172) Gharbavi, M.; Amani, J.; Kheiri-Manjili, H.; Danafar, H.; Sharafi, A. Niosome: A Promising Nanocarrier for Natural Drug Delivery through Blood-Brain Barrier. *Advances in Pharmacological Sciences* **2018**, *2018*. DOI: 10.1155/2018/6847971.

(173) Åkesson, A.; Lind, T.; Ehrlich, N.; Stamou, D.; Wacklin, H.; Cárdenas, M. Composition and structure of mixed phospholipid supported bilayers formed by POPC and DPPC. *Soft Matter* **2012**, *8* (20). DOI: 10.1039/c2sm00013j.

(174) Exerowa, D.; Todorov, R.; Nikolov, L. Amphiphile bilayer films from DPPC: bilayer lipid membranes and Newton black films. *Colloids and Surfaces A: Physicochemical and Engineering Aspects* **2004**, *250* (1-3), 195-201. DOI: 10.1016/j.colsurfa.2004.04.089.

(175) Maherani, B.; Arab-Tehrany, E.; Kheirolomoom, A.; Geny, D.; Linder, M. Calcein release behavior from liposomal bilayer; influence of physicochemical/mechanical/structural properties of lipids. *Biochimie* **2013**, *95* (11), 2018-2033. DOI: 10.1016/j.biochi.2013.07.006.

(176) Mason, R. P.; Gonye, G. E.; Chester, D. W.; Herbette, L. G. Partitioning and location of BAY-K-8644, 1,4-Dihydropyridine calcium-channel agonist, in model and biological membranes. *Biophysical Journal* **1989**, *55* (4), 769-778. DOI: 10.1016/s0006-3495(89)82875-9.

(177) Robinson, M.; Turnbull, S.; Lee, B. Y.; Leonenko, Z. The effects of melatonin, serotonin, tryptophan and NAS on the biophysical properties of DPPC monolayers. *Biochimica Et Biophysica Acta-Biomembranes* **2020**, *1862* (9). DOI: 10.1016/j.bbamem.2020.183363.

(178) Yuan, S. D.; Zhang, H.; Yuan, S. L. Theoretical insights into the uptake of sulfonamides onto phospholipid bilayers: Mechanisms, interaction and toxicity evaluation. *Journal of Hazardous Materials* **2022**, *435*. DOI: 10.1016/j.jhazmat.2022.129033.

(179) Zenker, A.; Cicero, M. R.; Prestinaci, F.; Bottoni, P.; Carere, M. Bioaccumulation and biomagnification potential of pharmaceuticals with a focus to the aquatic environment. *Journal of Environmental Management* **2014**, *133*, 378-387. DOI: 10.1016/j.jenvman.2013.12.017.

(180) Duncan, K. M.; Casey, A.; Gobrogge, C. A.; Trousdale, R. C.; Piontek, S. M.; Cook, M. J.; Steel, W. H.; Walker, R. A. Coumarin Partitioning in Model Biological Membranes: Limitations of log P as a Predictor. *J Phys Chem B* **2020**, *124* (38), 8299-8308. DOI: 10.1021/acs.jpcb.0c06109 From NLM Medline.

(181) Perkins, R.; Vaida, V. Phenylalanine Increases Membrane Permeability. *J Am Chem Soc* **2017**, *139* (41), 14388-14391. DOI: 10.1021/jacs.7b09219 From NLM Medline.

(182) Ng, C. A.; Hungerbuhler, K. Bioaccumulation of perfluorinated alkyl acids: observations and models. *Environ Sci Technol* **2014**, *48* (9), 4637-4648. DOI: 10.1021/es404008g From NLM Medline.

(183) EPA's PFAS Strategic Roadmap: Three Years of Progress. United States Environmental Protection Agency: 2024.

(184) Niemiec, S. S.; Kechris, K.; Pattee, J.; Yang, I. V.; Adgate, J. L.; Calafat, A. M.; Dabelea, D.; Starling, A. P. Prenatal exposures to per- and polyfluoroalkyl substances and epigenetic aging in umbilical cord blood: The Healthy Start study. *Environ Res* **2023**, *231* (Pt 2), 116215. DOI: 10.1016/j.envres.2023.116215 From NLM Medline.

(185) Sobolewski, T. N.; Trousdale, R. C.; Gauvin, C. L.; Lawrence, C. M.; Walker, R. A. Nanomolar PFOA Concentrations Affect Lipid Membrane Structure: Consequences for Bioconcentration Mechanisms. *Environ Sci Technol* **2024**. DOI: 10.1021/acs.est.4c03652 From NLM Publisher.

(186) Beesoon, S.; Martin, J. W. Isomer-Specific Binding Affinity of Perfluorooctanesulfonate (PFOS) and Perfluorooctanoate (PFOA) to Serum Proteins. *Environ Sci Technol* **2015**, *49* (9), 5722-5731. DOI: 10.1021/es505399w From NLM Medline.

(187) Cheng, W.; Ng, C. A. Predicting Relative Protein Affinity of Novel Per- and Polyfluoroalkyl Substances (PFASs) by An Efficient Molecular Dynamics Approach. *Environ Sci Technol* **2018**, *52* (14), 7972-7980. DOI: 10.1021/acs.est.8b01268 From NLM Medline.

(188) Sheng, N.; Li, J.; Liu, H.; Zhang, A.; Dai, J. Interaction of perfluoroalkyl acids with human liver fatty acid-binding protein. *Arch Toxicol* **2016**, *90* (1), 217-227. DOI: 10.1007/s00204-014-1391-7 From NLM Medline.

(189) Kosmachevskaya, O. V.; Topunov, A. F. Alternate and Additional Functions of Erythrocyte Hemoglobin. *Biochemistry (Mosc)* **2018**, *83* (12), 1575-1593. DOI: 10.1134/S0006297918120155 From NLM Medline.

(190) Qin, P.; Liu, R.; Teng, Y. Perfluorodecanoic acid binding to hemoproteins: new insights from spectroscopic studies. *J Agric Food Chem* **2011**, *59* (7), 3246-3252. DOI: 10.1021/jf200092y From NLM Medline.

(191) Yang, Y. D.; Lu, N.; Tian, R. The interaction of perfluorooctane sulfonate with hemoproteins and its relevance to molecular toxicology. *Int J Biol Macromol* **2024**, *254* (Pt 3), 128069. DOI: 10.1016/j.ijbiomac.2023.128069 From NLM Medline.

(192) Yang, Y. D.; Tian, R.; Lu, N. Binding of serum albumin to perfluorooctanoic acid reduced cytotoxicity. *Sci Total Environ* **2023**, *876*, 162738. DOI: 10.1016/j.scitotenv.2023.162738 From NLM Medline.

(193) Maso, L.; Trande, M.; Liberi, S.; Moro, G.; Daems, E.; Linciano, S.; Sobott, F.; Covaceuszach, S.; Cassetta, A.; Fasolato, S.; et al. Unveiling the binding mode of perfluorooctanoic acid to human serum albumin. *Protein Sci* **2021**, *30* (4), 830-841. DOI: 10.1002/pro.4036 From NLM Medline.

(194) Perera, N. L. D.; Betancourt, J.; Miksovska, J.; O'Shea, K. E. Detail study on the interaction between perfluorooctanoic acid (PFOA) with human hemoglobin (Hb). *Curr Res Toxicol* **2023**, *5*, 100130. DOI: 10.1016/j.crtox.2023.100130 From NLM PubMed-not-MEDLINE.

(195) Rout, J.; Swain, B. C.; Subadini, S.; Mishra, P. P.; Sahoo, H.; Tripathy, U. Spectroscopic and computational insight into the conformational dynamics of hemoglobin in the presence of vitamin B12. *Int J Biol Macromol* **2021**, *189*, 306-315. DOI: 10.1016/j.ijbiomac.2021.08.096 From NLM Medline.

(196) Monni, R.; Al Haddad, A.; van Mourik, F.; Aubock, G.; Chergui, M. Tryptophan-to-heme electron transfer in ferrous myoglobins. *Proc Natl Acad Sci U S A* **2015**, *112* (18), 5602-5606. DOI: 10.1073/pnas.1423186112 From NLM Medline.

(197) Liu, W.; Guo, X.; Guo, R. The interaction between hemoglobin and two surfactants with different charges. *International Journal of Biological Macromolecules* **2007**, *41* (5), 548-557. DOI: 10.1016/j.ijbiomac.2007.07.006.

(198) Moore, G. R. Pettigrew, G. W. Cytochromes c: Evolutionary, Structural and Physicochemical Aspects; Springer 1991. DOI: 3-642-74536-2.

(199) Diaz-Quintana, A.; Navarro, J. A.; Hervas, M.; Molina-Heredia, F. P.; De la Cerda, B.; De la Rosa, M. A. A comparative structural and functional analysis of cyanobacterial plastocyanin and cytochrome c (6) as alternative electron donors to Photosystem I. *Photosynth Res* **2003**, *75* (2), 97-110. DOI: 10.1023/A:1022841513592 From NLM PubMed-not-MEDLINE.

(200) Xu, Q.; Keiderling, T. A. Effect of sodium dodecyl sulfate on folding and thermal stability of acid-denatured cytochrome c: a spectroscopic approach. *Protein Sci* **2004**, *13* (11), 2949-2959. DOI: 10.1110/ps.04827604 From NLM Medline.

(201) Jones, M.N.; Manley, P.; Interaction between lysozyme and n-alkyl sulphates in aqueous solution. *Journal of the Chemical Society* **1980**, 76 (0), 654-664. DOI: https://doi.org/10.1039/F19807600654 From Royal Society of Chemistry

(202) Han, J. W.; Park, H. J. Perfluorooctanoic acid induces cell death in TM3 cells via the ER stress-mitochondrial apoptosis pathway. *Reprod Toxicol* **2023**, *118*, 108383. DOI: 10.1016/j.reprotox.2023.108383 From NLM Medline.

(203) Fronticelli, C.; Sanna, M. T.; Perez-Alvarado, G. C.; Karavitis, M.; Lu, A. L.; Brinigar, W. S. Allosteric modulation by tertiary structure in mammalian hemoglobins. Introduction of the functional characteristics of bovine hemoglobin into human hemoglobin by five amino acid substitutions. J Biol Chem 1995, 270 (51), 30588-30592. DOI: 10.1074/jbc.270.51.30588

(204) Christofi, E.; Barran, P. Ion Mobility Mass Spectrometry (IM-MS) for Structural Biology: Insights Gained by Measuring Mass, Charge, and Collision Cross Section. Chem Rev 2023, 123 (6), 2902-2949. DOI: 10.1021/acs.chemrev.2c00600

APPENDICES

APPENDIX A:

QUANTITATIVE MEMBRANE PARTITIONING STUDIES OF L-PHENYLALANINE

Structures of L-Phe and lipid vesicles used in this work

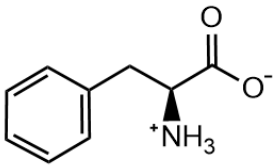

a) L-Phenylalanine

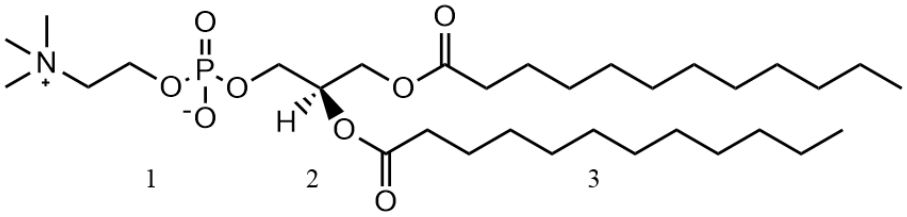

b) 12:0 DLPC: 1,2-dilauroyl-sn-glycero-3-phosphocholine

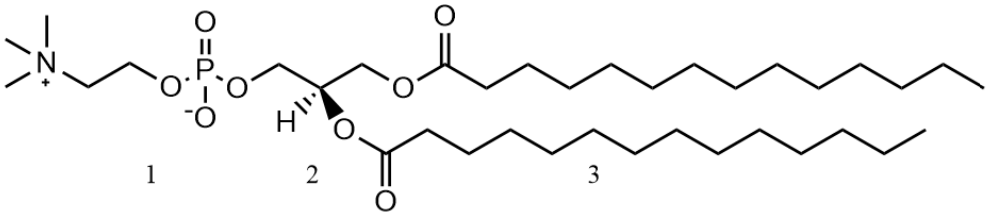

c) 14:0 DMPC: 1,2-dimyristoyl-sn-glycero-3-phosphocholine

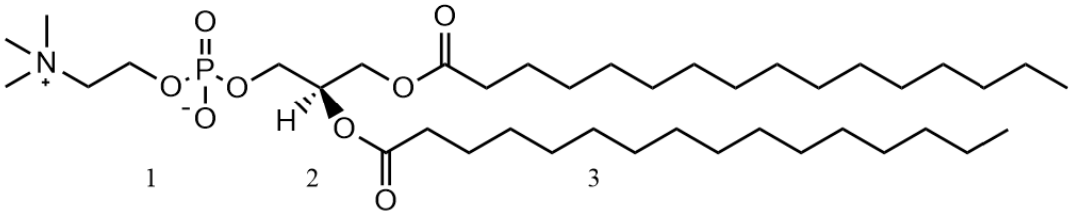

d) 16:0 PMPC: 1,2-Dipalmitoyl-sn-glycero-3-phsophocholine

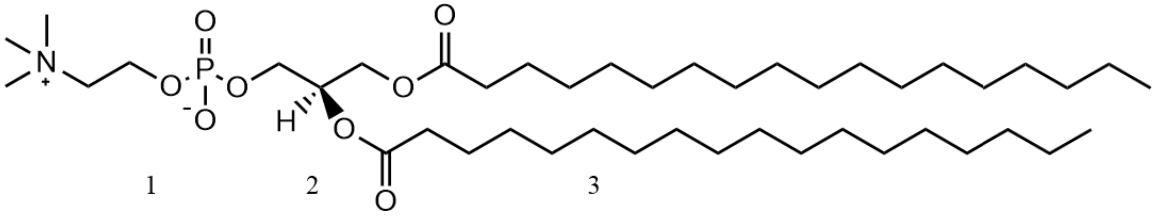

e) 18:0 DSPC: 1,2-distearoyl-sn-glycero-3-phosphocholine

Figure A-2.1. Chemical structures of (a) L-Phenylalanine, (b) 1,2-dilauroyl-sn-glycero-3-phosphocholine (12:0 DLPC) lipid, (c) 1,2-dimyristoyl-sn-glycero-3-phosphocholine (14:0 DMPC) lipid, (d) 1,2-Dipalmitoyl-*sn*-glycero-3-phsophocholine (16:0 DPPC) lipid, and (e) 1,2-distearoyl-sn-glycero-3-phosphocholine (18:0 DSPC) lipid. Number assignments refer to various

environments created by the lipid with 1) polar zwitterionic headgroup, 2) the polar glycerol-backbone and ester groups, and 3) nonpolar, hydrophobic hydrocarbon tails. The COOH pKa-value for L-Phe is 2.2 and amino pKa-value is 9.9 giving L-Phe local charges on structure at pH 7 used for these experiments.

Steady-State Spectra of L-Phe in Bulk Solvents.

Steady state measurements were collected using a Horiba Fluorolog-3 spectrofluorometer at concentrations of 10 mM for carbonate buffer and methanol, 1.4 mM in acetonitrile, and 0.1 mM for cyclohexane. The range in concentration is due to poor solubility of L-Phe in acetonitrile and cyclohexane. Excitation and emission spectra were taken at the solute's respective excitation and emission wavelengths in individual bulk solvents. Each spectrum was normalized to the maximum intensity between bulk solvents for each individual absorbance, excitation, and emission spectra.

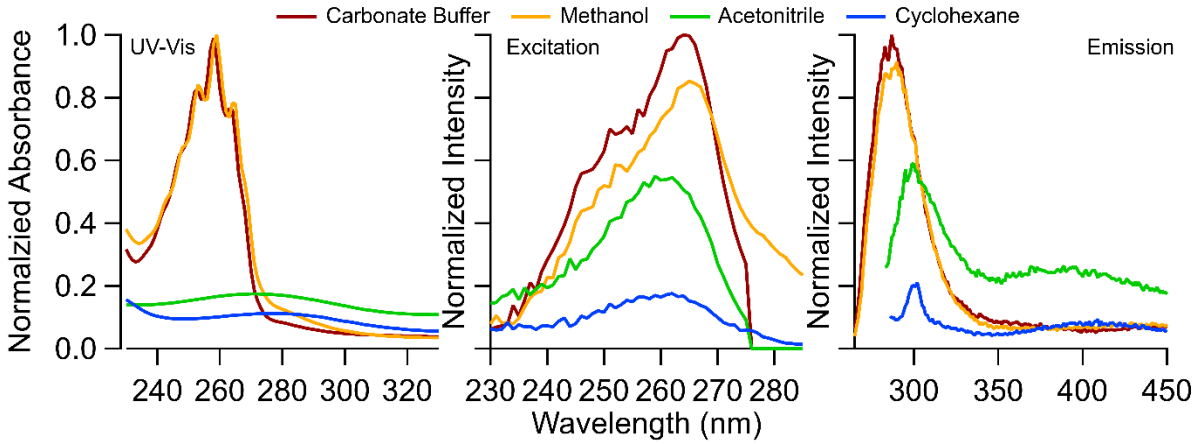

Figure A-2.2. Absorbance (left), excitation (middle), and emission (right) spectra for L-Phe in each of the bulk solvents.

Fluorescence lifetimes, quantum yield calculations, and radiative rate calculations of L-Phe in bulk carbonate buffer and methanol as a function of temperature.

Time-resolved emission of L-Phe in bulk carbonate buffer and methanol as a function of temperature can be seen in Figure SI-3 – SI-4, respectively. Each reported lifetime is a fit of each fluorescence decay using Equation 1. At each temperature, the solution was equilibrated for five minutes before data was accumulated. The resulting fluorescent lifetimes of L-Phe in bulk carbonate buffer and methanol can found in Table SI-1.

A brief explanation if how the quantum yields and radiative rates were collected will be described here with a further explanation of technique found in the references.[203-205] The quantum yields of L-Phe in bulk carbonate buffer and methanol were measured as a function of temperature from -5 °C to 80 °C. The quantum yield for L-Phe in acetonitrile was only measured at 20 °C. Calculations were not successfully measured for L-Phe in cyclohexane due to the low solubility as well as the extremely poor absorbance. Equation S1 was used for calculating the reference quantum yield ($\varphi_{f(x)}$) using Tyrosine in Millipore water as a reference ($\varphi_{f(s)}$).[206] The refractive indices for the sample and standard are n_x and n_s, respectively. The integrated fluorescence intensity was plotted as a function of absorbance for a sequence of four serial dilutions to create a slope of linear fits for the standard and sample, m_x and m_s, respectively. Each dilution was repeated at each reported temperature with an equilibration time of five minutes before data accumulation.

$$\phi_{f(x)} = \left(\frac{m_x}{m_s}\right)\left(\frac{n_x}{n_s}\right)^2 \phi_{f(s)} \qquad \text{(A1)}$$

To correct the amplitudes for only the radiative emission, the combination of the radiative (k_{rad}) and nonradiative (k_{nr}) rates must first be calculated using Equation S2. The experimental lifetime

(τ) of the solute in the respective environment at each respective temperature is used to calculate corresponding k_{rad} and k_{nr}.

$$\frac{1}{\tau} = k_{rad} + k_{nr} \quad \text{(A2)}$$

Using the quantum yield found in Equation S1 and the spontaneous emission rates from Equation S2, the k_{rad} can be calculated using Equation S3.

$$\phi_{f(x)} = \frac{k_{rad}}{k_{rad}+k_{nr}} \quad \text{(A3)}$$

A given amplitude at a specific temperature divided by the respective radiative rate at the same temperature is normalized against all other radiative rate corrected amplitudes of that system only at the corresponding temperature (Equation S4). Where A_i is the given amplitude that is produced using the FluoFit system software, $k_{r,i}$ is the corresponding radiative rate at the same temperature, and X_i is the resulting radiative rate corrected amplitude at the defined temperature.

$$X_i = \frac{\frac{A_i}{k_{r,i}}}{\left(\frac{A_i}{k_{r,a}}+\frac{A_i}{k_{r,b}}\right)} \quad \text{(A4)}$$

The radiative rate of L-Phe in carbonate buffer was used to correct the amplitude of L-Phe that remains in carbonate buffer when in the presence of a lipid vesicle system. The amplitude of L-Phe associated with the membrane and proposed to be a conformationally restricted rotamer (k_{rot}) was corrected using the radiative rate of L-Phe in bulk methanol. Methanol was chosen because it is the closest model available to mimic the polar protic environment of water permeating into the polar headgroup of the lipid bilayer. Temperatures reported in Table SI-1 are the same temperatures used throughout all experimental procedures for all lipid vesicles used in this study.

Table A-2.1. Fluorescence properties of L-Phe in bulk carbonate buffer and methanol from -5 °C to 80 °C. Lifetimes are ± 0.2 ns. Numbers in parenthesis next to lifetime are amplitudes of that lifetime. Quantum yields (φ_f) and radiative rates (k_f) were measured in this work

temp. (°C)	**Carbonate Buffer**			**Methanol**		
	τ_f (ns)	φ_f	k_f (10^6 s^{-1})	τ_f (ns)	φ_f	k_f (10^6 s^{-1})
-5	11.03	0.036	3.29	8.68	0.047	5.38
0	10.81	0.036	3.37	8.34	0.042	5.01
5	9.13	0.039	4.24	7.93	0.039	4.93
10	8.31	0.027	3.23	7.56	0.033	4.40
15	7.33	0.026	3.49	7.17	0.033	4.67
20	6.42	0.023	3.52	6.74	0.033	4.89
25	5.56	0.021	3.70	6.27	0.031	5.01
30	4.81	0.018	3.66	5.78	0.033	5.77
35	4.17	0.016	3.85	5.40	0.028	5.15
40	3.59	0.014	4.01	4.91	0.033	6.69
50	2.71	0.012	4.42	4.09	0.031	9.24
60	2.13 (0.89), 0.74 (0.11)	0.010	4.64	3.35	0.029	10.8
70	1.66 (0.84), 0.66 (0.16)	0.009	5.13	2.73	0.027	12.4
80	1.30 (0.80), 0.52 (0.20)	0.005	4.06	2.21	0.026	9.50

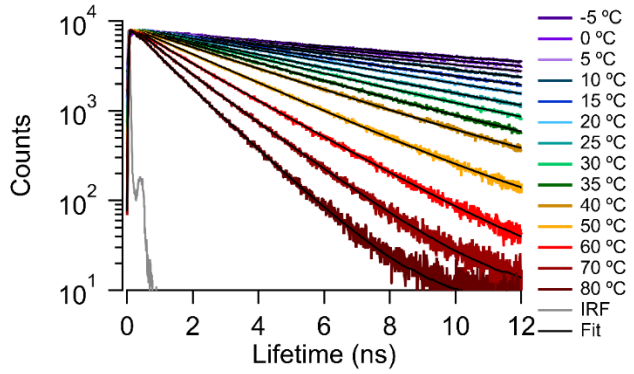

Figure A-2.3. TCSPC spectra of L-Phe in bulk carbonate buffer as a function of temperature. Results from fitting these emission traces to Eq 1 are reported in Table SI-1.

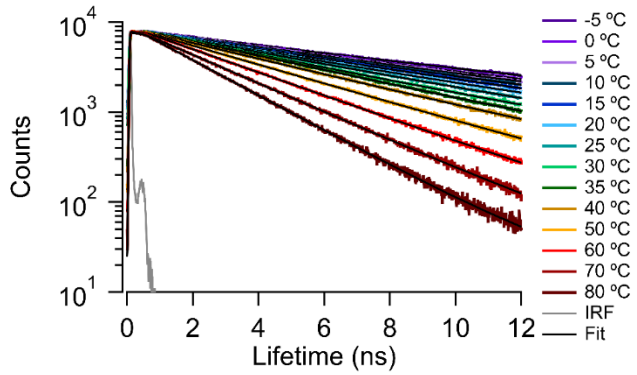

Figure A-2.4. TCSPC spectra of L-Phe in bulk methanol as a function of temperature. Results from fitting these emission traces to Eq. 1 are reported in Table SI-1.

Fluorescence behavior of 2.5 mM L-Phe in DPPC lipid vesicles.

The fluorescence behavior of 2.5 mM L-Phe in DPPC lipid vesicles was measured at selected temperatures can be found below. This was done to test aggregation effects of L-Phe at a 4-fold smaller concentration than what was used in this study. Results show that there was no significant change to the lifetimes and amplitudes of 10 mM L-Phe in DPPC lipid vesicles.

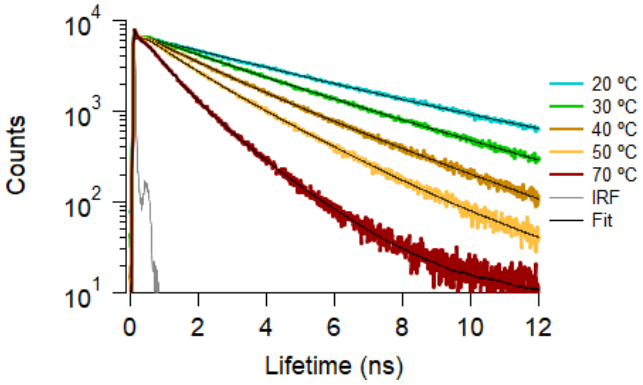

Figure A-2.5. TCSPC spectra of 2.5 mM L-Phe in DPPC lipid vesicles as a function of temperature. Results from fitting these emission traces to Equation 1 are reported in Table SI-2.

Table A-2.2. Fluorescence lifetimes (in ns) and amplitudes (in parentheses) of 2.5 mM L-Phe in DPPC vesicles at selected temperature ramp from 20 to 70 °C in and back down to 10 °C. Amplitudes have been corrected for their respective radiative rates. Uncertainties in lifetimes are ± 0.2 ns; uncertainties in amplitudes are ± 0.04.

temp. (°C)	buffer τ_1 (A_1)	K_{rot} τ_2 (A_2)
20	4.63	
30	3.75 (0.91)	1.49 (0.09)
40	3.12 (0.74)	1.66 (0.26)
50	2.39 (0.73)	1.24 (0.27)
70	1.59 (0.58)	0.74 (0.42)
50	2.44 (0.68)	1.27 (0.32)
40	2.93 (0.80)	1.47 (0.20)
30	3.86 (0.86)	1.73 (0.14)
20	4.57	

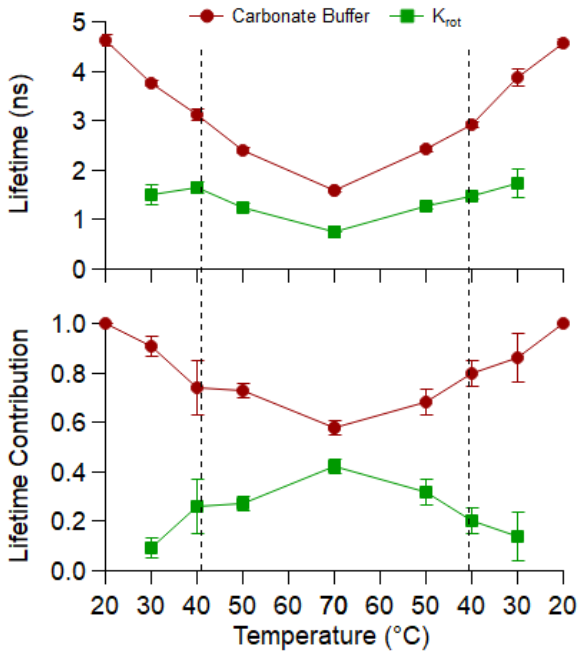

Figure A-2.6. Fluorescence lifetimes (top) and respective radiative rate corrected lifetime contribution (bottom) of 2.5 mM L-Phe in DPPC lipid vesicles. The major lifetime is assigned to a L-Phe in carbonate buffer (τ_1, burgundy circles), and a rotamer confinement lifetime (k_{rot}) of L-Phe in the DPPC polar headgroup region (τ_2, green squares). The dashed lines indicate the $T_{gel\text{-}lc}$ of the DPPC lipid bilayer at ~41.5 °C. Each point is an average of 2 independent trials and the respective error bars are one standard deviation based on the results of those 2 trials. In some instances, the uncertainty is smaller than the marker used to represent that data point.

Comparing fluorescence behavior of D_2O carbonate buffer to H_2O carbonate buffer

The fluorescence lifetimes of 10 mM L-Phe in H_2O carbonate buffer and D_2O carbonate buffer were measured as a function of temperature. This was done to measure the impact of H-bonding on the thermal stabilization of the rotamer lifetime. The lifetimes between the two buffer solutions are similar throughout the entire temperature ramp with the appearance of the second lifetime occurring at 60 °C for both solutions (Figure SI-7 and Table SI-3). However, the amplitude of the second lifetime in D_2O carbonate is significantly higher than that of H_2O carbonate buffer at 80 °C. There discrepancy between the two amplitudes is predicted to be due to the stronger H-Bonding capabilities of D_2O in comparison to H_2O allowing for more stabilization of the rotamer conformation.

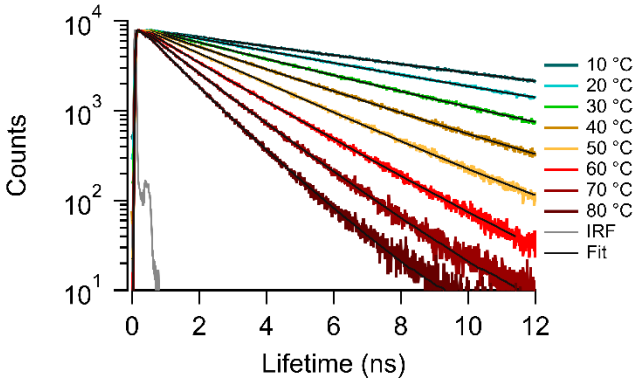

Figure A-2.7. TCSPC spectra of 10 mM L-Phe in D_2O carbonate buffer as a function of temperature. Results from fitting these emission traces to Equation 1 are reported in Table SI-3.

Table A-2.3. Fluorescence lifetimes (in ns) and amplitudes (in parentheses) of 10 mM L-Phe in H_2O carbonate buffer and D_2O carbonate buffer at temperature ramp from 10 °C to 80 °C.

Amplitudes have been corrected for their respective radiative rates. Uncertainties in lifetimes are ± 0.2 ns; uncertainties in amplitudes are ± 0.04.

temp. (°C)	H_2O Carbonate Buffer τ_f (ns)	D_2O Carbonate Buffer τ_f (ns)
10	8.31	7.91
20	6.42	6.17
30	4.81	4.63
40	3.59	3.47
50	2.71	2.62
60	2.13 (0.89), 0.74 (0.11)	2.09 (0.87), 1.02 (0.13)
70	1.66 (0.84), 0.74 (0.16)	1.63 (0.80), 0.88 (0.20)
80	1.30 (0.80), 0.52 (0.20)	1.37 (0.59), 0.81 (0.41)

Fluorescence behavior of 10 mM L-Phe in DLPC lipid vesicles at higher temperatures

Leroy et. al. described a change in non-radiative decay pathways at low temperatures.[5] To ensure L-Phe does not integrate into DLPC vesicles, the fluorescence lifetimes of L-Phe in DLPC vesicles were measured to a higher temperature to ensure there was no appearance of a second lifetime throughout the entire temperature run. The fluorescence decay and corresponding lifetimes can be seen in Figure SI-8 and Table SI-4, respectively. A visual representation of L-Phe in DLPC vesicles from -5 °C to 40 °C can be found in Figure SI-9. The results show L-Phe does not integrate into DLPC lipid vesicles.

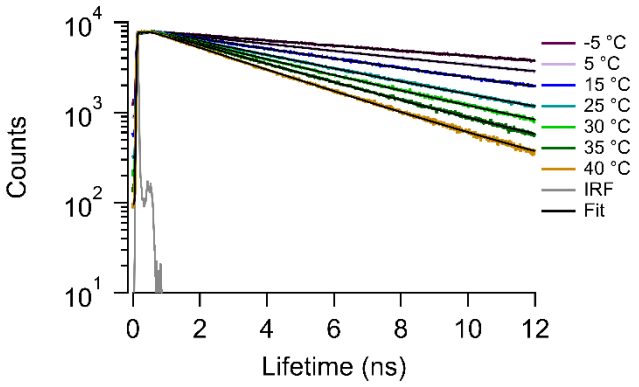

Figure A-2.5. TCSPC spectra of 10 mM L-Phe in DLPC lipid vesicles from -5 °C to 40 °C. Results from fitting these emission traces to Equation 1 are reported in Table SI-3.

Table A-2.4. Fluorescence lifetimes (in ns) and amplitudes (in parentheses) of 10 mM L-Phe in DLPC vesicles at selected temperature ramp from -5 to 40 °C in and back down to -5 °C. Uncertainties in lifetimes are ± 0.2 ns.

DLPC	
temp. (°C)	buffer τ_1 (A_1)
-5	13.3
5	10.1
15	7.36
25	5.5
30	4.73
35	4.08
40	3.52
35	4.03
30	4.7
25	5.47
15	6.8
5	9.89
-5	13.5

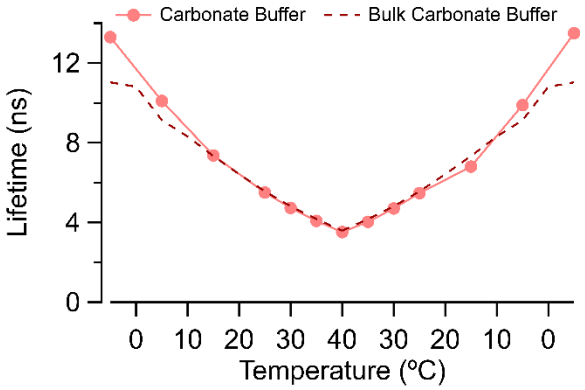

Figure A-2.6. TCSPC of 10 mM L-Phe in DLPC lipid vesicles from -5 °C to 40 °C. Fluorescence lifetimes of 10 mM L-Phe in DLPC lipid vesicles from -5 °C to 40 °C. The major lifetime is assigned to a L-Phe in carbonate buffer (τ_1, pink circles).

APPENDIX B:

NANOMOLAR PFOA CONCENTRATIONS AFFECT LIPID MEMBRANE STRUCTURE: CONSEQUENCES FOR BIOCONCENTRATION MECHANISMS

Structures of protonated and deprotonated PFOA

A 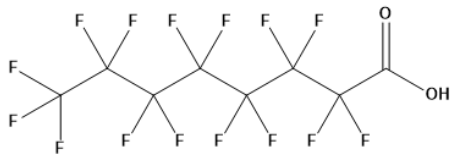 B 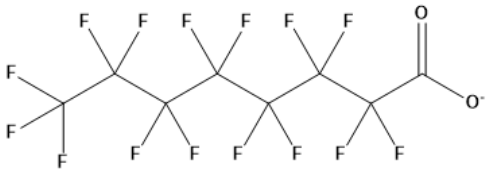

Figure B-3.1. Structure of A) neutral Perfluorooctanoic Acid (PFOA) and B) anionic PFOA

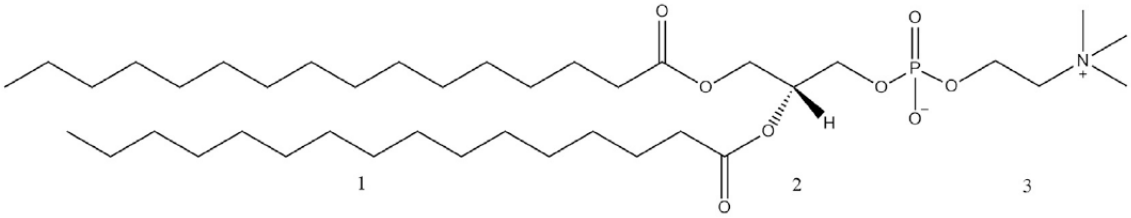

Figure B-3.2. Structure of 1,2-dipalmitoyl-sn-glycero-3-phosphocholine (DPPC)

TCSPC data of C152-DPPC control experiments

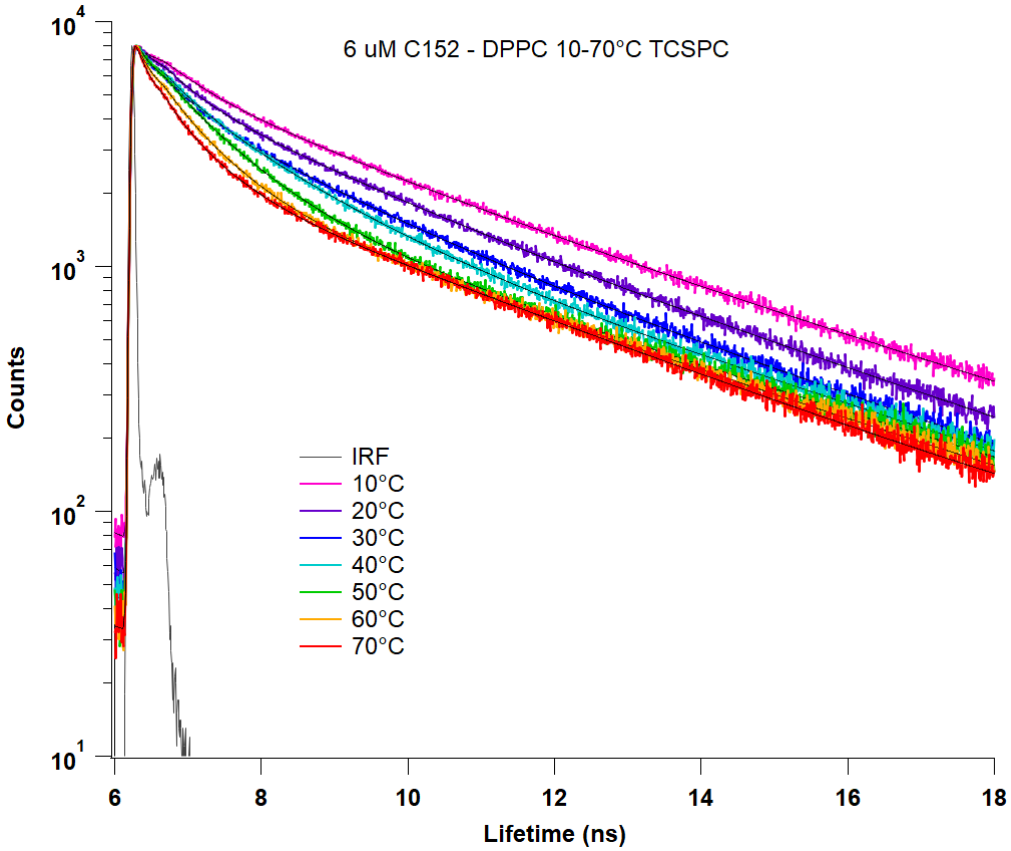

Figure B-3.3. TCSPC traces of 6 μM Coumarin 152 in solution with 1.5 mM DPPC vesicles from 10-70°C. These experiments are equivalent to those that led to the data presented in the manuscript's Figure 6 except that these experiments used DPPC vesicle solutions prepared in the absence of PFOA.

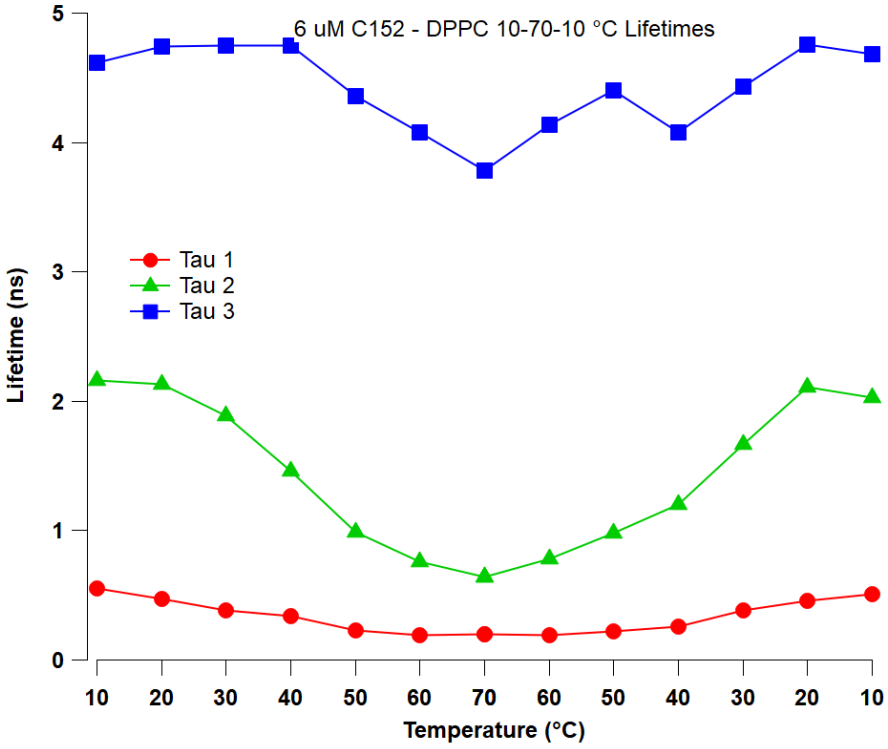

Figure B-3.4. C152 lifetimes derived from TCSPC decay traces shown in Figure B-2.3. Lifetimes are plotted as a function of temperature. These data can be compared directly to those shown in manuscript Figure 7. Uncertainties in lifetimes are ±0.10 ns.

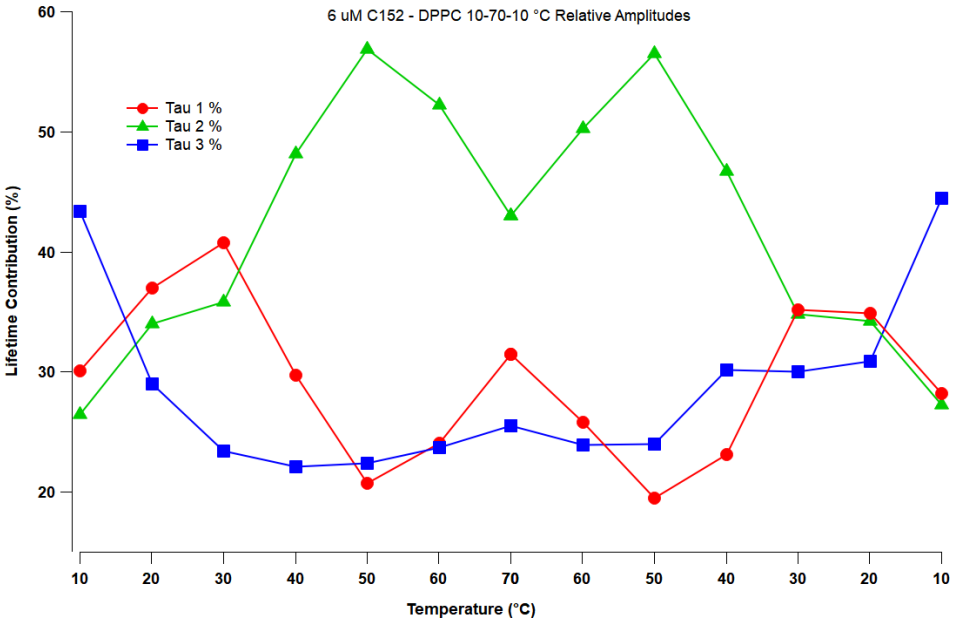

Figure B-3.5. Amplitudes of C152 lifetimes shown in Figure B-3.4 as a function of temperature. Amplitudes were determined from fitting shown in Figure B-3.3. These data can be compared directly to those shown in manuscript Figure 8. Uncertainties in lifetimes amplitudes are ±5 %.

TCSPC data of 1mM PFOA experiments

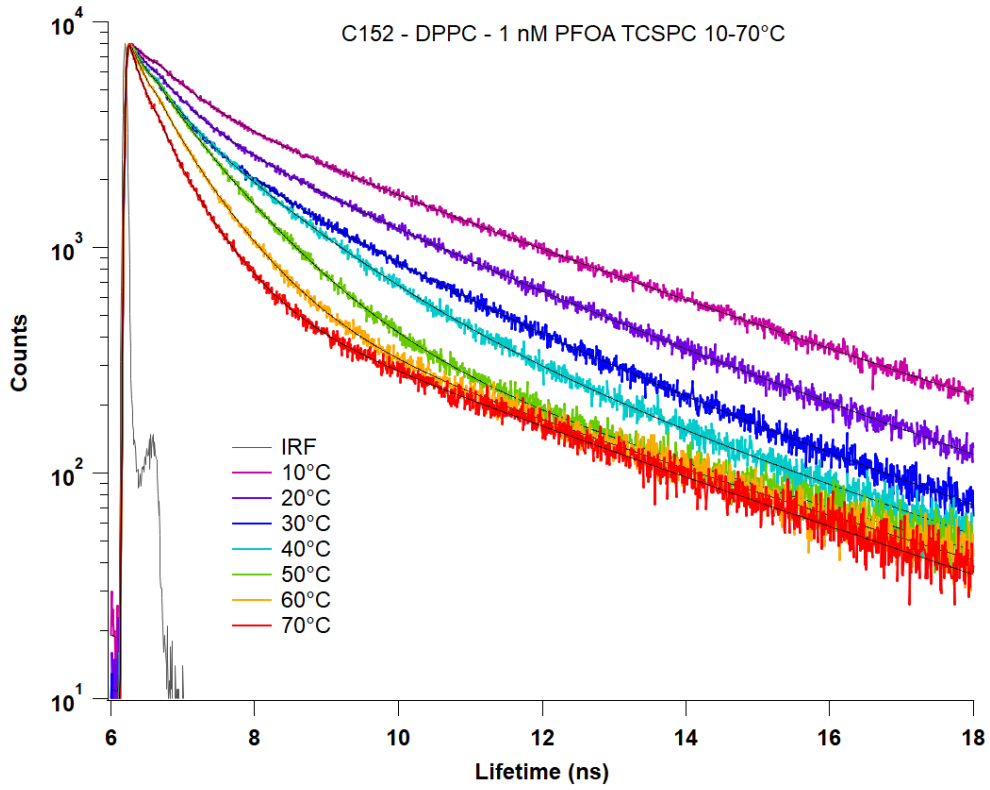

Figure B-3.6. TCSPC traces of 6 μM Coumarin 152 in solution with 1.5 mM DPPC vesicles from 10-70°C. These experiments are equivalent to those that led to the data presented in the manuscript's Figure 6 except that these experiments used DPPC vesicle solutions prepared in solutions containing 1 nM (vs. 100 nM) PFOA.

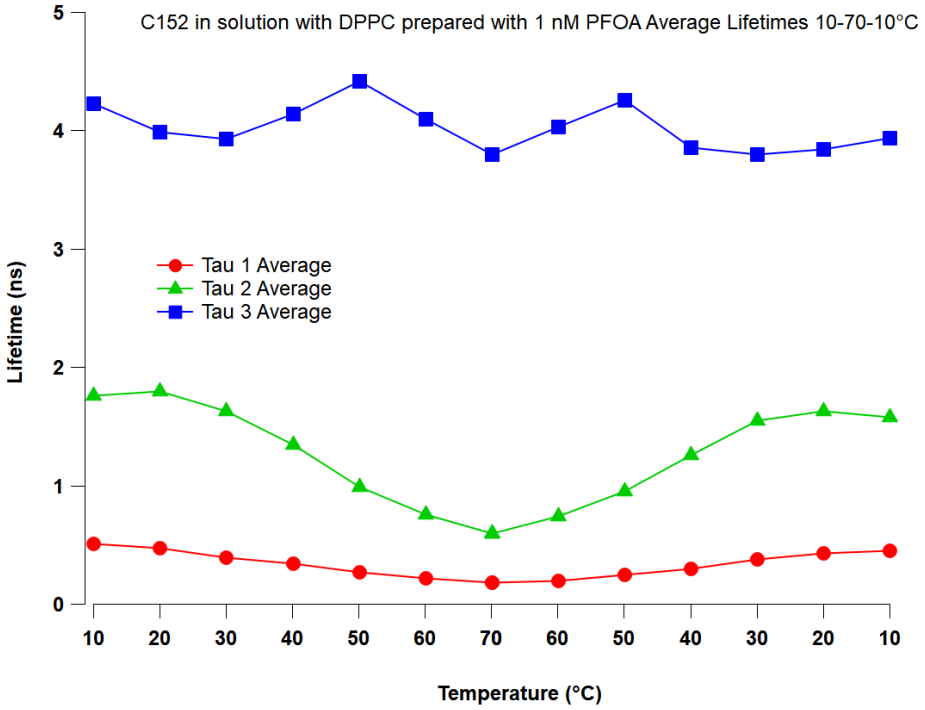

Figure B-3.7. C152 lifetimes derived from TCSPC decay traces shown in Figure B-3.6. Lifetimes are plotted as a function of temperature. These data can be compared directly to those shown in manuscript Figure 7. Uncertainties in lifetimes are ±0.10 ns.

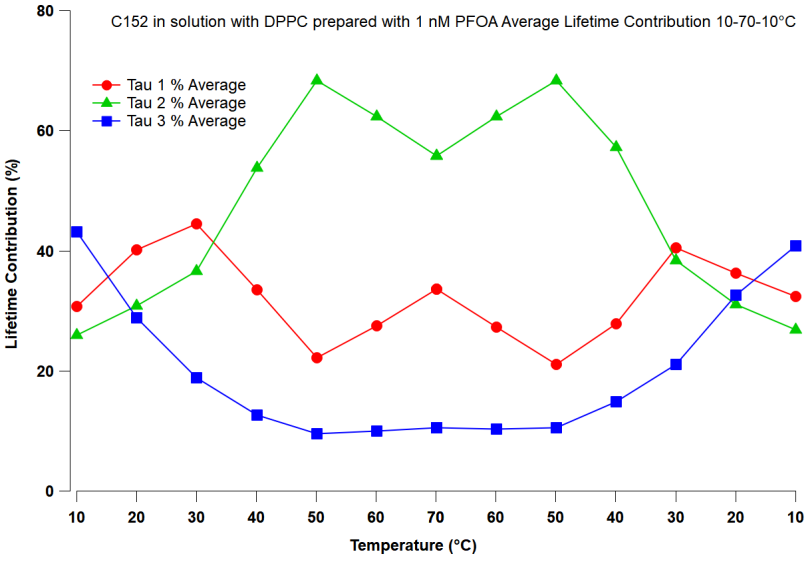

Figure B-3.8. Amplitudes of C152 lifetimes shown in Figure B-3.7 as a function of temperature. Amplitudes were determined from fitting shown in Figure B-3.6. These data can be compared

directly to those shown in manuscript Figure B-3.8. Uncertainties in lifetimes amplitudes are ±5 %.

TCSPC data of 100nM PFOA added after vesicle processing

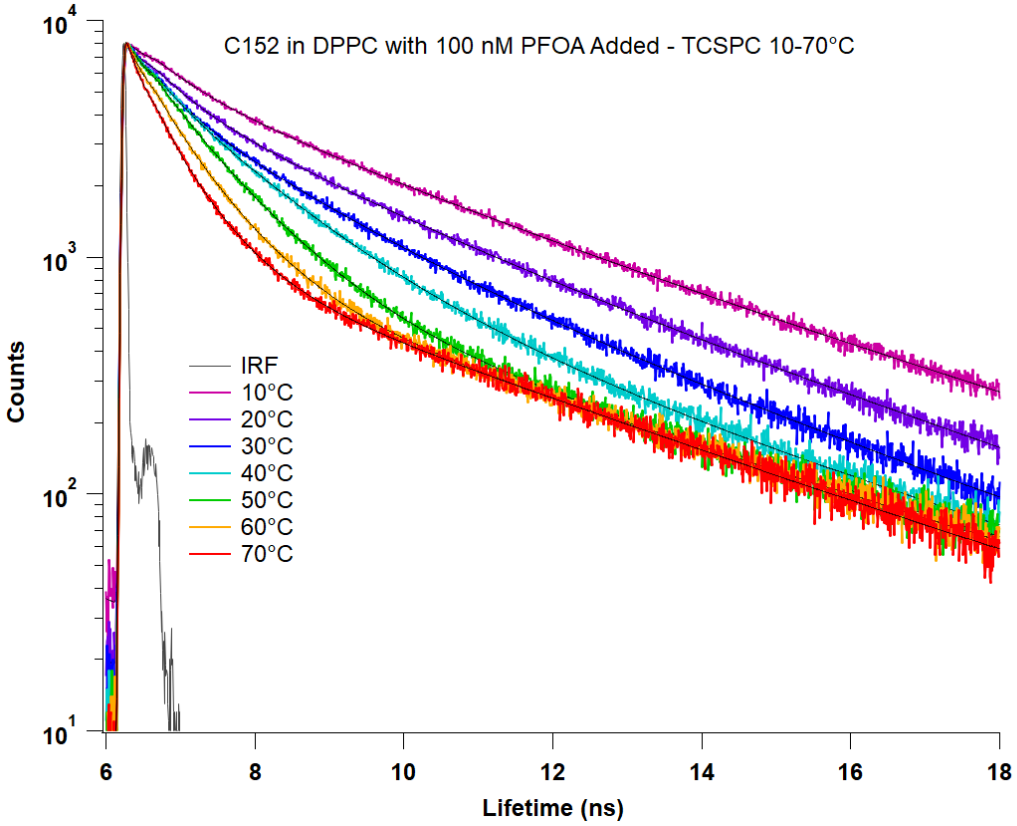

Figure B-3.9. TCSPC traces of 6 μM Coumarin 152 in solution with 1.5 mM DPPC vesicles from 10-70°C. These experiments are equivalent to those that led to the data presented in the manuscript's Figure 6 except that these experiments used DPPC vesicle solutions prepared in pure buffer solutions with 100 nM being added to solution after vesicle formation.

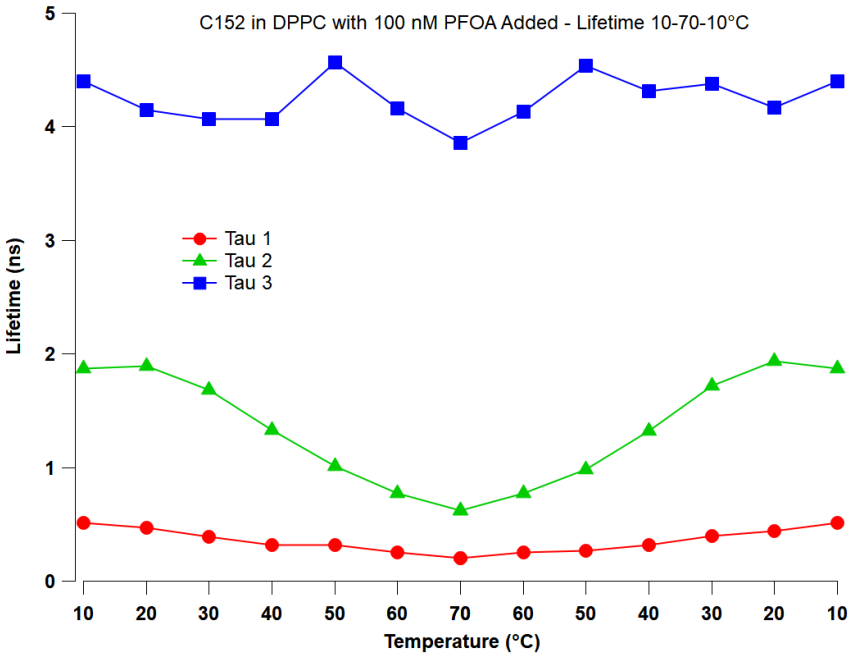

Figure B-3.10. C152 lifetimes derived from TCSPC decay traces shown in Figure B-3.9. Lifetimes are plotted as a function of temperature. These data can be compared directly to those shown in manuscript Figure B-3.8. Uncertainties in lifetimes are ±0.10 ns.

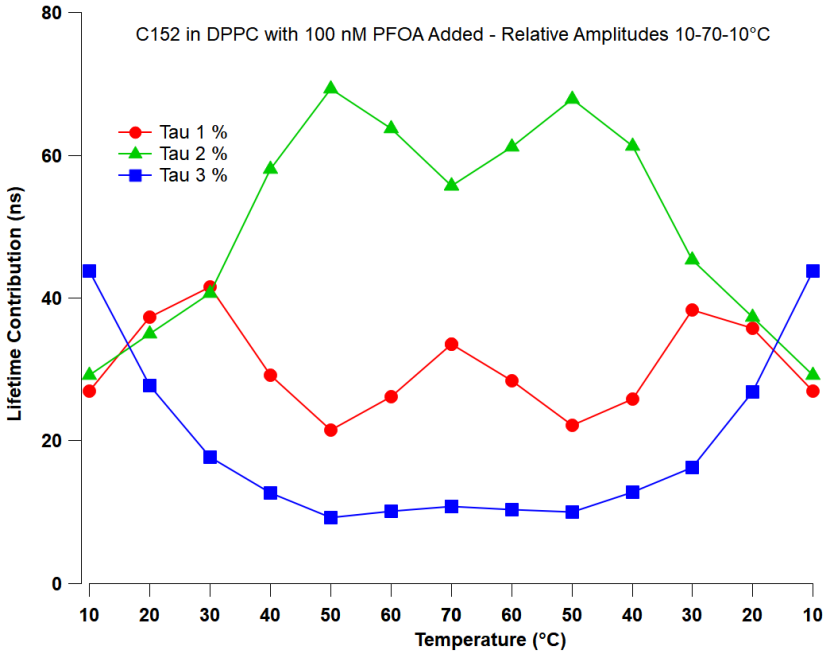

Figure B-3.11. Amplitudes of C152 lifetimes shown in Figure B-3.10 as a function of temperature. Amplitudes were determined from fitting shown in Figure B-3.9. These data can be compared directly to those shown in manuscript Figure 3.8. Uncertainties in lifetimes amplitudes are ±5 %.

Cryo-EM Images of pure DPPC vesicles

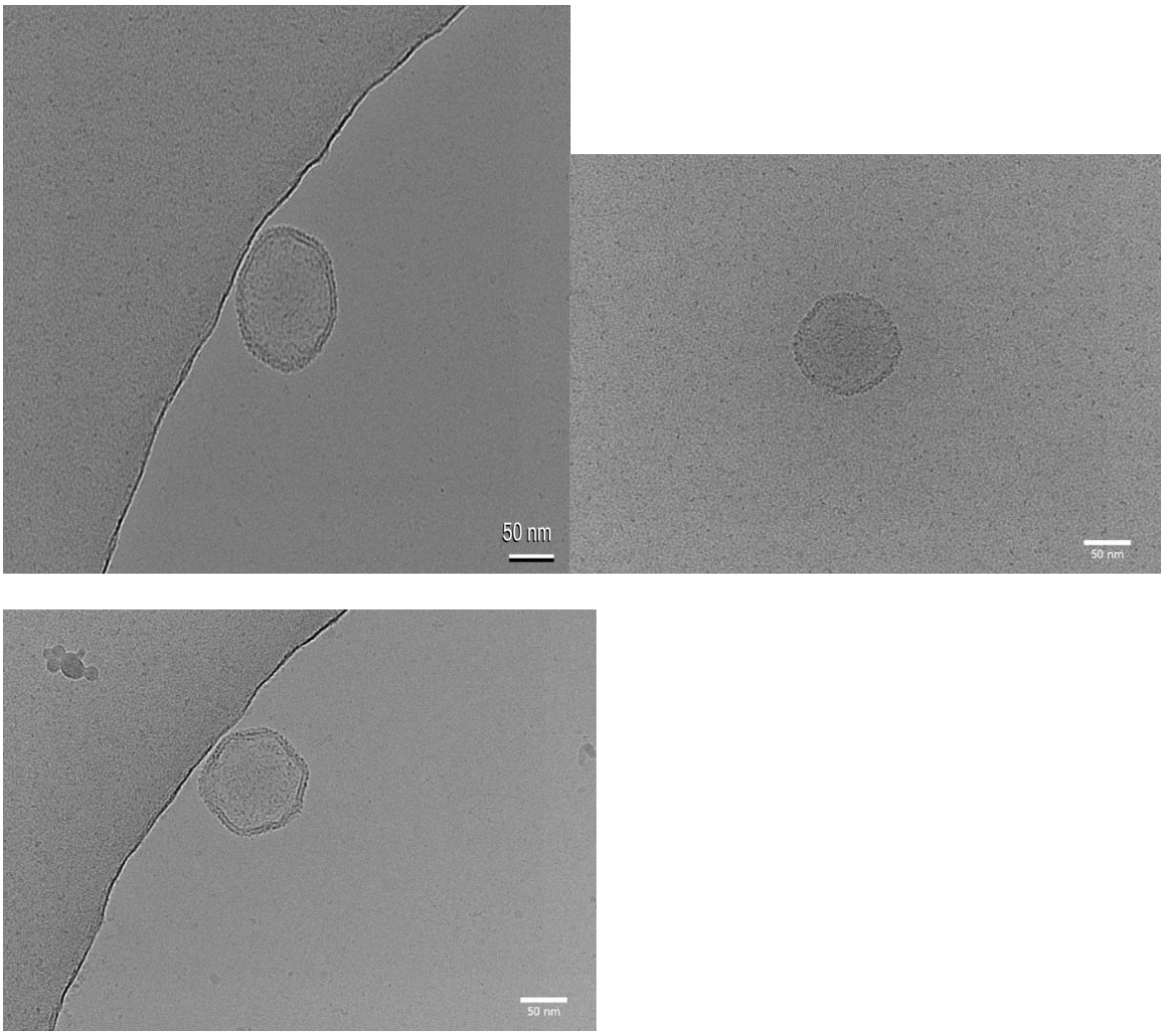

Figure B-3.12. Cryo-EM Images of DPPC vesicles prepared in pure buffer solutions containing no PFOA. These images can be compared directly to those in Figure 3.4 of the manuscript. These images are provided to demonstrate DPPC vesicle preparation generally leads to large unilamellar vesicles. Scale bars are 50 nm.

Cryo-EM images of DPPC Vesicles prepared with 100 nM PFOA

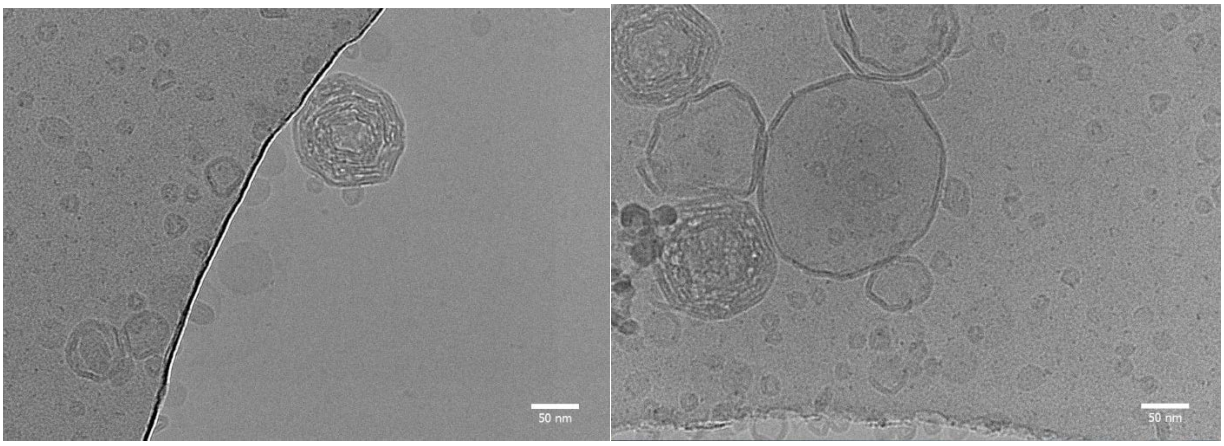

Figure B-3.13. Cryo-EM Images of DPPC vesicles prepared in solutions containing 100 nM PFOA. These images can be compared directly to those in Figure 2.5 of the manuscript. These images are provided to demonstrate generally that 100 nM PFOA introduces significant structural changes in DPPC vesicles. Scale bars are 50 nm.

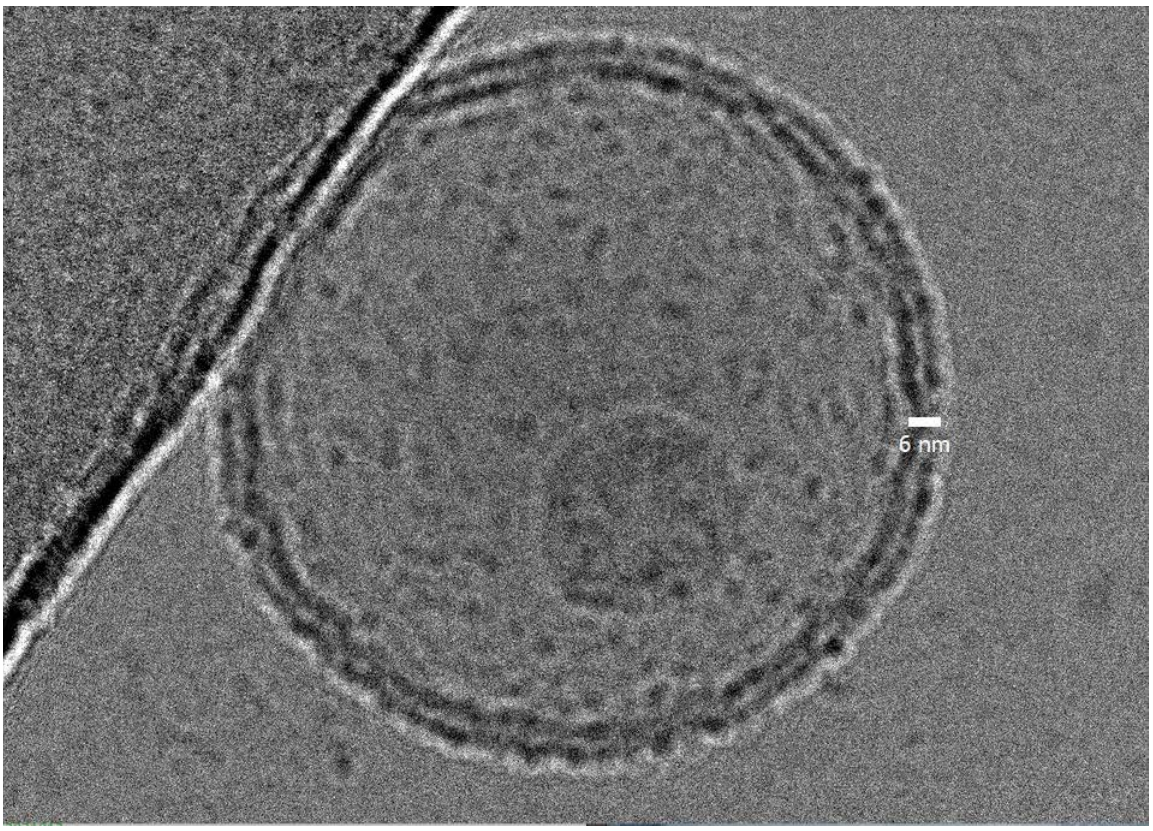

Figure B-3.14. Zoomed in image of a DPPC vesicle prepared in pure buffer solution. The scale bar is 6 nm and is chosen to span the bilayer width.

Tables containing raw TCSPC fitting data for all experiments

Table B-3.1. Averages of the raw fits of three TCSPC experiments with 1.5 mM DPPC Vesicles, 6 μM Coumarin 152, and 100 nM PFOA from 10 to 70˚C in 10 ˚C increments and then cooled back to 10˚C. The TCSPC decay traces are shown in Figure 6 in the manuscript and the data reported in the table below were used to create Figures 3.7 and 3.8 in the manuscript. Data were fit to 3 independent lifetimes. Attempting to fit data to 2 lifetimes led to unacceptably high χ^2 values. Uncertainties in lifetimes are ± 0.1 ns and uncertainties in amplitudes are ±5%.

Temp (°C)	χ^2	τ_1 (ns)	A_1 (%)	τ_2 (ns)	A_2 (%)	τ_3 (ns)	A_3 (%)
10	1.08	0.26	11.5	1.25	20.4	4.53	68.2
20	1.01	0.25	15.4	1.27	23.2	4.36	61.5
30	1.00	0.26	18.4	1.38	26.8	4.32	54.9
40	1.01	0.24	15.4	1.28	33.5	4.47	51.1
50	1.01	0.18	13.7	1.03	37.9	4.51	48.4
60	1.01	0.21	17.9	0.85	33.2	4.21	49.0
70	1.07	0.18	24.7	0.82	28.7	3.99	46.7
60	1.02	0.20	19.0	0.84	32.2	4.19	48.9
50	1.01	0.17	14.6	0.92	35.2	4.33	50.3
40	0.99	0.20	14.6	1.17	32.9	4.45	52.6
30	1.01	0.23	18.2	1.33	26.3	4.36	55.6
20	1.07	0.23	16.5	1.23	21.5	4.34	62.1
10	1.04	0.19	11.5	1.03	18.7	4.41	69.9

Table B-3.2. Averages of the raw fits of three TCSPC experiments with 1.5 mM DPPC vesicles and 6 μM Coumarin 152 with **no** PFOA. These data resulted from fitting the data in Figure B-3.1 to 3 independent lifetimes. Data in this table were used to create Figure 3.2 and Figure 3.3. Uncertainties in lifetimes are ± 0.1 ns and uncertainties in amplitudes are ±5%.

Temp (°C)	χ^2	τ_1 (ns)	A_1 (%)	τ_2 (ns)	A_2 (%)	τ_3 (ns)	A_3 (%)
10	1.09	0.55	30.1	2.16	26.5	4.62	43.4
20	1.05	0.47	37	2.13	34	4.74	29
30	1.05	0.38	40.8	1.89	35.8	4.75	23.4
40	0.99	0.34	29.7	1.46	48.2	4.75	22.1
50	1.03	0.23	20.7	0.99	56.9	4.36	22.4
60	0.95	0.19	24.1	0.76	52.2	4.08	23.7
70	0.97	0.2	31.5	0.64	43	3.78	25.5
60	1.02	0.19	25.8	0.78	50.3	4.14	23.9
50	0.94	0.22	19.5	0.98	56.5	4.4	24
40	1.07	0.26	23.1	1.2	46.7	4.08	30.2
30	1.04	0.38	35.2	1.67	34.8	4.43	30
20	1.05	0.46	34.9	2.11	34.2	4.76	30.9
10	1.05	0.51	28.2	2.03	27.3	4.68	44.5

Table B-3.3. Averages of the raw fits of three TCSPC experiments with 6 μM Coumarin 152 and 1.5 mM DPPC vesicles created in solutions containing 1 nM PFOA. These data resulted from fitting the data in Figure B-3.4 to 3 independent lifetimes. Data in this table were used to create Figure B-3.5 and Figure B-3.6. Uncertainties in lifetimes are ± 0.1 ns and uncertainties in amplitudes are ±5%.

Temp (°C)	χ^2	τ_1 (ns)	A_1 (%)	τ_2 (ns)	A_2 (%)	τ_3 (ns)	A_3 (%)
10	1.09	0.55	30.1	2.16	26.5	4.62	43.4
20	1.05	0.47	37	2.13	34	4.74	29
30	1.05	0.38	40.8	1.89	35.8	4.75	23.4
40	0.99	0.34	29.7	1.46	48.2	4.75	22.1
50	1.03	0.23	20.7	0.99	56.9	4.36	22.4
60	0.95	0.19	24.1	0.76	52.2	4.08	23.7
70	0.97	0.2	31.5	0.64	43	3.78	25.5
60	1.02	0.19	25.8	0.78	50.3	4.14	23.9
50	0.94	0.22	19.5	0.98	56.5	4.4	24
40	1.07	0.26	23.1	1.2	46.7	4.08	30.2
30	1.04	0.38	35.2	1.67	34.8	4.43	30
20	1.05	0.46	34.9	2.11	34.2	4.76	30.9
10	1.05	0.51	28.2	2.03	27.3	4.68	44.5

Table B-3.4. Averages of the raw fits of three TCSPC experiments with 6 μM Coumarin 152 and 1.5 mM DPPC vesicles created in pure buffer with PFOA being added after vesicle formation at a total PFOA concentration of 100 nM. These data resulted from fitting the data in Figure B-3.7 to 3 independent lifetimes. Data in this table were used to create Figure B-3.8 and Figure B-3.9. Uncertainties in lifetimes are ± 0.1 ns and uncertainties in amplitudes are ±5%.

Temp (°C)	χ^2	τ_1 (ns)	A_1 (%)	τ_2 (ns)	A_2 (%)	τ_3 (ns)	A_3 (%)
10	0.99	0.53	30.2	1.94	27.5	4.28	42.3
20	1.03	0.47	37.3	1.89	35	4.15	27.7
30	1.05	0.39	41.7	1.68	40.6	4.07	17.7
40	0.99	0.32	29.2	1.33	58.1	4.07	12.7
50	1.05	0.31	21.5	1.01	69.3	4.57	9.2
60	1.06	0.25	26.2	0.77	63.7	4.16	10.1
70	1.05	0.2	33.5	0.62	55.7	3.86	10.8
60	1.08	0.25	28.4	0.77	61.2	4.13	10.4
50	1.04	0.27	22.2	0.98	67.8	4.54	10
40	0.97	0.32	25.9	1.31	61.3	4.31	12.8
30	1.03	0.4	38.3	1.72	45.4	4.38	16.3
20	0.98	0.44	35.8	1.94	37.3	4.17	26.9
10	0.96	0.51	27	1.87	29.2	4.4	43.8

APPENDIX C:

PERFLUOROOCTANOIC ACID DESTABALZIES HEMOGLOBIN STRUCTURE AT SUB-MICROMOLAR CONCENTRATIONS

TCSPC histogram and raw fitting data

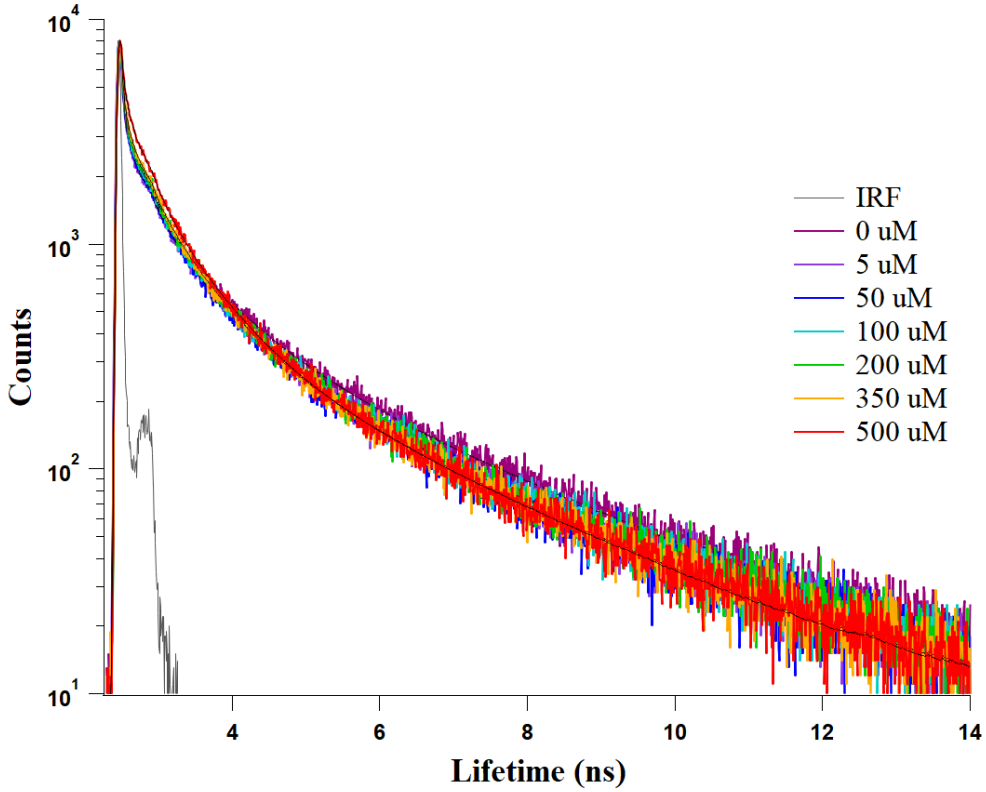

Figure C-4.1. TCSPC spectra of 5 μM Hemoglobin with increasing PFOA concentration. Excitation was 290 nm collecting emission at 335 nm

Table C-4.1. Averages of fluorescence lifetimes and relative amplitudes of Human Hemoglobin from 3 separate TCSPC experiments with standard deviations. These data are plotted in Figure 2 of the manuscript.

	t1 avg	**a1 avg**	**t2 avg**	**a2 avg**	**t3 avg**	**a3 avg**
0 μM PFOA	≤ 0.03	85.3 ± 1	0.45 ± 0.02	11.2 ± 0.8	2.34 ± 0.07	3.5 ± 0.22
5	≤ 0.03	85.5 ± 1	0.46 ± 0.02	11.2 ± 0.8	2.32 ± 0.11	3.3 ± 0.39
20	≤ 0.03	84.6 ± 0.3	0.47 ± 0.01	11.8 ± 0.1	2.4 ± 0.1	3.6 ± 0.2
50	≤ 0.03	85.1 ± 1	0.45 ± 0.01	11.5 ± 0.7	2.28 ± 0.1	3.4 ± 0.42

100	≤ 0.03	84.6 ± 0.6	0.44 ± 0.01	12.1 ± 0.4	2.24 ± 0.06	3.3 ± 0.25
200	≤ 0.03	84.1 ± 0.9	0.44 ± 0.01	12.5 ± 0.7	2.23 ± 0.07	3.4 ± 0.29
350	≤ 0.03	82.4 ± 0.8	0.44 ± 0.01	14 ± 0.5	2.20 ± 0.06	3.6 ± 0.34
500	≤ 0.04	73.4 ± 2.5	0.43 ± 0.02	22.3 ± 2.7	2.09 ± 0.15	4.3 ± 0.22

Steady state optical characterization of Hb

Human Hemoglobin was subjected to fluorescence characterization studies to obtain parameters for time-resolved emission experiments. UV-Vis experiments were performed to ensure absorption from PFOA doesn't impact absorption of the protein, find maximum absorbance of the fluorescence residues of the protein, and to witness changes to the soret band from heme when PFOA is present. Steady-state fluorescence measurements were performed to find the best excitation and emission wavelengths from the fluorescent residues of the protein. Excitation and emission maxima were then used to perform TCSPC experiments.

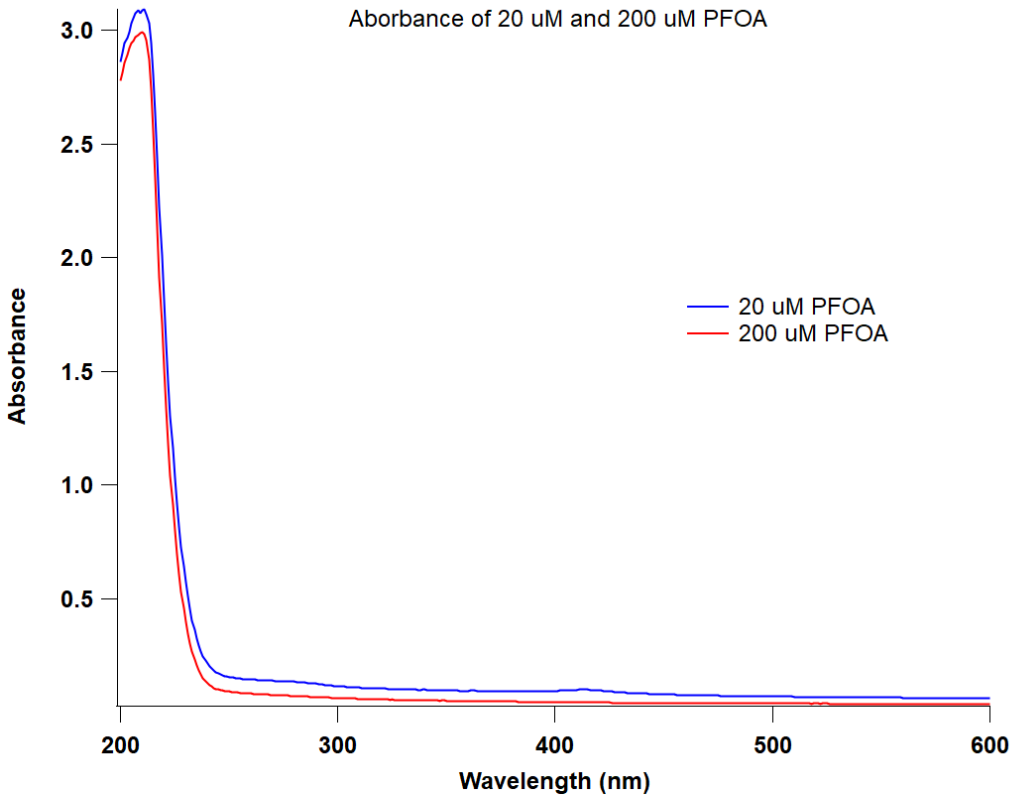

Figure C-4.2. UV-Vis absorbance of pure PFOA at concentrations of 20 □M and 200 □M in ammonium acetate buffer

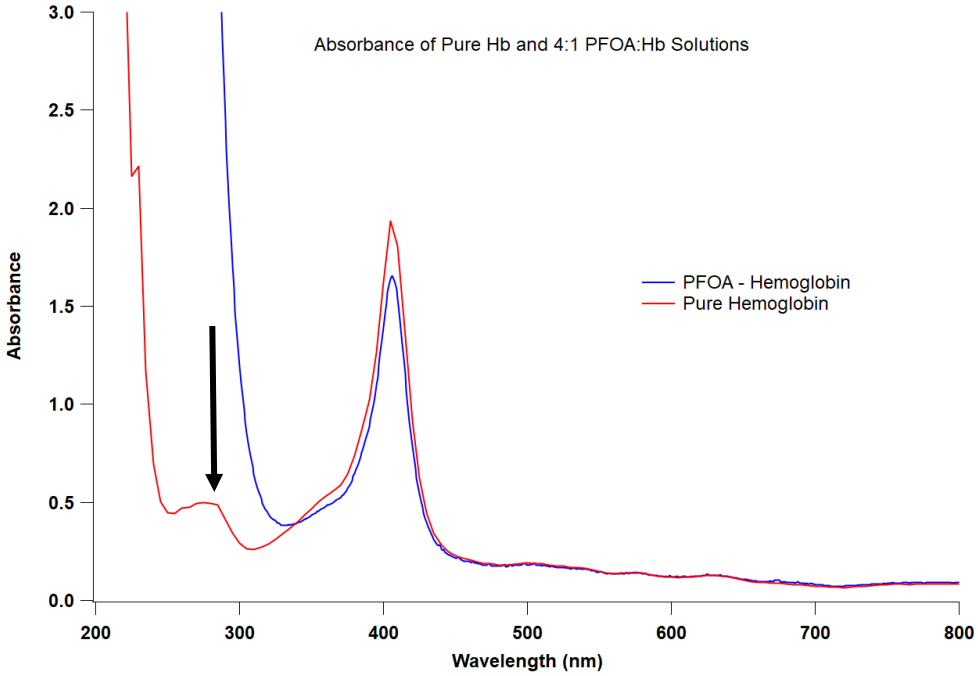

Figure C-4.3. UV-Vis of 5 μM Human Hemoglobin with 20 μM PFOA in ammonium acetate buffer pH 7. The arrow (280 nm) indicates absorption of the fluorescent residues of the protein chain.

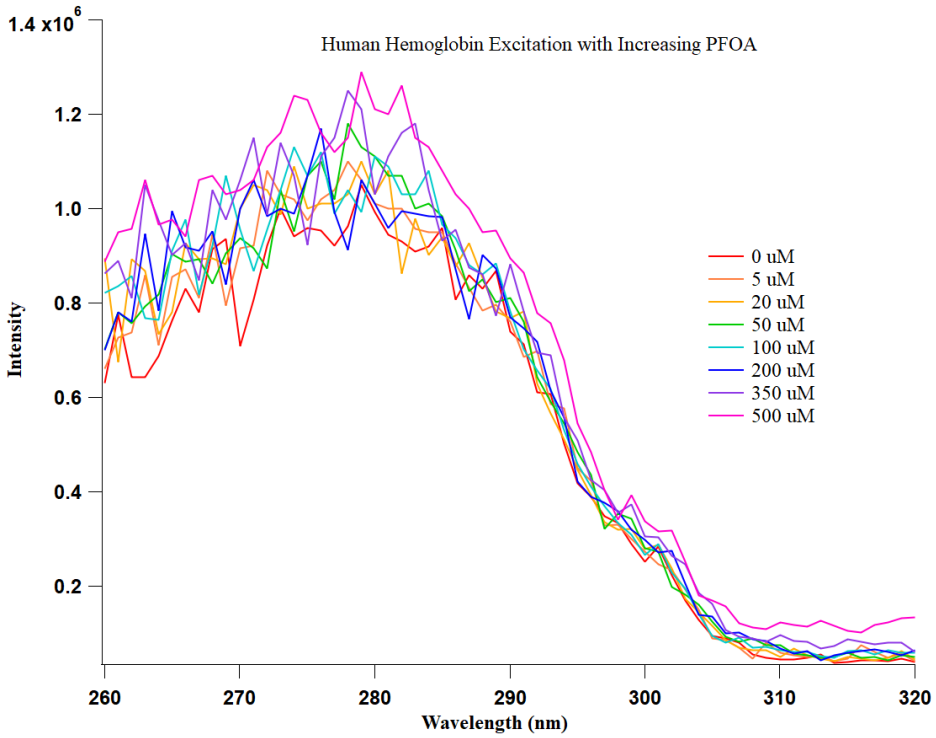

Figure C-4.4. Human Hemoglobin with increasing PFOA concentration steady-state excitation, Emission was measured at 335 nm.

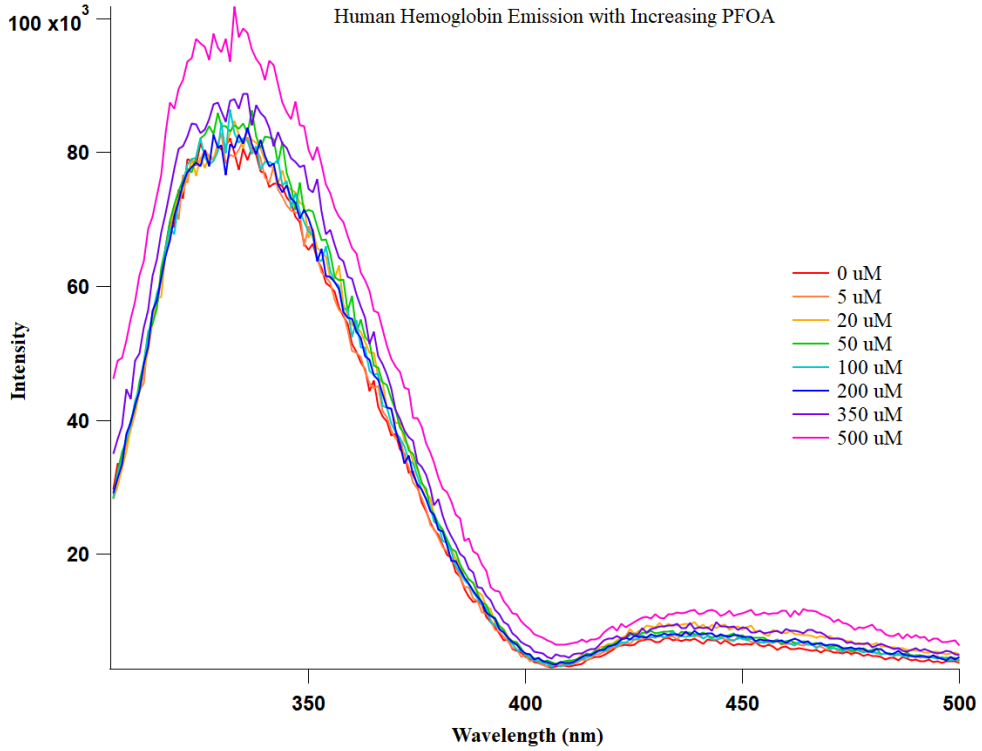

Figure C-4.5. Human Hemoglobin with increasing PFOA concentration steady-state emission. excitation was parked at 290 nm.